First-Ply Failure Behaviour of Pretwisted Delaminated Rotating Composite Conical Shells Due to Static & Impact Loading

A Thesis Submitted by

SUMAN KARMAKAR

[REG. NO.: 1021911007]

Doctor of Philosophy (Engineering)

DEPARTMENT OF MECHANICAL ENGINEERING

FACULTY COUNCIL OF ENGINEERING & TECHNOLOGY

JADAVPUR UNIVERSITY

KOLKATA, INDIA-700 032

2024

JADAVPUR UNIVERSITY

KOLKATA – 700 032

INDEX NO. 107/19/E

1. Title of Thesis:

First-Ply Failure Behaviour of Pretwisted Delaminated Rotating Composite Conical Shells Due to Static & Impact Loading

2. Name, Designation & Institution of the Supervisors:

Dr. Tanmoy Bandyopadhyay,

Assistant Professor,
Mechanical Engineering Department,
Jadavpur University, Kolkata -700032, India.

&

Dr. Amit Karmakar,
Professor
Mechanical Engineering Department,
Jadavpur University, Kolkata -700032, India.

3. List of Publications

i. Karmakar S, Singha T D, Rout M, Bandyopadhyay T, Karmakar A. First‑ply failure load prediction of delaminated pre‑twisted rotating composite conical shells. **Journal of the Brazilian Society of Mechanical Sciences and Engineering. 2023 Apr 26: 45(271)** doi.org/ 10.1007/s40430-023-04194-x

ii. Karmakar S, Bandyopadhyay T, Karmakar A. Additively Transient Behaviour and Impact Induced First‑Ply Failure of Delaminated Composite Conical Shells. **Journal of Vibration Engineering & Technologies. 2023 July 27.** doi.org/ 10.1007/s42417-023-01078-1

4. List of Patents: Nil

5. List of Presentations in National/International/Conferences/Workshops:

i. Karmakar S, Bandyopadhyay T, Karmakar A. "First-ply failure load prediction of pre-twisted delaminated composite cantilever conical shells." International Conferences on Advances in Mechanics, Modelling, Computation and Statistics (ICAMMCS-2022)", March 19 – 21, 2022, Department of Mathematics, Bits Pilani.

ii. Karmakar S, Bandyopadhyay T, Karmakar A.. "A Finite Element Approach for Prediction of First Ply Failure Load of Delaminated Composite Conical Rotating Shell." Industrial Problems on Machines & Mechanisms (IPRoMM-2022) December 22-23, 2022. Mechanical Engineering Department, IIT-ISM Dhanbad. doi.org/10.1007/978-981-99-4270-1_44

JADAVPUR UNIVERSITY

KOLKATA–700032, INDIA

STATEMENT OF ORIGINALITY

I, Suman Karmakar registered on 06/06/2019 do hereby declare that this thesis entitled "First-Ply Failure Behaviour of Pretwisted Delaminated Rotating Composite Conical Shells Due to Static & Impact Loading" contains literature survey and original research work done by the undersigned candidate as part of Doctoral studies.

All information in this thesis have been obtained and presented in accordance with existing academic rules and ethical conduct. I declare that, as required by these rules and conduct, I have fully cited and referred all materials and results that are not original to this work.

I also declare that I have checked this thesis as per the "Policy on Anti Plagiarism, Jadavpur University, 2019", and the level of similarity as checked by iThenticate software is 9%.

Suman Karmakar

Signature of Candidate:

Date: 03/05/2024

Certified by Supervisor(s):

(Signature with date, seal)

1. Bandyopadhyay 03/05/24

Assistant Professor
Dept. of Mechanical Engineering
Jadavpur University, Kolkata-32

2. Amit Karmakar 03/05/24

Professor
Dept. of Mechanical Engineering
Jadavpur University, Kolkata-32

JADAVPUR UNIVERSITY

KOLKATA–700032, INDIA

CERTIFICATE FROM THE SUPERVISOR(S)

This is to certify that the thesis entitled "First-Ply Failure Behaviour of Pretwisted Delaminated Rotating Composite Conical Shells Due to Static & Impact Loading", submitted by Mr. Suman Karmakar, who got his name registered on 06/06/2019 for the award of Ph.D. (Engineering & Technology) degree of Jadavpur University is absolutely based upon his own work under our guidance and supervision. Neither the results obtained from this work nor any part of this thesis has been submitted for any degree / diploma or any other academic award anywhere before.

(Dr. Tanmoy Bandyopadhyay)
Assistant Professor,
Mechanical Engineering Department,
Jadavpur University,
Kolkata-700032,
India.

Assistant Professor
Dept. of Mechanical Engineering
Jadavpur University, Kolkata-32

(Dr. Amit Karmakar)
Professor
Mechanical Engineering Department,
Jadavpur University,
Kolkata-700032,
India.

Professor
Dept. of Mechanical Engineering
Jadavpur University, Kolkata-32

ACKNOWLEDGEMENT

The author expresses his deep sense of gratitude to his supervisors, Dr. Tanmoy Bandyopadhyay & Dr. Amit Karmakar for their keen interest, cherished guidance and constant inspiration during the research work. The author is grateful to him for his guidance to enter a new field of composite structure. Above all, without his moral support and constant guidance the author would have not been completed the work.

The author acknowledges to the reviewers of journals and conference papers and from the audience, while presenting papers in conferences. The author extends specials thanks to the Applied Mechanics Laboratory of Jadavpur University, Kolkata for providing facility and support during this research work.

The author takes great pleasure to thank Dr. T. D. Singha & Mr. P Mandal from whom he received immense support and assistance. The author expresses extreme gratefulness to his wife (Antara) and daughter (Isha) for their constant support and motivation, without that he would not have come to this stage.

Above all, it is the wish of The Almighty that the author has been able to complete this work.

Suman Karmakar

Date: 03/05/2024

Suman Karmakar

LIST OF PUBLICATIONS

The below technical papers are prepared based on the present research work which have been published/accepted or submitted in the International Journals and International/National conferences:

INTERNATIONAL JOURNAL:

1. Karmakar S, Singha T D, Rout M, Bandyopadhyay T, Karmakar A. First‐ply failure load prediction of delaminated pre‐twisted rotating composite conical shells. **Journal of the Brazilian Society of Mechanical Sciences and Engineering. 2023 Apr 26: 45(271)** doi.org/ 10.1007/s40430-023-04194-x

2. Karmakar S, Bandyopadhyay T, Karmakar A. Additively Transient Behaviour and Impact Induced First‐Ply Failure of Delaminated Composite Conical Shells. **Journal of Vibration Engineering & Technologies. 2023 July 27.** doi.org/ 10.1007/s42417-023-01078-1

INTERNATIONAL/ NATIONAL CONFERENCE:

1. Karmakar S, Bandyopadhyay T, Karmakar A. "First-ply failure load prediction of pre-twisted delaminated composite cantilever conical shells." International Conferences on Advances in Mechanics, Modelling, Computation and Statistics (ICAMMCS-2022)", March 19 – 21, 2022, Department of Mathematics, Bits Pilani.

2. Karmakar S, Bandyopadhyay T, Karmakar A. "A Finite Element Approach for Prediction of First Ply Failure Load of Delaminated Composite Conical Rotating Shell." Industrial Problems on Machines & Mechanisms (IPRoMM-2022) December 22-23, 2022. Mechanical Engineering Department, IIT-ISM Dhanbad. doi.org/10.1007/978-981-99-4270-1_44

ABSTRACT

In the field of materials science, composite materials have gained attraction as scientist and researchers can improve different mechanical properties as per choice. Due to high stiffness and lesser in weight compared to conventional materials, composites are suitable for weight sensitive application in the field of marine, automobile, sports, aeronautic structure and power plant. In recent past extensive use of laminated composites are found in many engineering discipline like aerospace, mechanical, civil, marine, automobile, and power plant. Composite materials are used in structural application due to reduction in weight and enhancement of strength. Therefore it is an important area for researchers and scientist to analyze different structural parameters and their effects.

Turbomachinery blades are fixed at one end on disc or hub and other end is free. Thus it behaves like a cantilever beam fixed at one end and conical in shape with trapezoidal planform. During rotation blades are subjected to centrifugal forces. In power plants, the composite blades are subjected to high operating temperatures. So it is necessary to understand the dynamic behaviour of conical shell operating under thermal and centrifugal loading.

Delamination or separation of layers is one of the failure mode of laminated composite materials. It may occur at any arbitrary location due to manufacturing defect, loading condition, environmental effect etc. Delamination creates geometrical and material discontinuities. It reduces structural strength and stiffness and as a result the load carrying capacity of the material reduces. Therefore it is necessary to study the effect of delamination on structural strength of composite blades.

It is required to predict the maximum safe load in design of a composite material which depend on several structural parameters, size and location of delamination, rotation and environmental condition. The initial separation of any two layers of laminated composite are known as first-ply failure (FPF). There are several established FPF theories available which are maximum strain (independent), maximum stress (independent), maximum stress (polynomial) Hoffman, Tsai-Hill, and Tsai-Wu. The present work illustrates the effect of some vital parameters like stacking sequence, pre-twist angle, aspect ratio, presence and location of delamination, and rotational speed on the FPF in the delaminated composite conical shell with an initial twist. It is found that the FPF strengths increase on increasing the non-dimensional rotational speed whereas the strength decreases

with size and number of delaminations, aspect ratio and pretwist angle. The stresses developed at the FPF loads are lower in non-rotating conical shells compared to rotating shells.

Dynamic behaviour of composite materials under random impact is a serious concern since the impact phenomenon inevitably arises during manufacturing, maintenance, transport and hostile operating conditions. The presence of delamination intensifies the damage caused by impact which in turn significantly reduces the strength and stiffness of the composite structure. The critical impact velocity at which the first-ply failure may initiate is of utmost engineering concern and importance since failure will propagate at an enhanced rate due to reduced strength of the resulting composite structure. The effect of delamination, aspect ratio, fiber orientation angle on contact force, shell displacement, impact or displacement, impactor velocity are significant parameters as it initiates impact induced first-ply failure. Results include the effects of different parameters like delamination length, aspect ratio, fibre-orientation angle and impact location on the dynamic behaviour of conical shell at maximum safe impact velocity beyond which first-ply failure (FPF) will commence. The Tsai-Wu failure criterion which is the most general and consistent criterion for biaxial stresses is used to predict the critical velocity of impact for first-ply failure initiation in composite conical shells. It is observed that critical velocity decreases on increase of aspect ratio and size of delamination. It is also found that contact force, shell displacement, impactor displacement, impactor velocity decreases on increasing the aspect ratio, size & number of delamination. When the impact location moves from near fixed end to near free end, the contact force, shell displacement, impactor displacement, and impactor velocity decreases.

The FEM codes are developed first validated with available benchmark literatures and the percentage variation between current and published results are found to be between 3%. Then the codes are used for present analysis. The FEM codes are developed using MATLAB and FORTRAN and the results are plotted using standard graph plotting software (ORIGIN).

KEYWORDS

First-ply failure; conical shell; FEM; delamination; pretwist; composite; impact; Critical Velocity of Impact

NOMENCLATURE

z	Mid-plane of the conical shell laminate.
$R_{y,}$	Chordwise radius of the conical shell.
R_{xy}	Pre-twist radius of the conical shell
L,	Span length
b_o,	base width
α_0	major radii
β_0	minor radii
h	thickness
θ_v	vertex angle
θ_0	base subtended angle
ψ,	Pre-twist angle
ω_z,	Rotational speed (rad/s),
Ω	Non-dimensional rotational speed ($\Omega = \frac{\omega_z}{\omega_o}$),
ω_0	Angular speed at resonance
d	Delamination size
d_1	spanwise location of the delamination centre from the fixed end
L	span length of the conical shell
h_{Del}	Delaminated ply location from bottom
n_d	Number of delaminations (for multiple-delaminations).
E	Young's modulus
G	Rigidity modulus
v	Poisson's ratio
ρ	Density

$[N]$	Shape function matrix
$[B]$	Strain-displacement matrix
$[D]$	Elasticity matrix
$[M]$	Mass matrix
$[K]$	Linear stiffness matrix
U	Total strain energy
$[K_{\sigma e}]$	Geometric stiffness matrix at element
$[K_{\sigma}]$	Geometric stiffness matrix at global
F_P	Externally applied point load
σ_1,σ_2, σ_6	Normal stress components, shear stress components in the principal material directions.
ε_1,ε_2, ε_6	Normal strain components, shear strain components in the principal material directions.
X_T,Y_T	Tensile strengths (based on stress) of the lamina in the principal material directions (x- and y-directions) assuming plane-stress conditions for the present analysis.
X_C,Y_C	Compressive strengths (based on stress) of the lamina in the principal material directions (x- and y-directions).
R, S, T	Shear strengths (based on stress) of the lamina in the principal material directions (x- and y-directions).
$X_{\varepsilon T}$,$Y_{\varepsilon T}$	Tensile strengths (based on strain) of the lamina in the principal material directions (x- and y-directions).
$X_{\varepsilon C}$,$Y_{\varepsilon C}$	Compressive strengths (based on strain) of the lamina in the principal material directions (x- and y-directions).
R_ε, S_ε, T_ε	Shear strengths (based on strain) of the lamina in the principal material directions (x- and y-directions).
m_i	Mass of the impactor
$\ddot{\delta}$	Acceleration of the impactor

F_c	Global contact force vector
k_c	Contact stiffness
α_0	Permanent indentation

Numbering of Figures, Tables and Equations

Figures, tables, and equations have been numbered in accordance with the chapters in which they appear in the thesis. Each table, figure and equation have two distinct numbers. The first number specifies the number of the chapter, and the second number denotes to the actual number of the figure, table, and equation in that chapter.

Representation of References

The list of references has been furnished at the end of the thesis. These references have been represented by the respective name of the author(s) along with the year of publication.

CONTENTS

LIST OF TABLES

LIST OF FIGURES

CHAPTER 1: INTRODUCTION

1.1 Overview

1.1.1 Preface

With the advancement of technology and computing facilities in the field of material science, composite materials have gained superior attention by many researchers and scientists. The improvement of different mechanical properties as per choice encouraged researcher to tailor the fibre orientations in order to obtain desired properties of composite materials. With the advancement of composite materials designers got freedom to improve structural properties of same dimension by analysing/optimizing different properties. Owing to its high stiffness, low weight compared to conventional materials, alloys and ceramics and other preferred properties like corrosion resistance, wear resistance, durability, composites are considered as potential materials for weight sensitive applications like marine structure, aeronautic structure, automobile applications and sports equipment. In the past few decades, the extensive use of laminated composites was found in various engineering disciplines such as aerospace, mechanical, civil, marine, automobile, and power plant. The use of composite materials in structures for reduction in weight and enhancement of strength are growing for last few decades. Analysis of different parameters and their effects are necessary to understand the design of composite materials for some specific use. Therefore it is a thrust area for many researchers to investigate effect of different parameters and their response.

Usually turbomachinery blades are fixed on a disc or hub which rotates about an axis perpendicular to the plane of hub. Thus turbomachinery blades can be assumed as a cantilever beam whose one end is fixed at hub and conical in shape. During rotation the blades are subjected to centrifugal forces. Therefore, it is necessary to understand the dynamic behaviour of conical shells. Delamination of a composite shell is a serious concern as it reduces structural strength and initiate failure at lower load.

Like other materials it is required to predict failure load of laminated composite at different operating condition. Initiation of first ply failure (FPF) will reduce the strength of laminated composite materials for static and impact loading. As laminated composites are made of different layers, separation of different layers or presence of delamination will reduce the strength. Thus first ply failure of laminated shells is not desirable as it degrades stiffness and strength of a structure.

Composite laminates are made of several layers and each layer is made of matrix material & fibre. The matrix material that holds the individual layers of laminate together has a considerably smaller strength of the layers. Under certain loading, large stresses can be generated in a direction perpendicular to the interface between the layers. These stresses are mostly localized and cause breaking of bond between the layers within a small region. However, presence of small size delamination effects the integrity of structure and aids to initiate failure at lower load.

An open conical shell has a trapezoidal planform that is wider at the base and this end is fixed to the hub of the turbomachines with a definite pre-twist. However, delamination is a serious concern because it deteriorates the structural strength resulting in premature failure of the composite blades.

1.1.2 Turbo Machinery Blades

Development in the field of turbomachinery mainly in aviation, wind turbine and marine has taken place rapidly in previous century. Turbomachinery blades are fixed at hub which rotates/revolves about an axis perpendicular to the blades. The laminated composites are considered as potential materials for turbomachinery blades that are normally wider near the hub region and narrow at free end which can be consider as a cantilever beam. In most of the cases turbomachinery blades are pretwisted in nature. During rotation at speed centrifugal forces are generated which effects the strength and stiffness of the composite structure. Presence of delamination in the composite blades reduces the stiffness and strength of the structure resulting in decrease of failure load. So it is necessary to investigate and predict the failure loads to ensure safe operating conditions of rotating turbomachinery blades.

1.1.3 Shell Modelling

The initial approach was using Euler Bernoulli's beam equation to study the behavior of turbomachinery blades and other structural components. It is acceptable when the width of the blades are smaller compared to length and blades are reasonably thick. But if the blades having small aspect ratio with less thickness will behave as shell rather than beam for which Euler Bernoulli's beam equation does not give accurate result. For precise result blades are considered as pretwisted shell structure with small aspect ratio and less thickness. Due to consideration of shallow shell a three dimensional problem can be reduced to two dimensional by applying plane strain condition.

1.1.4 Pre-twisted Composite Conical Shell Modeling

Pretwisted composite conical shell have wide application in turbo machinery blades, aviation's, automobiles etc. due to low weight and higher stiffness and strength result in better fuel efficiency and reliability. Hence composites are very advantageous as the desired material properties can be tailored in any specific directions. Modelling of composite blades are complex because due complex geometry and variations in curvature and thickness may occur in chordwise direction and along the length. The width of the blades is usually higher in the hub region compared to its free end. The turbomacinery blades can be represented as open conical shell with trapezoidal planform. During Finite Element Analysis (FEA) pretwisted composite blades are considered as it represents the actual situation. The pretwist angle is constrained to a certain limit as excessive increase of pretwist angle reduces structural stiffness and strength.

1.1.5 Finite Element Modeling

Turbomachinery blades, wings of aircraft, haul of ship, automobile components etc. are made of composite materials subjected to various types load such as static, impact and centrifugal resulting in deflection and stress generation. Therefore, it is necessary to predict the effect of aspect ratio, pretwist angle, fiber orientation angle, delamination and rotational speed on dynamic behaviour on composite shells. Due to complicated shape the dynamic behavior of blade is difficult to predict accurately using analytical beam theory and the results are insufficient as it provides

preliminary/basic results. Hence, Finite Element Method (FEM) is very useful to predict the dynamic behavior of complex shaped composite blades. In FEA of composite shells complex shape with direction dependent material properties can be analysed in details by discretizing the domain in small elements as per requirement.

1.1.6 Delamination Modeling

Delamination is the separation between layers which is one of the failure mode laminated composites. It may occur at any arbitrary location along the span of the composites. Delamination generates due to manufacturing defect, loading condition, environmental effect etc. The strength and stiffness significantly reduces depending upon the size, shape and number of delamination present inside the composite structures. Delamination creates geometrical and material discontinues and analysis of effect of delamination on failure load is important from structural failure point of view as it may not be visible by bare eyes. The frequency analysis of delaminated structure is mathematically complicated. Delamination may occur within the composite laminate either during manufacturing or transportation and it may also be induced dynamically owing to the application of external loadings during service or due to rapid impact or blast loads under severe working conditions. The presence of delamination severely deteriorates the load-bearing capacity of the composite structures. The determination of the first-ply failure loads of delaminated composite shallow shells is extremely complex and mathematically intricate.

1.1.7 First Ply Failure due to Static Loading

It is necessary to predict the maximum safe load which a composite structure can withstand before its failure. The different parameters effect the maximum safe load are aspect ratio, fiber orientation angle, vertex angle, base subtended angle, pretwist angle, presence of delamination and its location, rotational speed, environmental conditions etc. The initial separation of any two layers of laminated composites is termed as first-ply failure (FPF) and it reduces the structural strength and stiffness leading to failure of composites. Several established theories have been developed to predict the FPF and among them some important theories are maximum strain (independent), maximum stress (independent), maximum stress (polynomial) Hoffman, Tsai-Hill, and Tsai-Wu.

1.1.8 Impact Induced First Ply Failure

Dynamic behaviour of composite materials under random impact is a serious concern since the impact phenomenon inevitably arises during manufacturing, maintenance, transport and hostile operating conditions. The damage occurring in the composite laminates due to low-velocity impact mostly remains undetected by visual inspection owing to its insidious nature. The presence of delamination intensifies the damage caused by impact which in turn significantly reduces the strength and stiffness of the composite structure. The critical impact velocity at which the first-ply failure may initiate is of utmost engineering concern and importance since failure will propagate at an enhanced rate due to reduced strength of the resulting composite structure. The effect of delamination, aspect ratio, fiber orientation angle on contact force, shell displacement, impact or displacement, impactor velocity are significant parameters to be considered during analysis as it initiates impact induced FPF and failure propagation resulting in reduction of strength and stiffness of the structure.

1.1.9 Transient Response

The structural strength and stiffness is the major concern to withstand maximum safe load and stresses under impact condition. Therefore, prediction of impact response of composite shells is necessary under different service condition to estimate service life and safety. Structural elements like fuselage, blades of jet engine and turbine are usually subjected to impact load. If the loads or stresses crosses the permissible limit catastrophic failure may occur of the entire structure resulting loss of life and property. Therefore, the time dependent responses of contact force, shell displacement, impactor displacement, impactor velocity, stresses at critical velocity of impact are major concern to predict the impact response over time in design and analysis of composite structure.

1.2 Literature Review

Composite materials are widely used in various industries like automobile, aerospace, marine, defense, engineering etc. due to their light weight combined with high strength and excellent ability to be tailored to meet desired properties. The literature review related to modelling, design, analysis, impact response and failure of composite shells encloses a wide area

related to present work. An enormous knowledge is presented in various books and research articles. Related to the present work emphasis is given to pretwisted delaminated composite shells both stationary and rotating, their FPF, impact response and progressive failure.

Flow Chart for Literature Review

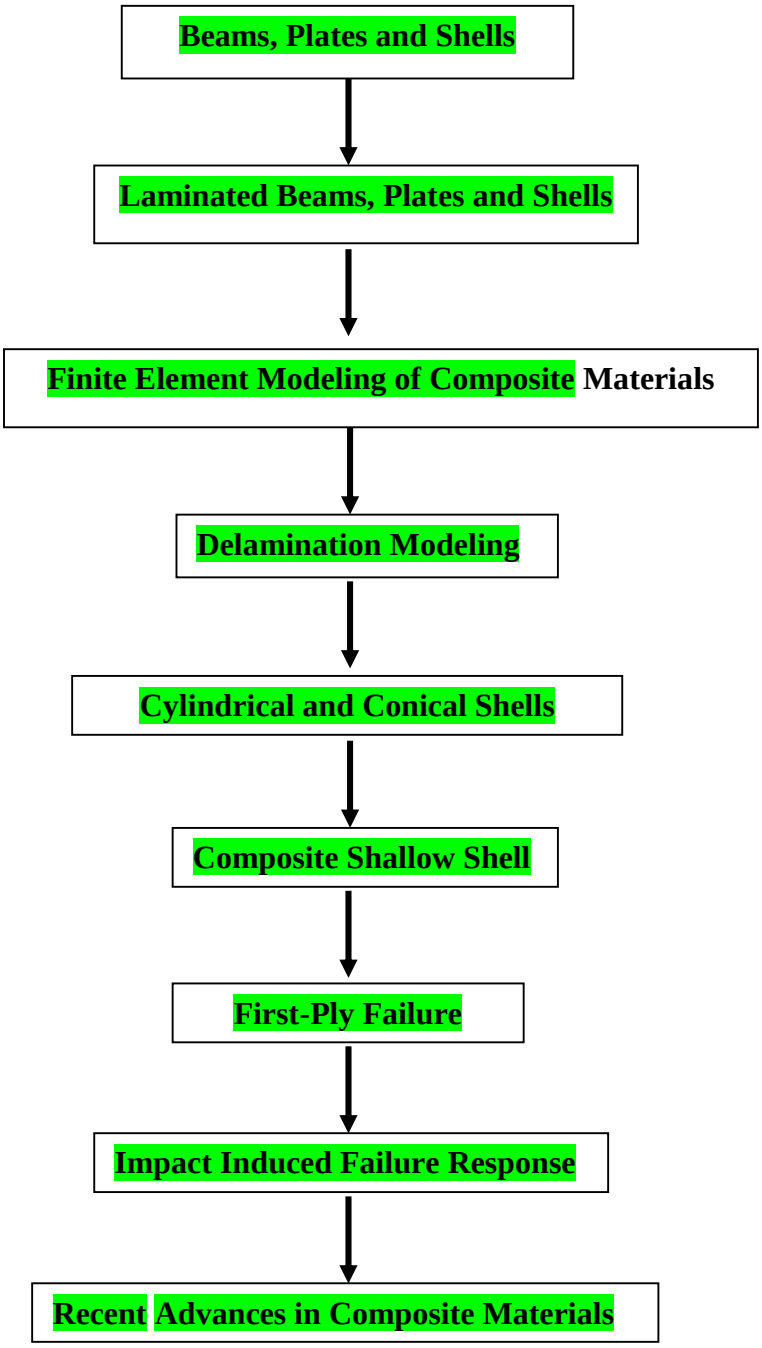

1.2.1 Beams, Plates and Shells

Liew et al. [1] analyzed the vibration characteristics of stationary pre-twisted isotropic cantilever shallow conical shells employing the Ritz method. For a larger conical shell fundamental physical frequency (ω) decreases monotonically. Outcomes signifies that a rise in angle of twist does not confirm greater torsional stiffness for the shell, which was in ambiguity for a pretwisted beam or plate. The regularity of modes was found for non-zero twist angle.

Sreenivasamurthy and Ramamurti [2] performed the modal analysis of a pre-twisted tapered blade fixed on the periphery of a rotating hub using finite element (FE) techniques considering certain parameters like pre-twist angle, skew angle, skew angle, disc radius, taper angle and disc radius. The effect of disc radius on frequency parameters on ratating pre-twisted and tapered cantilever blades were presented. Triangular shell element was employed to model the blade and mass and stiffness matrix were derived using Lagrange's equation to the energy expression.

Kumar and Srivastava [3] analyzed the FPF of laminated stiffened plates using a stiffened plate element subjected to uniformly distributed load and sinusoidal load, considering various well-known first –ply failure criteria. Some parametric studies were made for I section and hat section with fibre angles ranging from 15°to 75°.

Leissa et al. [4] studied vibrational behavior, displacement and mode shape of blades both rotating and nonrotating with camber using shallow shell theory and Ritz method. The effect of variable twist angle, thickness ratio and setting angle on frequency and mode shape were presented for assuming a blade model having both twist and camber.

Gu et al. [5] presented a new vibration model of cantilever pretwisted rotating blade with initial exponential type geometric imperfection using shallow shell theory. The effect of Coroilis force and centrifugal force was considered for the homogeneous and isotropic blade. Using Rayleigh-Ritz method and continuous algebraic polynomial function natural frequency and mode shape were computed. Different parameters like geometry, imperfection size and location, degree of imperfection, twist angle and rotational speed were considered to study vibration behavior.

Carnegie et al. [6] constructed a test rig to test the vibration characteristics of turbine blade at high (20,000 rpm) and low rotational speed. The dynamic behavior of turbine blade was predicted considering different parameters such as amplitude, frequency and stress is considered separately or together with to predict failure.

Dokainish and Rawtani [7] developed a FE model for a cantilever plate attached on the circumference of a rotating disc to find natural frequencies and mode shapes. It was assumed that plane of the plate makes any arbitrary angle with the plane of the disc. The centrifugal force was divided in two components, one in plane of the plate and another perpendicular to the plate. The stresses produced in the mid surface of the plate were obtained which cause the increase in bending stiffness of the plate. The effect of aspect ratio, rotational speed, disc radius and setting angle was the vital parameters to find the vibration behavior.

Gupta and Rao [8] presented torsional vibration characteristics of a thin cantilever plate considering shallow shell theory and displacement fields were employed to determined potential and kinetic energies of vibration. Hamilton's principle was used to reduce the problem in fourth-order differential equation, which was solved to obtain first four modes of torsional vibration. Plates with different aspect ratios and pretwist angles were taken for the analysis.

Frequencies and mode shapes of a thin rotating cantilever plate were presented by Henry and Lalanne[9]. The structure was discretized using triangular elements with three nodes, then mass and stiffness matrices were calculated using area co-ordinate. First initial stresses due to rotation were calculated and then frequencies and modes were determined using iterative technique.

Kielb et al. [10] presented vibration characteristics of pretwisted cantilever plates using FEM, shell theory and beam theory. Vital parameters like pretwist angle, aspect ratio and thickness ratio were considered for the analysis. They found that first bending frequency decreases for the short specimen whereas it remains constant for long specimen and first torsion frequency increases significantly for all configurations.

Li and Cheng [11] developed a model of rotating variable thickness pretwisted blade with elastic constraints using shallow shell theory for free vibration analysis. The effect of Corilis and centrifugal force due to rotation were taken into account in the formulation. Based on Lagrange equation of motion, natural frequencies and modes were solved. Parameters like thickness to taper ratio, pretwist angle and rotational speed were considered for the analysis.

Cao et al. [12] analysed the vibration behaviour of a pre-twisted rotating cantilever sandwich blade with thermal barrier coatings (TBC). The von Karman plate theory and FSDT were employed to derive the energy equation. The Chebyshev-Ritz method was utilized to get the frequency of the rotating TBC blade. The finite-element method (FEM) was employed to relate and confirm the results from the Chebyshev-Ritz method for static frequency and modal analysis. The results were analyzed in detail considering the effect of some parameters like thickness of the TBC layer, the working temperature, and the pre-twisted and pre-set angle.

Sinha and Turner [13] derived the partial differential equation of motion for a thin rotating cantilever pretwisted blade using shallow shell theory to study vibration behaviour. The derived equation of motion was used to derive the free vibration of a distinctive turbo-machinery airfoil blade by assuming it plate of an equivalent rectangular cross-section subjected to a centrifugal force field. The derivation reflects both the stress-stiffening and stress-softening effects due to centrifugal forces on the rotating airfoil. The partial differential equation was transformed into a matrix-eigenvalue form employing Rayleigh–Ritz technique.

Sreenivasamurthy and Ramamurti [14] developed a FE model to predict vibration characteristics of rotating pretwisted tapered cantilever plate. The plate was assumed as an assemblage of three noded shell element having six degrees of freedom per node. The eigenvalues of the model has been solved by using a simultaneous iteration technique. Frequencies were found by considering different parameters like pretwist angle, taper angle, skew angle and disc radius.

Vadiraja and Sahasrabudhe [15] made a vibrational analysis of rotating pretwisted thin walled composite beam with embedded macro fiber composite (MFC) actuators and sensors using HSDT. The governing equation was derived from Hamilton's principle and solved by using Galerkin's method. They found that gyroscopic coupling between lagging-extension motions could not be ignored in the investigation because it was important. Properties of vibration suppression using MFC actuators and sensors were emphasized.

1.2.2 Laminated Beams, Plates and Shells

The vibrational behavior of pre-twisted multi-layered composite cantilever plates was studied by Qatu and Wang [16] utilizing the Ritz technique and thin-shell theory. The effect of twist angle, fiber orientation angle and thickness ratio on natural frequency and mode shape were studied for three layer graphite-epoxy and E-glass epoxy angle-ply composite plates were studied.

McGee and Chu [17] focused on the 3-D continuum vibration analysis of rotating multi-layered composite blades. A mathematical model was developed using Ritz method to minimize the dynamic energies with displacements which satisfied the displacements were zero at blade root. Numerical convergence study satisfy the validity of present model. Numerical results presented the effect of aspect ratio, chord radio, thickness ratio, variable thickness distribution, fiber orientation angle, pretwist angle and angular velocity on vibration characteristics. The effect of Coriolis acceleration also include in the study.

Reddy and Liu [18] developed a higher-order shear deformation theory (HSDT) to obtain the exact solutions for bending and vibration analysis of laminated composite cylindrical and spherical shells for simply supported boundary condition which was modification of Sander's theory and can take parabolic distribution of transverse shear strains throughout the thickness.

Belarbi et al. [19] developed a two dimensional isoparametric finite element model for bending analysis of sandwich thin and thick plates based on layerwise approach. Using first order shear deformation theory the face sheet was modeled and utilizing higher order shear deformation theory the core was modelled. The accuracy and convergence of the model were in good agreement with

existing literature. They have been examined, for symmetric/unsymmetric composite laminated, sandwich and skew plates to test the performance and convergence of the existing FE model.

Belarbi et al. [20] established a FE model using higher order shear deformation theory for static analysis of laminated composite and sandwich plates. For the analysis of natural frequency laminated composite plates and sandwich plates were considered with various material mixtures, aspect ratios, boundary conditions, number of layers and geometry and ply orientations angel.

In another study, Belarbi et al. [21] developed an efficient eight-node quadrilateral element to study the vibration of multi-layer sandwich plates with arbitrary boundary conditions. In this analysis an eight-node serendipity quadrilateral element was selected based on layerwise model to predict accurately the natural frequencies of laminated sandwich plates. In the analysis effect of different parameters were considered like modular ratio, aspect ratios, core-to-face thickness ratio, boundary conditions, skew angle, number of layers, geometry and ply orientations.

Caliri et al. [22] also implemented a new elastic solution technique for thick laminated composites and sandwich using a generalized unified FE formulation. A quadrilateral four-node element was implemented for the analysis. Accuracy and convergence rate of the formulation was carried out.

Planninc et al. [23] developed a computational procedure using strain based FEM for non-linear analysis of composite timber with interlayer slips. Attention was given on load bearing capacity of two-layered beams. It was found that the crucial parameter was the nonlinear timber constitutive law which was significantly influenced by condition of stress and strain state and mainly the ultimate load of the timber composite beam.

Chen and Li [24] developed a dynamic model of pretwisted rotating laminated composite blade using shallow shell theory to investigate the vibration behaviour considering Coriolis and centrifugal forces due to rotation. The frequencies and mode shapes were obtained by using Rayleigh-Ritz and continuous algebraic polynomial functions. The effects of pre-twisted angle,

stagger angle, aspect ratio, rotational speed and hub radius on modal characteristics of the blade was conducted.

Pan et al. [25] modeled a vibration behaviour with large amplitude of pretwisted carbon nanotube reinforced composites (CNTRC). Based on differential geometry the shell model was made. The von Karman strains were employed to capture the geometrically non-linear behavior of blade and Ritz method was used to solve the problem. The model was studied on the large amplitude vibration with variation of different parameters.

Xiang et al. [26] studied the vibration characteristics of rotating pretwisted laminated functionally graded CNTs reinforced composite (FG-CNTRC) shallow conical shells using FSDT. Governing equations of the rotating pretwisted conical shell was derived and solved by kp-Ritz method. Comprehensive parametric studies were performed considering the CNT configuration, pre-twisted angle and stacking sequence which plays an important role on vibration characteristics of rotating FG-CNTRC blades.

Zhao et al. [27] analyzed analytically the free vibration behaviour FG pretwisted blade-shaft reinforced with graphene nanaoplatelets (GPLs). The material properties of blade and shaft were anticipated to fluctuate constantly along their thickness and radius directions and were estimated by Halpin-Tsai micromechanics model and rule of mixture. With the background of Rayleigh theory and Euler-Bernoulli beam theory governing equations were obtained using Lagrange's equation. The effects of GPL weight fraction, distribution pattern, geometry and dimensions of the blade length, pre-twist angle, the shaft length and rotational speed were included in parametric study. They found that improvement in dynamic performance due to presence graphene in shaft and blade material.

Zhang et al. [28] examined the saturation phenomena and nonlinear resonances due to subsonic air flow of rotating composite cantilever blade. The blade was assumed to be a rectangular plate which was clamped on the rigid disk with the pretwisted and preset angles. The governing equation

derived from third order shear deformation plate theory, von-Karman nonlinear geometry and Hamilton's principle. Chebyshev-Ritz technique was utilize to find the natural frequencies.

Chen et al. [29] analyzed the vibration behaviour of rotating pretwisted FG sandwich blades exposed to steady state thermal environment. The FG sandwich blades were composed of single metallic core and two FG surfaces and its material properties were temperature dependent. A two stage solving method was presented which was based on first-shear shell deformation theory (FSDST) and modified Fourier spectral approach (MFSA). They found that important effects of temperature rise, rotating speed, layer thickness ratio, volume fraction, pretwist and presetting angle on the vibration response of the rotating blades.

Chen et al. [30] studied free vibration of rotating pretwisted FG blades with a quasi-3D dynamic model based on three dimensional elasticity shell theory. The eigenvalue formulation were derived utilizing Hamilton's principle on the base of the kinetic, strain, centrifugal potential and boundary potential energy. Parametric studies were then performed to investigate the effect of centrifugal stress, rotational speed, volume fraction and pre-twisted angle on the vibration characteristics.

Hajianmaleki and Qatu [31] reviewed the vibration characteristics of straight and curved composite beams related to engineering applications. They emphasized on the beam theory (thin, thick & layerwise), different solving methods (FEM, differential transform and others), experimental methods and effect of complex geometry and materials properties.

Kumari [32] investigated the free vibration behaviour of rotating plate type composite blades using finite element method. The formulation was derived using FSDT considering the effect of centrifugal force. Parameters like rotational speed, setting angle, twist angle, fibre orientation angle and variable thickness of panels were used to study the vibration characteristics of pretwisted cantilever blade.

Nabi and Ganesan [33] compared vibration of metal matrix pretwisted composite blades using beam and plate theories. In beam analysis a beam element with eight degrees of freedom was

selected with torsion-flexure, flexure-flexure and shear-flexure couplings. A triangular plate element was employed for the composite material to model the beam as a plate structure. A parametric investigation was done considering twist angle, fiber orientation angle and taper ratio.

Zhang et al. [34] investigated vibration characteristics of matrix cracked pretwisted hybrid composite blades having CNTRC layers. They studied the change of vibration characteristics due to degradation of stiffness caused by matrix cracks. The degraded stiffness of matrix cracked composite was modeled using self-consistent model (SCM) micromechanical framework. A shell model was proposed based on differential geometry. The effect of transverse shear deformation and rotary inertia were considered with the using of FSDT which can adopt the kinematics of blade.

1.2.3 Finite Element Modeling of Composite Materials

Teotia and Soni [35] presented a complex and nonlinear damage behavior model based on Finite Element Method (FEM) of composites. The article signifies applications of FE methodology in failure prediction and analysis of laminated glasses. Development of modelling and different theories like single layer, layerwise and zig-zag models were represented to highlights basic ideas for modelling. Suggested FE models were helpful guides for researchers and engineers to fabricate laminated composites.

Bathe [36] presented elaborately physical and mathematical characteristics of Finite Element procedures which are useful for FE analysis.

Gim [37] modelled a plane finite element of delaminated composite plate based on based on lamination theory which can incorporate the effect of transverse shear deformation. Single layer plate element was used to model the undelaminated region whereas the delaminated region was modelled using two layer plate elements whose interface contains delamination. A multipoint constrain algorithm was developed to incorporate deformation and equilibrium of resultant forces and moments at delaminated crack tip.

Reddy and Liu [38] developed a HSDT for laminated shells which was modification of Sanders' theory and can incorporate parabolic distribution of the transverse shear strain along the thickness. The Navier-type exact solution were presented for bending and natural vibration of spherical and cylindrical shells under simply supported boundary condition.

Alnefaie [39] developed a three dimensional FE model to investgate dynamics of fiber-reinforced delaminated composite plates. For different dimensions and delamination characteristics natural frequencies and modal displacements were computed. The above study also indicate a method for detecting delamination in composite plates.

Beheshti-Aval and Lezgy-Nazargah [40] developed FE model of beams with distributed piezoelectric sensors and actuators. For modelling of mechanical displacements along the thickness, a sinus model was employed which satisfy continuity condition of transverse shear stresses and boundary condition on the upper and lower surfaces of the beam layers.

Chung and Sotelino [41] investigated flexural behavior of composite steel girder bridges using FE modelling techniques Different modelling technique were studied and selection of element was discussed. The accuracy of each model was verified with the experimental results and with the available literatures. Finally the efficiency of each model were presented.

Gama and Gillespie [42] investigated damage progress and penetration of thick section composites utilizing explicit FE investigation. A 3D model of impact on thick section of composites were developed. The investigation included beginning and progressive damage through impact and penetration for various impact velocities.

Khalili et al. [43] studied FE modelling of composite laminates and shell structures subjected to low velocity impact. In this study, different example were considered with different conditions and rationality of the present modeling procedure was investigated. In every instance, results were compared with available experimental results, and then best process was suggested as standard technique for low-velocity impact modeling of composite shells.

Mitchell et al. [44] investigated by developing two FE models of cured fabric-reinforced composites. In beam-shell model the beam elements represents the fiber and matrix was represented by shell element. In double-orthotropic shell model, two shells, each express a set of fibers, were superimposed.

Peeters et al. [45] developed a detailed FE model of composite wind turbine blades. The novel approach was the blade consist of parametric predefined blocks which allows the turbine blade models consist of shell elements, solid elements or combination of both. By partitioning outer mold layer, offsetting the surfaces and accurate element-wise material orientations a high level and detailed model was developed.

Reddy and Robbins Jr. [46] reviewed equivalent-single-layer and layerwise laminated plate theories and their FE models. A variable displacement FE formulation and mesh superposition method were presented. A simultaneous multiple model method which was based on kinematic theory and mesh superposition methods were also presented. The objective of the said model was to validate the best suitable math model with each subregion based on physical properties.

Shi et al. [47] discussed FE modeling of composite beams and plates based on higher order shear deformation theories. They described selection of proper strain expressions to formulate accurate elements under the same nodal degrees of freedom. Numerical examples were presented to describe that existing composite beam element was perfect than the higher order beam elements but using a different expression for bending strain.

Stemple and Lee [48] developed a FE model for large deflection which can take the wrapping effect of composite beams. The existing derivation could be utilized for FE model having combined bending, torsional and extensional behavior of composite rotor blade. The said method could model shallow to moderately thick walled composite beams with arbitary cross section.

1.2.4 Delamination Modeling

Some preliminary works both analytically and experimentally on vibration study of delaminated beams were carried out by Shen and Grady [49]. A generalized variational principal employed to derive the equation of motion considering boundary condition and delamination of arbitrary size and location.

Krawczuk et al. [50] modeled cracked beam, delaminated beam and delaminated plate using FEM and analyses the dynamic characteristics of those composite materials. Numerical calculations were presented considering some vital parameters like position and depth of crack or length and position of delamination and their effect on natural frequencies.

Tracy and Pardoen [51] experimentally demonstrate the effect of delamination on natural frequency and the results were in good agreement with the result obtained using FEM for simply supported graphite epoxy beam specimen.

Gim [52] developed a plane FE model based on lamination theory of plates which can include transverse shear deformation. The undelaminated zone was modeled using a single layer plate elements and the delaminated area was modelled using two layer plate elements and its interface contains delamination. A multipoint constraint algorithm has been developed to incorporate deformation and resultant force and moments at delamination crack tip and strain energy release rate could be estimated using the plate elements.

Zak et al. [53] using various approaches (i.e., analytical, experimental and FEM) investigated the vibration characteristics of a composite plate with single and closing delamination. Contact force between the layers were modelled between node to node contact models. A harmonic force was applied in the plate and the vibration response were analysed using Fast Fourier Transformation (FFT). The influence of delamination length and position on vibration response were presented.

Bandyopadhyay and Karmakar [54] and Bandyopadhyay et al. [55, 56] formulated an FE procedure in conjunction with Mindlin's plate theory to predict the bending, dynamic responses

vibration characteristics of rotating delaminated composite conical blades with pre-twist in hot and moist environments. The effect of rotary inertia and transverse shear deformation included in the FEM analysis.

Singha et al. [57] studied the free vibration of multiple debonded rotating pre-twisted composite sandwich conical shells exposed to hygrothermal environments. For existing analysis an eight noded isoparametric shell element was employed with five degrees of freedom in each node. The effects of thickness ratio core to face sheets, twist angle and rotational speed were included in the analysis.

Parhi et al. [58] employed the displacement type FE method to examine the nonlinear free vibration of composite conical shells having clusters of delamination in hot and moist environments. The panel has been discretized with an eight noded isoparametric shell element to maintain C° continuity mathematical complexity of C^1 continuity was avoided. Effect of different parameters like fiber orientation angle, support conditions, thickness ratios, aspect ratios, curvature ratios and material properties were considered for the linear and nonlinear free vibration response.

Rao and Shu [59] developed a mathematical model to investigate the buckling behaviour of double layered beam with single delamination under simply supported and clamped boundary condition. Critical buckling loads were obtained and a new parameter effective slenderness ratio introduced for perceptive of local, mixed and global buckling phenomenon.

Wan-Lee Yin [60] investigated the effect of cylindrical buckling on symmetric composite structures having clamped boundary condition with mid plane delamination. The energy dissipation rate was observed at the delamination zone to define the stability characteristics of the flaw progress. Postbucling deformations were drastically decreases by bending and streaching coupling.

Yin et al. [61] computed the ultimate load capacity of axially loaded beam and plate with delamination located symmetrically at an arbitrary depth. The energy release rate allied with

delaminaion growth were computed for different delamination length and axial load.

Shu [62] developed a generalized Finite Element model for composite plate considering weak interfacial bonding condition i.e. perfect bonding, weak bonding and local delamination. The FE model created based on Smeared laminate theory and number of displacement parameters were fixed.

Paolozzi and Peroni [63] developed finite element models to investigate the effect of delamination on frequency shift. A relationship between the peaks of the frequency shift vs order of the mode, and the addition of the delamination were presented.

Tracy [64] et al. evaluated numerically and experimentally the impact of delamination length on frequency for simply supported beam. Modal analysis was carried out to investigate the effect of delamination length on first four frequencies.

Tenek et al. [65] investigated using FEM and three dimensional theory of linear elasticity for cantilever laminated plate and found that on increase of size and number of delamination natural frequency reduces.

Yin et al. [66] performed an analytically buckling and post-buckling analysis of plate and beam having delamination located symmetrically at an arbitrary depth.

Chen and Qiao [67] presented an analytical model to investigate the delamination buckling of beam/column with delamination along the width considering transverse and shear deformation. To establish the continuity condition between the two substrates in the intact areas a deformable interface was employed in the existing model which accounts for global deformations of the intact region in the delaminated composites. It was capable for taking the buckling mode shape, transitions from the global to global–local coexistent and to local buckling. Parametric studies were carried out to observe the effects of various parameters on the critical buckling load.

Wang and Zhang [68] developed a computational model for buckling, post-buckling and delamination propagation in debonded composite laminates. The initial buckling load were often much lesser in comparison the global buckling load. The delamination evolution has major influence on the post-buckling characteristics and strength of the composites.

Parlapalli et al. [69] represented an analytical model to predict buckling load of a composite beam with enclosed delaminations by using Euler–Bernoulli beam and classical lamination theory. They also performed linear and non-linear FE Analysis to validate the model. For upper bounds S-shaped buckling modes have higher domination compared with single hump buckling mode, whereas, for lower bounds of the buckling load, mixed or local buckling modes were found.

1.2.5 Composite Cylindrical and Conical Shell

Parhi et al. [70] employed the displacement type FE technique to investigate the nonlinear free vibration of conical composite shells having clusters of delaminations in hot and moist environments. The governing equation of the vibrated structure was obtained from the principle of virtual displacement. The model was discretized using eight-nodedisoparametric element and a delamination model was employed which could incorporate single and cluster of delamination.
To explain vibration problem of FG-CNTRC Qin et al. [71] presented a unified Fourier series solution for cylindrical shells, conical shells and annular plates subjected to different boundary conditions. FSDT and virtual boundary method were employed to obtain energy expressions of FG-CNTRC structures.

Safarpour et al. [72] analyzed static and free vibration of FG graphene-platelets reinforced composite (FG-GPLRC) conical shells, cylindrical shells and annular plates with different boundary conditions using theory of elasticity. A semi-analytical solution was proposed employing differential quadrature method (DQM) to solve the existing formulation. The effect of GPLs weight fraction, patterns of GPLs distribution through the thickness direction, semi vertex angle, length to radius ratio on natural frequencies and bending features were investigated.

Maji et al. [73] computed free vibration of functionally graded carbon nanotubes reinforced composites (FG-CNTRC) pretwisted conical shells under thermal environment. An eight nodedisoparametric shell element and FSDT was used to model the derivation. The dynamic equilibrium equation was obtained from Lagrange's equation of motion at modest rotational speed and Coriolis effect was neglected. The effect of twist angle, aspect ratio, rotational speed and temperature on vibration was investigated.

Singha et al. [74] investigated free vibration characteristics of rotating pretwisted sandwich FG-CNTRC conical shells using FE method under thermal environments. In the shell thickness direction the carbon nanotubes were distributed homogeneously. The material properties of the FG-CNTRC face sheets and core were temperature dependent and estimated using micromechanics model. The thin conical shell was modeled using FEM within the structure of HSDT.

Patel et al. [75] studied the vibrational characteristics of some structural elements such as cylindrical, conical and joined conical-cylindrical composite shells. A two-noded shear flexible axi-symmetric shell element was employed for the FE investigation. The in-plane and effect of rotary inertia were included in the existing formulation. The model developed was used to obtain natural frequencies and mode shape of cross-ply composites.

He et al. [76] investigated free vibration behaviour of laminated composite conical shells, cylindrical shells and annular plates with arbitrary boundary conditions by adopting power series method. The governing equation of the shell structure was established by using FSDT. The effect of geometric parameters and material constraints on vibration characteristics were investigated.

Kamaloo et al. [77] investigated the non-linear free vibration of laminated composite conical shells having circumferential delamination. The governing equation of the shell structure was derived using energy method. Using the Galerkin method the non-linear partial differential equations were reduced to coupled ordinary differential equations. The effect of delamination, delamination length, conical shell geometry and material properties on vibration were investigated.

Karmakar et al. [78] investigated the effect of delamination, delamination length and stacking sequence on free vibration of graphite epoxy composite pretwisted shallow cylindrical shells. An eight-noded isoparametric shell element was employed which was compatible with deformation and equilibrium of resultant forces and moments. A multipoint constraint algorithm was developed to model the delamination. The non-dimensional natural frequencies were obtained for angle-ply and cross-ply orientation of long, intermediate and short cylindrical shells defined by Aas-Jakobsen's parameters with definite pretwist.

Karmakar and Kishimoto [79] developed a FE model to investigate the vibration response of graphite epoxy pretwisted delaminated rotating shells. The dynamic equilibrium equation at moderate rotational speed was derived from Lagrange equation of motion where Coriolis effect was neglected. An eight noded isoparametric element was considered based on Mindlin's theory which can incorporate the effect of rotary inertia and transverse shear deformation. The effect of delamination, fibre orientation angle, pretwist angle and rotational speed on vibration characteristics were investigated.

Maji and Singh [80] studied free vibration response of 3D braided rotating composite cylindrical shells utilizing third order shear deformation theory. The material properties of composites were found based on volume averaging method. In the eight-noded isoparametric 3D-finite element formulation twelve degrees of freedom per node was applied. At modest rotational speed the dynamic equilibrium equation was obtained from Lagrange's equation of motion and the Coriolis effect was ignored.

Mohammadrezazadeh and Jafari [81] presented non-linear vibration analysis of laminated composite angle-ply conical and cylindrical shells. The shells were modelled considering rotary inertia and shear deformation whereas the geometrical nonlinearity was modeled using von Karman approach. The influence of different parameters such as layers' angle, number of layers, semi- vertex angle, length, radius was considered on vibration characteristics.

Rout et al. [82] presented free vibration characteristics of pretwisted delaminated shallow cylindrical shells using FEM. At modest rotational speed the dynamic equilibrium equation was obtained from Lagrange's equation of motion and the Coriolis effect was ignored. The multipoint constraint algorithm was employed to model the delamination at desired location. Vibration response were obtained for cantilevered long, intermediate and short shells based on Aas-Jakobsen's criteria.

Rout et al. [83] analyzed the free vibration response of pretwisted delaminated stiffened composite cylindrical shells. To incorporate transverse shear deformation and rotary inertia an eight-noded isoparametric shell element was employed and for stiffener a three noded beam element was employed. A multipoint constraint algorithm was employed which account for deformation, resultant forces and moments at delamination crack tip. Utilizing Lagrange's equation of motion, the dynamic equilibrium equation was obtained for modest rotational speed and the Coriolis effect was ignored. Applying QR iteration algorithm eigenvalue problem was evaluated. The effect of delamination, fiber orientation, twist angle, stiffener depth-to-shell thickness ratio, and rotational speed on vibration response was computed.

Sobhani et al. [84] studied the free vibration response of sandwich composite joined conical-cylindrical- conical shells utilizing FSDT. The sandwich shell was made of two face sheets and one core. Each layers were reinforced with FG- CNTs and FG graphene nanoplatelets (FG-GNPs). The equivalent mechanical properties of each layer was obtained by utilizing rule of mixture. The Hamilton's principle was used to derive governing partial differential equation of joined shells and solved by Generalized Differential Quadrature Method (GDQM).

Wagner et al. [85] presented the stability failure of the axially loaded cylindrical shell which was considered as the last unresolved classical stability problem. Perturbation approaches for the design of axially loaded cylindrical and conical shells were presented.

1.2.6 Composite Shallow Shell

Lim et al. [86] to demonstrate the effects of stacking sequence on the vibrational behavior of non-rotating pre-twisted cantilever E-glass/epoxy composite conical shells. Energy principle was used to compute eigen-value equation and a flexible global function was developed to account geometric boundary condition.

Karimiasl et al. [87] investigated the post-buckling behaviour of doubly curved composite shells in hygrothermal environment using multiple scale perturbation method. The displacement-strain were obtained by employing third order shear deformation theory and von-Karman non-linear shell theory. The governing equation was derived from Hamilton's principle. The effect of different parameters such as volume fraction, temperature raise, aspect and curvature ratio was included in this investigation.

Beakou and Touratier [88] presented a new four node C^1 rectangular element generated from standard interpolation. The element allows the continuity conditions for displacement and stresses at the interfaces between the laminated shell and boundary condition at upper and lower surface of shell. The element was investigated on standard problems and compared with exact three dimensional and analytical solutions for multilayered plates and shells in statics, vibration and buckling.

Biswal et al. [89] investigated both numerically and experimentally the free vibration response of laminated composite shells in hygrothermal environments. A doubly curved shell model was created based on FSDT and a quadratic eight-noded isoparametric element was used for the analysis. Parametric study was carried out by changing curvature ratios, number of layers, lamination sequence at different hygrothermal situation with different boundary conditions. Numerical and experimental outcomes indicate that there was a decrease in natural frequency of laminated shells on rise of temperature and moisture concentration.

Sciuva et al. [90] presented the effect of damage interface on load carrying capacity of multilayered composite shallow shells using non-linear third order theory which accounts for arbitrary displacement of tangential displacements through the shell thickness and continuity conditions of

transverse shear stresses at the layer interfaces. The pertinent equations of motions and variationally consistent boundary conditions were derived from virtual work principle. A numerical assessment of the existing model was carried out and non-linear response under transverse loading were presented.

Duc et al. [91] investigated dynamic response and vibration of doubly curved shallow shell with auxetic honeycombs core on elastic foundations subjected to blast and damping loads. The core was made of three layers with top and bottom skin were isotropic aluminium material. Using the FSDT with the geometrical nonlinearity in von Karman and using Airy stress functions, Galerkin and the fourth-order Runge-Kutta method, the resulting equations were evaluated to get expressions for nonlinear equations.

Guo et al. [92] investigated non-linear large amplitude and multi-mode response of shallow composite shell at elevated temperature with rectangular planform using FEM. The system of equation in structural degrees of freedom were changed to modal coordinates and stiffness matrices were changed into non-linear modal stiffness matrices. A numerical integration was performed to determine random response. The natural frequencies of the vibration about thermally buckled position were studied.

Hirwani et al. [93] presented non-linear transient response of delaminated curved composite shell under different kind of mechanical loading using FEM. The nonlinear transient response were calculated using Newmark's time integration scheme together with direct iterative method and finite element steps. The effect of size and location of delamination, aspect ratio, curvature ratio, modular ratio and shell configuration on non-linear transient response were presented.

Fatt and Sirivolu [94] developed an analytical model for blast response prediction of doubly curved composite sandwich thin shell with PVC foam core. The core made of PVC foam was modeled with isotropic and transversely isotropic elastic–plastic properties employing Donnell's nonlinear shallow shell model. For sandwich shell with large curvature, blast resistance was lower for transversely isotropic core rather than isotropic core.

Huang and Qiao [95] evaluated nonlinear stability response of rotationally-restrained stiffened laminated composite curved shells with imperfection subjected to shear and compression loading. The Galerkin method was employed to solve non-linear governing equation derived in present semi-analytical method. The effect of imperfection, load ratio, curvature and distribution of stiffener on non-linear response of stiffened shell were studied.

Kurtaran [96] performed geometrically non-linear transient analysis of moderately thick shallow laminated composite shells using generalized differential quadrature method. FSDT was employed to consider the effect transverse shear and Von-Karman nonlinear strain-displacement equation was incorporate geometric nonlinearities. The equation of motion was derived from Virtual work principle and time integration was carried out using using Newmark average acceleration scheme.

Li et al. [97] presented a Jacobi-Ritz method for analysis of laminated composite shallow shells with arbitrary boundary conditions. The theoretical model was developed using FSDT and displacement function in each segment of the shell was denoted by Jacobi polynomials along the length and width orientation. For solution procedure the Raleigh-Ritz method on the basis of energy function was utilized.

Matsunaga [98] investigated natural frequencies and buckling stresses of cross ply laminated composite thin shells by considering the effect of transverse shear and normal deformation, and rotary inertia. A set of dynamic equations were derived through Hamilton's principle. Higher order deformation theories with thickness change and rotary inertia were used to resolve the vibration and stability of laminated shells.

Nguyen et al. [99] investigated non-linear dynamic and vibration response of FG-CNTRC doubly curved thin shells exposed to blast load and temperature. The shallow shells were reinforced with single-walled carbon nanotubes (SWCNTs) which vary as a linear functions of the shell thickness. The material properties of the shells were temperature dependent and predicted by the rule of mixture. By using higher order shear theory, Galerkin approach, fourth-order Runge–Kutta method

and the Airy stress function, nonlinear dynamic behaviour and natural frequency of imperfect FG-CNTRC shells were determined.

Singh and Panda [100] analysed large amplitude free vibration response of doubly curved composite shallow shells using non-linear FEM. The model was derive using Green Lagrange type geometric non-linearity in the framework of HSDT. The governing equation was derived using Hamilton's principle and solved numerically by direct iterative method. The effect of orthotropicity ratios, stacking sequences, thickness ratios, amplitude ratios, symmetric and unsymmetrical lamination and support conditions were included in the study.

Qatu and Leissa [101] analyzed free vibration of laminated plates and shallow shells with rectangular planform using Ritz method with algebraic polynomial displacement function. The effect of various parameters such as material, stacking sequence and number of layers on frequencies were studied. The first ten frequencies of different curvatures such as spherical, circular cylindrical, hyperbolic paraboloidal and flat plate were presented.

1.2.7 First-Ply Failure

Said and Hallett [102] presented damage initiation in composite laminates. The said method associate the meso-scale models to produce complete idea of damage beginning under all possible combinations of bi-axial loading. The 2-D biaxial failure envelope were then combined with the composites physical behavior and surface compatibility conditions to generate 3D failure manifolds using Gauss surface equation.

Zimmermann and Wang [103] studied the failure of a laminated composite shell was a highly complex phenomenon owing to complex shell geometries and the associated shell dynamics under different loading conditions. The composite laminates were inherently weak in transverse shear, and the actual failure occurs owing to a complex interaction between different failure modes.

Kam et al. [104] analyzed the deformation and FPF of thin laminated composite plates using nonlinear FEM utilizing the von Karman-Mindlin plate theory and the principle of minimum total

potential energy. The load displacement curves of a number of laminated composite plates were determined using proposed FEM. The correctness of the FE outcomes were validated with the existing experimental results.

Reddy and Pandey [105] formulated an FE procedure to investigate the FPF of layered composite plates based on FSDT and a tensor polynomial failure criterion which contains maximum stress, maximum strain, Tsai-Hill, Tsai-Wu and Hoffman as special case. Composite laminates subjected to in plane or bending loads were considered for FPF.

Kam and Lai [106] predicted the FPF strength of laminated composite plates through experimental and theoretical approaches. An acoustic emission technique was used to compute the energy release rate during the failure. The first-ply failure loads were then computed from energy vs load diagram which was made on the basis of energy emission. Using layerwise linear displacement theory and Tsai-Wu failure criteria a FE analysis was done to predict the FPF loads.

Prusty et al. [107] focused on the damage initiation in composite panels based on various failure criteria utilizing FEM and FSDT. An eight noded isoparametric shell element was employed for the FE analysis. Failure of the weakest ply under transverse load was investigated using different failure theories. Different plates and shells with different lamination schemes was selected for the analysis.

Błachut [108] numerically studied the bifurcation buckling, and the FPF of CFRP filament wound toroidal shells having closed circular and arbitrary cross-sections. The influence of boundary conditions, variable wall thickness, stacking sequence and initial imperfection on load carrying capacity was investigated.

Ramtekkar et al. [109] developed a 3-D layer-wise mixed FE model to study the FPF of composite plates and concluded that the 3-D failure theories yield roughly the same failure loads as the 2-D ones. For calculation of stress and strain mechanics of advanced materials and structures was used. FPF was estimated by using various theories like maximum stress, maximum strain, Tsai-Wu,

Tsai-Hill and Hoffman. FE results were computed for angle-ply, cross-ply, symmetric, anti-symmetric and thin-thick plates.

Bakshi and Chakravorty [110] focused on the FPF of thin laminated composite conoidal shells using FEM. Simply supported thin shell with uniformly distributed load were considered for the investigation. Failure loads were computed using some established failure theories. Apart from failure loads, failure location and failure modes were also studied.

Bakshi and Chakravorty [111] investigated the FPF of laminated composite cylindrical shells using geometrically nonlinear approach. FE investigation were carried out using eight noded doubly curved elements along with modified Sander's first approximation for shallow shells and von Karman nonlinear strains were included. Failure loads, failure modes and failure locations were reported in the present study.

Romanowicz [112] determined the FPF strengths of cross-ply laminates under compression, tension, and shear using computational micromechanics. The random distribution of fibers, fiber–matrix decohesion and matrix plastic deformations were considered in the simulations.

Kam et al. [113] analyzed the failure of composite wind blades subjected to quasi-static loads using geometrically nonlinear FEM and various failure theories to identify the buckling, debonding, and FPF of a blade by an incremental loading approach. The failure loads, failure locations and failure modes were determined to study the appropriateness of the failure criteria.

Karmakar and Sinha [114] estimated the FPF strengths of pre-twisted rotating laminated composite plates under centrally applied point loads utilizing FEM based on a nine-noded 3-D degenerated shell element. Effects of transverse shear deformation and rotary inertia were included and for moderate rotational speed Coriolis effect was neglected. Lagrange's equation of motion was employed to derive the dynamic equilibrium equation.

A combination of experimental and FE approaches was employed by Biswas and Ray [115] to

carry out the FPF analysis of hybrid composite laminates under transversely applied static loads. An eight noded quadratic isoparametric plate bending element based on higher order zigzag theory (HRZT) was formulated to evaluate the interlaminar stresses of multilayered composite laminates.

Gohari et al. [116] formulated an analytical approach to demonstrate the influence of thickness, aspect ratio, and fiber orientation on the FPF of unsymmetrical ellipsoidal composite shells subjected to internal pressure using linear interpolation technique. The experimental results was indicate that failure happened close to the shell's edge as predicted by analytical method.
Rao and Rao [117] determined the FPF loads of fiber metal laminate (FML) under uniformly distributed loads using FEM combined with classical laminated plate theory (CLPT). The failure loads and deformation of FMLs were studied in the form of dimensionless parameters, and their changes was investigated.

Mondal and Ramachandra [118] presented a layer-wise FE approach to analyze the effect of size and location of delamination, area of heating surface, and boundary conditions on the FPF load and buckling temperature of delaminated composite plates. Prebuckling stress distribution within the plate was computed by computing thermoelasticity problem because applied thermal loading was non-uniform. Thermal buckling temperature was evaluated by employing prebuckling stress distribution. Postbuckling behaviour of the plate was found by considering the von Karman type geometric nonlinearity.

Kumar et al. [119] implemented an efficient FEM within the framework of higher-order zigzag theory (HOZT) to explore the FPF load, location and failure index of layered composite and sandwich cylindrical shells. The two dimensional FE model satisfied the interlaminar shear stress continuity at layer interfaces and zero transverse shear stress at top and bottom of the shell. The parabolic shear stress deviation across the thickness of each layer was measured and shear deformation was perfectly modelled for composites and sandwich shells.

Anish et al. [120] used the improved HSDT kinematic conditions in the FE formulation to demonstrate the failure mode of composite sandwich plates. The proposed 2D improved HSDT

satisfied the interlaminar shear stress continuity at each layer and zero transverse shear stress condition at the top and bottom of the plate. The parabolic shear stress distribution was piecewise across the thickness of each layer so no shear correction factor was used. The tentative modes of failure was transverse matrix cracking, fiber breakage and inter-fiber shear failure of the matrix.

Ang et al. [121] presented an artificial neural network scheme to predict the FPF of laminated composite pipes subjected to multi-axial loads. The model was expected to predict the FPF loads under several biaxial stress ratios. The biaxial failure envelope was then explained by highlighting axial stress against hoop stress.

Mustafa et al. [122] examined the probabilistic FPF of composite plates employing the micromechanics for static failure (M-SaF) method. To compute the damage condition distinct failure criteria was considered.

Recently, the stochastic influences of the parameters like stacking sequence, lamina thickness, material properties and strengths on the FPF of laminated composite plates subjected to unidirectional static loading have been studied by Martinez and Bishay [123].

Saha et al. [124] presented a parametric study of the FPF of mid plane delaminated shallow conical shells. The dynamic equilibrium equation was obtained from Lagrange's equation of motion for modest rotational speed neglecting the Coriolis effect. The theoretical calculation was carried out based on Mindlin's theory and an eight noded isoparametric shell element was employed for FE model. Multipoint constraint algorithm was used to ensure the equilibrium of resultant forces and moments at delaminated crack tip. The first ply failure loads was evaluated considering various failure theories.

1.2.8 Impact Induced Failure Response

The pioneering investigation of impact on isotropic beam was carried out by Timoshenko & Young [125] and Sairam et al. [126] investigated the low velocity impact response of AA5083 alloy plate using FEA package by measuring the impact resistance in terms of depth of indentation. The

investigation was carried out for different orientation of the alloy plate with respect to horizontal datum. They found that impact resistance was dependend on the angle of inclination and is minimum when the inclination was 90°.

M. V. Shitikova [127] developed a mathematical model and carried out numerical calculations to predict impact resistance and indentation of a viscoelastic plate and compared with the experimental results.

Feli and Das [128] analysed the low velocity impact performance of piezoelectric plates using FEM. The plate kinematics was modelled using FSDT and governing equations were formulated utilizing Hamilton's principle and Maxwell's law and contact behaviour was modelled using Hertz's contact law. Parameters like volume fraction, slenderness ratios and in plane dimensions were considered to predict impact response for simply supported and clamped boundary condition.

The central impact response of simply supported composite plates under initial stress was studied by Sun and Chattopadhyay [129]. The contact force and dynamic response were found by resolving nonlinear integral equation. It was also found that greater initial stress result in smaller energy transfer from the striking mass to the plate.

Sun and Chen [130] investigated impact response of initially stresses composite laminates using FEM. The Newmark time integration algorithm was used to solve time dependent equation of the plate and impactor. The effect of impact velocity, initial stress, and mass and size of impactor on contact force, deflection and strain were included in the result.

Mortimer et al. [131] performed in plane and shear bending impact experiments on laminated angle ply and cross ply composite plates and compared the results with theoretical predictions. Results indicated that under given loading condition the lamination theory adequately predicts wave velocities and strains in composite plates.

E. H. Lee [132] developed an approximate solution for a beam impacted by a mass to find out energy distribution among the different modes of vibration. Solution using energy and momentum consideration was developed to give motions beam and mass resulting from the impact.

Shen et al. [133] represents a nonlinear study of low velocity impact response of graphene reinforced sandwich composite plates with functionally graded (FG) cores which enhances impact resistance and bending strength significantly. Parameters like thermal environments, FG configurations, strut radii, volume fractions, impact velocities were considered in FE simulation to predict bending, shear and axial deformation.

Song et al. [134] prepared a parametric approach to investigate the effect of temperature deviation, geometry, weight fraction, impactor radius and initial velocity of FG plates under simply supported boundary condition. The material properties were estimated from Halpin–Tsai model and Hertz contact law was used to predict contact forces.

He et al. [135] made a FE simulation of fiber reinforced composite laminates predict effects of material parameters, shape of impactor including flat, hemispherical, and conical under low and high velocity impact. It was found that amount of energy absorbed in damaged area and impactor displacement were maximum for conical impactor and minimum for flat impactor.

Ebrahimi et al. [136] represented a nonlinear FE simulation of laminated FG carbon nanotube reinforced composite (FG-CNTRC) plate under low-velocity impact using higher-order shear deformation theory (HSDT) and von Karman geometrical nonlinearity conventions in thermal atmosphere. The effect of temperature change, stacking sequence, distribution of carbon nano tubes, volume fraction, mass and the velocity of the impactor on CNTRC laminates were investigated thoroughly.

Ceyla and Şenel [137] made an experimental study of low velocity impact on E-glass/epoxy symmetric laminated plates for different stacking sequence under clamped boundary condition. It

was found that more energy required to damage the plate when two sides were clamped compared to all the four sides.

Ansari and Chakrabarti [138] investigated numerically and experimentally of Glass Fiber Reinforced Polymer (GFRP) plates under ballistic impact. The effect of plate thickness, projectile nose shapes and incidence velocity on residual velocity, contact force- energy absorption, ballistic limit, time histories, damage pattern and area in the composite plate were studied.

Chun and Lam [139] developed a numerical method to investigate low velocity impact response of composite plates using Hertzian contact law and Lagrange principle. The governing equations were decoupled according to the second-order terms by the method of principal transformation, and then solved numerically. The contact force, deformation, energy transferred and stresses were presented.

Hu [140] developed a generalized Finite Element model for composite plate considering weak interfacial bonding and local delamination and represented the transient response of composite laminates having multiple delamination subjected to low velocity impact by a spherical mass. The FE model was based on Mindlin plate theory and Hertzian indentation law was used to compute the impact force between the ball and the laminates. Modified Lagrange multiplier technique was used to deal with the dynamic contacts between delaminated layers.

Sekine et al. [141] investigated the impact response of partially delaminated composite plates by employing Hertzian contact law and Newmark algorithm and Karmakar et al. [142] analyzed centrally impacted transient response of delaminated pretwisted rotating shallow cylindrical shell under low velocity impact. The dynamic equilibrium equation was obtained from Lagrange equation of motion for modest rotational speed where Coriolis effect was negligible. For FE formulation an eight noded isoparametric element was selected based on Mindlin's theory, including rotary inertia and effects of transverse shear deformation.

Bandyopadhyay et al. [143] investigated the transient response of pretwisted delaminated conical shallow shell impacted by multiple impactors in hygrothermal environments. An eight noded shell

element was employed for the analysis based on Mindlin's theory. The dynamic equilibrium equation was obtained from Lagrange's equation of motion and Coriolis effect was neglected for modest rotational speed. A multipoint constraint algorithm was used to confirm the compatibility of deformation and equilibrium of forces and moments at delamination crack-tip.

Reis et al. [144] studied experimentally the effect of thickness on static compression and multiple impact response of laminated semi cylindrical shells and found impact damages were localized with the increase of thickness due to dissipation of energy at the interfaces.

Sharifi et al. [145] investigated the low velocity impact response of shallow laminated composite cylindrical shell using FEA package. The variation of stress and displacement along circumferential and radial directions were investigated and found that 90° along the circumferential and radial directions were critical point.

Rout et al. [146] made a FE model to investigate dynamic behaviour of twisted delaminated stiffened cylindrical shell under low velocity multiple impact. The contact forces were modelled with modified Hertzian contact law. Lagrange's equation of motion was used to formulate governing equations and solved by Newmark's algorithm to execute the analysis.

Coelho et al. [147] and Paramasivam and Johnson [148] performed experimental and FE analysis of low velocity axial impact of both anisogrid and unstiffened cylindrical shells made of composite materials. The results indicated that anisogrid structures have greater load carrying capacity than unstiffend shell under dynamic loading.

Parhi et al. [149] studied analytically free and forced vibration, first-ply failure due to low velocity impact of laminated composite plates, cylindrical and spherical shells using FSDT. Sander's shallow shell theory was employed for the analysis. To solve time dependent equations of the plate and impactor Newmark's time integration algorithm was used. Tsai-Wu failure criteria was utilize to predict FPF of laminate due to impact at every time step. Numerical results were presented by varying size and location of delaminations and stacking sequence.

1.2.9 Recent Advances in Composite Materials:

Hirwani et al. [150] investigated the effect of delamination on the free vibration response of laminated composites curved panels with different geometry. The presence of delamination is modelled using higher order shear deformable kinematic models. The governing equation was acquired from classical Hamilton's principle and discretised by FEM. The effect of different materials and geometrical properties such as size, location and position of the delamination on the free vibration response of laminated composite shell was analysed numerically.

Hirwani et al. [151] analyzed the transient response of composite plate with internal debonding under transverse sinusoidal loading. The composite plate with internal debonding was modelled mathematicaly by using Reddy's simple shear deformation kinematic theory and geometrical nonlinearity of the debonded plate was taken care by Lagrangian method. The governing equation of motion was derived with the help of Lagrangian method and solved by Newmark's time integration scheme. The effect of size, location and position of internal damage, material and geometrical factors on the nonlinear transient behaviour of composite plate was found numerically.

Hirwani et al. [152] developed a mathematical model using higher order kinematic model to investigate the flexural strength of delaminated composite plate and compared the outcomes with experimental results. The governing equation was found from variational approach and discretised with isoparametric FE steps. The flexural responses was evaluated numerically and experimental bending response was found by three-point bend test. The analysis include effect of material and geometrical properties such as size and location of delamination on bending behavior of the plate.

Hirwani et al. [153] investigated numerically the effect of various mechanical loading on transient response of internally delaminated composite plate and shallow shells. Higher-order displacement kinematics was used to model the problem followed by FE steps and the domain was discretized with the biquadratic nine-noded quadrilateral element. The effect of design parameters, geometries and delaminations on transient response was analyzed.

Hirwani and Panda [154] investigated the thermal free vibration of delaminated composite shell including large geometrical deformation. The model was derived using various higher-order polynomial kinematics considering nonlinear structural geometry.

They analyzed the influence of design parameters, delamination size, interlayer position and location on the nonlinear frequency response.

Hirwani et al. [155] examined numerically the effect of thermomechanical loading on deflection response of delaminated doubly curved shallow shells. Using higher order kinematic theories the delaminated shell structure was modelled mathematically. The investigation includes the effect of delamination size and position and structural parameters on deflection response under combined loading.

Dewangan et al. [156] investigated numerically the effect of shape and size on modal response of impregnated composite panels using higher order isoparametric FE formulation and higher order polynomial kinematic model. The effect of design and structural parameters on modal response was found with different boundary conditions.

Hirwani and Panda [157] investigated numerically the effect of delamination on structural stiffness and modal response of layered composite using higher order FEM and kinematic models. The effect of different parameters such as material properties, geometrics and delamination size and position on frequency behaviour was presented.

Hirwani et al. [158] examined nonlinear transient response of delaminated composite shell under different kind of mechanical loading. The delaminated shell was modelled using higher order midplane theories in association with the Green-Langrage theories. The nonlinear frequency response was computed numerically by applying Newmark's time integration scheme. The effect of delamination size, location and position and design parameters on frequency response was found.

Hirwani et al. [159] examined numerically and experimentally the nonlinear frequency behaviour of laminated curved composite panels. The mathematical model was developed by using different kinematic models and Green-Lagrange nonlinear strains. The effect of design parameters and different geometrical formations on linear and nonlinear frequency behaviour was found.

Hirwani and Panda [160] investigated numerically thermoelastic deflection and stresses of a delaminated layered structure under the variable temperature field. The formulation was developed using various polynomial kinematic theories considering the stretching effect. For nonlinear equilibrium conditions variational norm was selected and solved using Lagrangian method. The different input parameters such as delamination size, position and location was selected for the analysis.

Hirwani and Panda [161] examined numerically nonlinear deflections and stress response of pre damaged single and doubly curved composite shell under quasi-static loading and validated the result experimentally. For mathematical model higher-order kinematic theories and Green-Lagrange nonlinear strain theories was used. The necessary governing equation was found by minimizing the energy expression and solved by using FE steps.

Hirwani et al. [162] evaluated numerically the nonlinear bending and stress values of internally debonded flat composite panel using higher-order kinematic theories considering thickness stretching effect. The model was developed considering Green–Lagrange strain kinematics and higher order strains. Various examples was solved considering the effect of delamination size, location and position on nonlinear deflection.

Hirwani and Panda [163] investigated nonlinear time-dependent displacement results of delaminated composite curved shell under various pulse loading. The mathematical model was developed using higher-order displacement theories in association with thickness stretching effect and sublaminate method was selected for presence of delamination. The governing equation was reduced by 2D FE formulation through nine-noded isoparametric elements and solved by using by direct iterative technique and Newmark's average acceleration approach.

Srivastava et al. [164] investigated experimentally and numerically dynamic deflection of delaminated carbon–epoxy composite shallow shell panels. Initially composite panels were fabricated and the material properties were obtained. For modelling delaminated panels higher-order displacement kinematics and FE method was used. The equation of motion was derived from Lagrangian method and solved by Newmark's time integration scheme. The effect of delamination size, shape, material and geometrical properties on transient deflection were analyzed.

Erukala et al. [165] examined mathematically delaminated structural strength of laminated composite using higher-order displacement field. The impact of crack on frequency estimated numerically by using FE method. The decrease in strength due to rise in temperature and presence of crack were found using the developed model. Enhancement of strength/stiffness was achieved by reinforcing the shape memory alloy.

Erukala et al. [166] analyzed nonlinear transient deflection laminated composite shell assimilated with shape memory alloy (SMA) with or without the presence of damage. The mathematical model employed HSDT and transient response were found using the Newmark's average acceleration approach.

Kumar et al. [167] investigated the effect of delamination and crack inside layered composite on modal response and strain energy release rate (SERR) numerically using FEM and higher-order mathematical model. The effect of delamination and presence of crack on eigenvalue and SERR were analyzed.

Kumar et al. [168] examined transient behavior of curved composite shell panels with the presence of crack and delamination under thermo-mechanical loading and verified experimentally. They developed mathematically a model for damage shell using higher-order polynomials and isoparametric FE steps. The dynamic behaviour were computed numerically employing Newmark's constant average acceleration approach. The FE results were compared with the experimental outcomes. The effect of delamination, crack, structural parameters and temperature on the curved shell was presented.

Jones [169] describes the basic knowledge of mechanical behavior of laminated composite materials. He also discussed the micromechanics and macromechanics behaviour of composites, lamination theory and plate bending, buckling and vibration theories.

Cook [170] presented elaborately the FEM for beginners to use it in computational problems. He represented modest amount of FE theory, nature of FE solution, suggestion for modelling and computational problems.

1.3 Motivation of the present Research

It is evident from the literature review that earlier research works mostly focused on the first-ply failure of composite plates without considering the influence of internal anomalies of the structure. In general, the composite blades fitted to the hub of the turbomachinery blades are wider near the fixed end where the highest bending stresses tend to develop. The trapezoidal planform of the composite blades may be suitably analyzed by idealizing them as thin conical shells. The presence of delamination and matrix-cracking are detrimental and hazardous to the service life of the composite structures owing to their insidious presence. The first-ply failure of composite conical shells is widely affected by the presence of delamination. The delamination may occur in the composite conical shell structures during transportation, tool drop, hailstorm and impact of slow moving projectiles during harsh working conditions. As such, the critical velocity of impact at which the first-ply failure of delaminated composite conical shells initiates is of utmost importance from their design point of view. The present work thereby focuses on the first-ply failure behavior of pretwisted delaminated composite conical shells due to static and impact loading.

1.4 Objective of the present work

The objective of current research work is to predict the failure behaviour and transient response of pretwisted delaminated rotating composite conical shells under static and impact loading. The pre-twisted rotating conical shells are assumed to be subjected to a center point transverse load, and the FPF loads are evaluated based on the well-established failure-criterions namely, maximum strain, maximum stress (Independent and polynomial based), Hoffmann, Tsai-

Hill, and Tsai-Wu criteria under static loading condition. For impact loading, first the critical velocity of impact will be calculated at which the first-ply failure begins. Obtaining critical velocity of impact is necessary because contact force depends on the velocity of impact. Then the transient response of single delaminated and multiple delaminated shells will be studied at critical velocity of impact for different aspect ratio. Also size and location of delamination and location of impact will be considered as vital parameters for present analysis.

1.5 Scope of the Present work

The scope of present work is restricted to the study of first-ply failure behavior of pretwisted delaminated rotating conical shells under static and impact loading. Under static loading some well-established failure criterion are selected and the pre-twisted conical shells are assumed to be subjected to a transverse central point load with cantilever boundary condition. During impact loading critical velocity of impact is found at which first-ply failure begins. The shells are assumed to have single and multiple delamination with different size and location of impact on the conical shell are varied.

CHAPTER 2: Theoretical Formulation

2.1 Introduction

This chapter presents the theoretical formulation and solution procedures and use of Finite Element Method (FEM) adopted for the first-ply failure of composite conical shells. The conical shell geometry are presented initially followed by discretization of domain, lamina stress strain relationship, governing equation, first ply failure theories and impact relationship. The conical shell is discretized using an eight-noded isoparametric shell bending element and multipoint constraint algorithm is employed to model the delaminated conical shell. Different first ply failure theories are described and impact relationships are explained. Further computer codes are developed based on existing formulation and graphs are plotted using Origin software.

2.2 Conical Shell Model

A shallow conical shell is employed for present analysis shown in **Fig.1.** The span length, base width, major radius, minor radius, thickness, vertex angle, base subtended angle are L, b_0, α_0, β_0, h, θ_v , θ_0 respectively. The geometric orientation of the mid-plane of an untwisted shallow shell is [1]

The radius of twist (R_{xy}), length (L) of the shell and twist angle (ψ) are related by the expression [1]

$$z = -\frac{1}{2}\left(\frac{x^2}{R_x} + \frac{2xy}{R_{xy}} + \frac{y^2}{R_y}\right) \quad \text{and} \quad \tan\psi = -\frac{L}{R_{xy}} \tag{2.1}$$

where R_x is the span-wise radius, R_y is the chord-wise radius, R_{xy} is the curvature radius, length of the shell is L and twist angle is ψ. However, there is no curvature of the conical shell along the spanwise direction. The cantilevered shallow conical shell, assumed to be clamped at x=0, is pretwisted at a twist angle of ψ and a radius of twist R_{xy}. Any cross section of the conical shell is a part of an ellipse with α and β are major and minor radii. The equation of the ellipse is given by [1]

$$\left(\frac{y}{\alpha}\right)^2 + \left(\frac{z+\beta}{\beta}\right)^2 = 1 \tag{2.2}$$

The chord-wise radius R_y of the conical shell is [86]

$$R_y = \frac{[1+(\frac{dz}{dy})^2]^{3/2}}{\frac{d^2z}{dy^2}} = \alpha^2\beta^2[\frac{1}{\beta^2} + \frac{y^2}{\alpha^2}\left(\frac{1}{\alpha^2} - \frac{1}{\beta^2}\right)]^{\frac{3}{2}} \quad (2.3)$$

$$= s(\frac{\alpha}{s})^2(\frac{\beta}{s})^2\{\left(\frac{s}{\beta}\right)^2 + \left(\frac{s}{b_0}\right)^2\left(\frac{b_0}{s}\right)^2\left(\frac{s}{\alpha}\right)^2[\left(\frac{s}{\alpha}\right)^2 - \left(\frac{s}{\beta}\right)^2\}^{3/2} \quad (2.4)$$

$$\text{where } \frac{\alpha}{s} = \frac{(\frac{b}{s})(\frac{\beta}{s})\tan(\frac{\theta_0}{2})}{\sqrt{tan^2(\frac{\theta_0}{2} - (\frac{\beta}{s})^2)}} \quad (2.5)$$

$$\frac{\beta}{s} = \tan\left(\frac{\theta v}{2}\right)[1 - \left(\frac{x}{s}\right)]$$

$$\frac{b}{s} = (\frac{b_0}{s})[1 - \left(\frac{x}{s}\right)]$$

$$\frac{b_0}{s} = 2\sin(\frac{\theta_0}{2})\sqrt{\frac{tan^2(\frac{\theta_0}{2})}{cos^2\left(\frac{\theta_0}{2}\right) + tan^2\left(\frac{\theta_0}{2}\right)}} \quad (2.6)$$

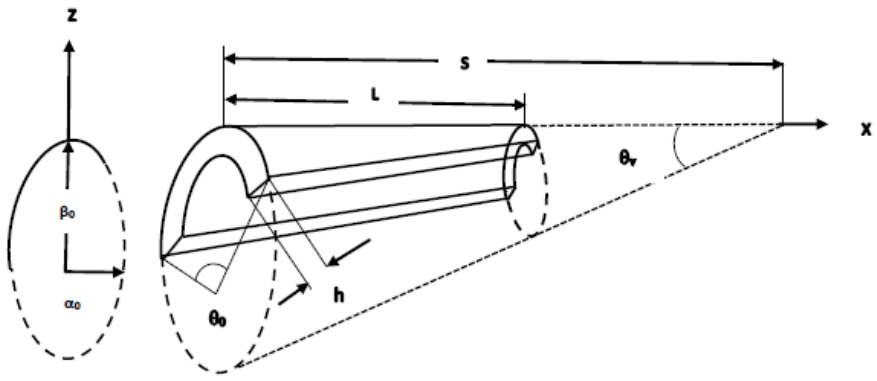

2.1(a)

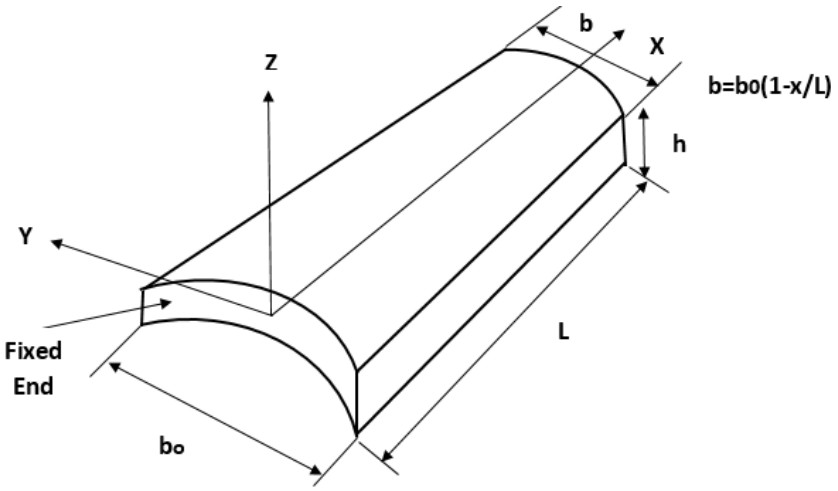

2.1(b)

Fig. 2.1(a & b) Schematic diagram of a shallow conical shell

2.3 Finite Element Formulation

The domain is discretized by 8X8 mesh division of the planform of the conical shell and an eight-noded isoparametric shell element is selected for present analysis **(Fig. 2.2).** The isoparametric shell element is shown in *x-y* ($\xi - \eta$) plane and $\xi - \eta$ plane **(Fig. 2.3 and Fig. 2.4).**

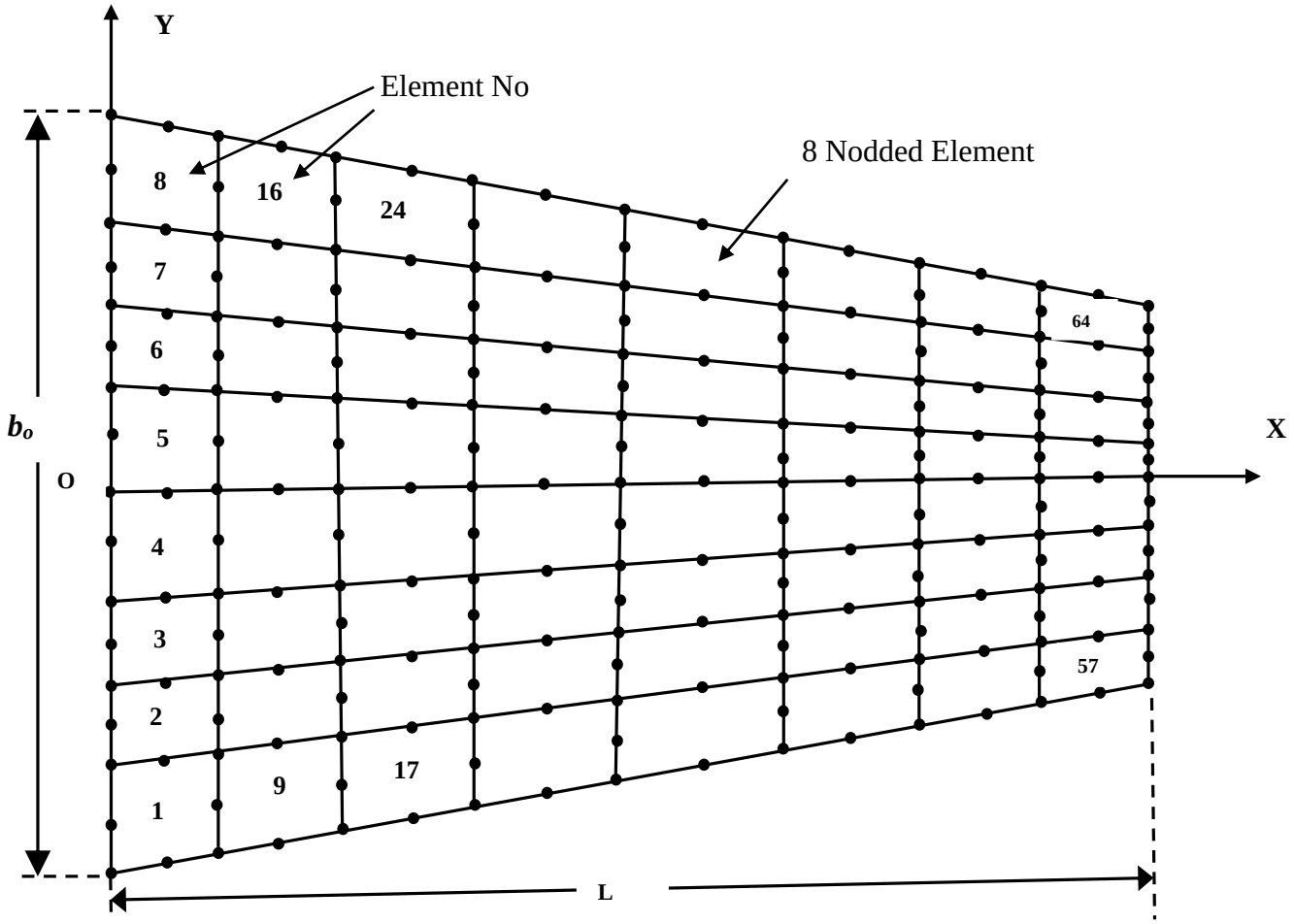

Fig. 2.2 FE Mesh discretization of the planform of the conical shell

The geometry of the element and displacement fields can be described by the following quadratic shape functions(N_i). [36]

$$x = \sum_{i=1}^{8} N_i x_i;\ y = \sum_{i=1}^{8} N_i y_i \tag{2.7}$$

$$u^0 = \sum_{i=1}^{8} N_i\, u_i^0\ ;\ v^0 = \sum_{i=1}^{8} N_i\, v_i^0\ ;\ w^0 = \sum_{i=1}^{8} N_i\, w_i^0 \tag{2.8}$$

$$\theta_x = \sum_{i=1}^{8} N_i\, \theta_x^i;\ \theta_y = \sum_{i=1}^{8} N_i\, \theta_y^i \tag{2.9}$$

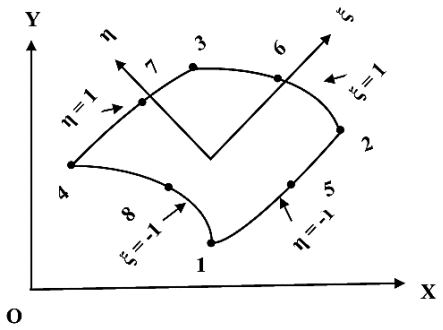

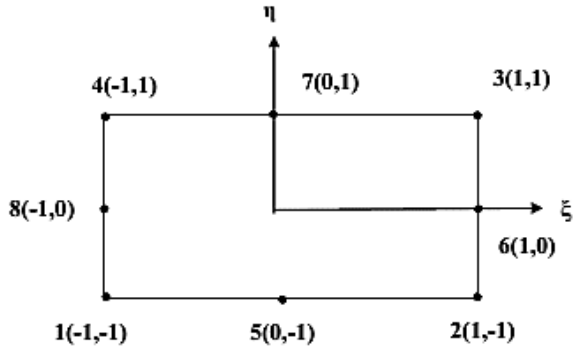

Fig. 2.3 An element in *x-y* (ξ – η) plane

Fig. 2.4 An isoparametric element in the ξ – η space

The on axis stiffness of the k^{th} lamina is [169]

$$[Q_{ij}]_k=\begin{bmatrix} Q_{11} & Q_{12} & 0 \\ Q_{12} & Q_{22} & 0 \\ 0 & 0 & Q_{66} \end{bmatrix}; \; i, j=1, 2, 6 \tag{2.10}$$

$$[Q_{ij}]_k=\begin{bmatrix} Q_{44} & 0 \\ 0 & Q_{55} \end{bmatrix}; \; i,j=4, 5 \tag{2.11}$$

where $Q_{11}=\frac{E_1}{1-\nu_{12}\nu_{21}}$, $Q_{12}=\frac{\nu_{12}E_2}{1-\nu_{12}\nu_{21}}$, $Q_{22}=\frac{E_2}{1-\nu_{12}\nu_{21}}$, $Q_{44}=G_{13}$, $Q_{55}=G_{23}$ and $Q_{66}=G_{12}$

The transformation matrices can be expressed as [169]

$$[T_1]=\begin{bmatrix} m^2 & n^2 & 2mn \\ n^2 & m^2 & -2mn \\ -mn & mn & m^2-n^2 \end{bmatrix} \tag{2.12}$$

$$[T_2]=\begin{bmatrix} m & -n \\ n & m \end{bmatrix} \tag{2.13}$$

The off axis stiffness for the k^{th} lamina is [169]

$$[\bar{Q}_{ij}]_k=[T_1]^{-1}[Q_{ij}]_k[T_1]^T, \; i, j=1,2,6 \tag{2.14}$$

$$[\bar{Q}_{ij}]_k=[T_2]^{-1}[Q_{ij}]_k[T_2] \quad , \; i, j=4,5 \tag{2.15}$$

2.4 *Stress Strain Relationship*

The linear strains of each lamina at a distance 'z' from the mid-surface of the laminate are [36, 169]

$$\varepsilon_x = u_{,x} + \frac{w}{R_x};$$

$$\varepsilon_y = v_{,y} + \frac{w}{R_y};$$

$$\gamma_{xy} = u_{,y} + v_{,x} + \frac{2w}{R_{xy}}$$

(2.16)

The in-plane strain vector is the summation of the mid-surface strain vector and vector of the variation in curvature due to external applied loads, wherek_x, k_y, and k_{xy}represents the curvature vectors of the conical shell [169]

$$\begin{Bmatrix} \varepsilon_x \\ \varepsilon_y \\ \gamma_{xy} \\ \gamma_{xz} \\ \gamma_{yz} \end{Bmatrix} = \begin{Bmatrix} u_{,x} \\ v_{,y} + w/r_y \\ u_{,y} + v_{,x} + w/r_{xy} \\ u_{,z} + w_{,x} \\ v_{,z} + w_{,y} - v/r_y \end{Bmatrix} = \begin{Bmatrix} \varepsilon_{xx}^0 \\ \varepsilon_{yy}^0 \\ \gamma_{xy}^0 \\ \varphi_{xz} \\ \varphi_{yz} \end{Bmatrix} + z \begin{Bmatrix} \kappa_{xx} \\ \kappa_{yy} \\ \kappa_{xy} \\ \kappa_{xz} \\ \kappa_{yz} \end{Bmatrix}$$

(2.17)

The in-plane strain and transverse strains can be calculated by the following relations [169]

$$\varepsilon_x = \varepsilon_x^0 + zk_x; \quad \varepsilon_y = \varepsilon_y^0 + zk_y; \quad \gamma_{xy} = \gamma_{xy}^0 + zk_{xy}$$

$$\gamma_{xz} = \varphi_{xz} + z\kappa_{xz} \text{ and } \gamma_{yz} = \varphi_{yz} + z\,\kappa_{yz}$$

(2.18)

For the k^{th} lamina the strains in the principal material directions can be obtained by using the transformation given below [169]

$$\begin{Bmatrix} \varepsilon_1 \\ \varepsilon_2 \\ \varepsilon_6 \end{Bmatrix}_k = \begin{bmatrix} p^2 & q^2 & 2pq \\ q^2 & p^2 & -2pq \\ -pq & pq & p^2 - q^2 \end{bmatrix}_k \begin{Bmatrix} \varepsilon_x \\ \varepsilon_y \\ \frac{\gamma_{xy}}{2} \end{Bmatrix}_k$$

(2.19)

Where $p=cos\theta_k$ and $q=sin\theta_k$, θ_k being the fiber-angle of the k^{th} lamina

The strain vector $\{\varepsilon\}$and nodal displacement vector $\{\delta_e\}$ of an element are associated by the relation provided below [170]

$$\{\varepsilon\} = [B]\{\delta_e\}$$

(2.20)

where $[B]$ is the strain-displacement matrix.

The five lamina stresses for the k^{th} lamina can be computed using the following stress-strain relations considering plane stress conditions [169,170]

$$\begin{Bmatrix}\sigma_{11}\\ \sigma_{22}\\ \tau_{12}\\ \tau_{13}\\ \tau_{23}\end{Bmatrix}_k = \begin{bmatrix}Q_{11} & Q_{12} & 0 & 0 & 0\\ Q_{12} & Q_{22} & 0 & 0 & 0\\ 0 & 0 & Q_{66} & 0 & 0\\ 0 & 0 & 0 & Q_{44} & 0\\ 0 & 0 & 0 & 0 & Q_{55}\end{bmatrix}_k \left(\begin{Bmatrix}\varepsilon_{11}\\ \varepsilon_{22}\\ \gamma_{12}\\ \gamma_{13}\\ \gamma_{23}\end{Bmatrix}\right)_k$$

Where

$$Q_{11} = \frac{E_{11}}{1-\nu_{12}\nu_{21}},\ Q_{22} = \frac{E_{22}}{1-\nu_{12}\nu_{21}},\ Q_{12} = \frac{\nu_{21}E_{11}}{1-\nu_{12}\nu_{21}},$$

$$Q_{66} = G_{12}, Q_{44} = G_{23},\ Q_{55} = G_{13}$$

(2.21)

For orthotropic laminate the stress-strain relationship is

$$\{\sigma\} = [D]\{\varepsilon\}$$

(2.22)

where $[D]$ is the elasticity matrix.

For a generalized representation of the overall displacement field over the element, the shape functions may be defined based on the natural or intrinsic co-ordinates ξ and η. The displacement variable $u(\xi,\eta)$ may be defined as a polynomial of the natural coordinates in order to arrive at the interpolation or shape functions, [170]

$$u(\xi,\eta) = k_1 + k_2\xi + k_3\eta + k_4\xi\eta + k_5\xi^2 + k_6\eta^2 + k_7\xi^2\eta + k_8\xi\eta^2 \qquad (2.23)$$

where, $k_i (i = 1,2,3,\ldots,8)$ are the degrees of freedom for the element considered.

The interpolation functions N_i for the i^{th} node may be represented as below [170]

$$N_i = (1+\xi\xi_i)(1+\eta\eta_i)(\xi\xi_i+\eta\eta_i-1)/4 \quad (\text{for } i = 1, 2, 3, 4) \qquad (2.24)$$

$$N_i = (1-\xi^2)(1+\eta\eta_i)/2 \quad (\text{for } i = 5, 7) \qquad (2.25)$$

$$N_i = (1-\eta^2)(1+\xi\xi_i)/2 \quad (\text{for } i = 6, 8) \qquad (2.26)$$

where ξ_i and η_i are the natural coordinates at i^{th} node.

The shape functions considered must satisfy the following conditions, [170]

$$\sum_{i=1}^{8} N_i = 1, \quad \sum_{i=1}^{8} \frac{\partial N_i}{\partial \xi} = 1, \quad \sum_{i=1}^{8} \frac{\partial N_i}{\partial \eta} = 1, \tag{2.27}$$

Based on the isoparametric formulation, the coordinates x and y of a point within the element may be expressed as below, in terms of shape functions N_i and the coordinates (x_i, y_i) as [170]

$$x = \sum_{i=1}^{8} N_i \, x_i \qquad\qquad y = \sum_{i=1}^{8} N_i \, y_i \tag{2.28}$$

Where, N_i's denotes the shape functions and x_i and y_i are the nodal coordinates.

The mid-plane displacements within the finite element may be expressed in terms of the nodal displacement as given below, [170]

$$u_0 = \sum_{i=1}^{8} N_i \, u_{0i} \; ; v_0 = \sum_{i=1}^{8} N_i \, v_{0i} \; ; \; w_0 = \sum_{i=1}^{8} N_i \, w_{0i} \; ;$$
$$\theta_x = \sum_{i=1}^{8} N_i \, \beta_{xi} \; ; \theta_y = \sum_{i=1}^{8} N_i \, \beta_{yi} \tag{2.29}$$

The derivatives of the shape functions in the (x, y) and (ξ, η) systems are related as mentioned below, [169]

$$\begin{Bmatrix} N_{i,x} \\ N_{i,y} \end{Bmatrix} = [J]^{-1} \begin{Bmatrix} N_{i,\xi} \\ N_{i,\eta} \end{Bmatrix} \tag{2.30}$$

where $[J]$ denotes the Jacobian matrix and is may be defined as below, [169]

$$[J] = \begin{bmatrix} x_{,\xi} & y_{,\xi} \\ x_{,\eta} & y_{,\eta} \end{bmatrix} \tag{2.31}$$

The generalized displacements $\{u\}$ in **Eq. (2.29)** may be expressed in terms of the nodal displacement vector $\{\delta_e\}$ and the matrix of the shape functions $[N]$ as below, [170]

$$\{u\} = [N]\{\delta_e\} \tag{2.32}$$

where $\{u\} = [u_0 \quad v_0 \quad w_0 \quad \theta_x \quad \theta_y]^T$ is the vector representing generalized displacement parameter and $\{\delta_e\} = [u_{0i} \quad v_{0i} \quad w_{0i} \quad \theta_{xi} \quad \theta_{yi}]^T$ represent nodal displacement parameter vector. The shape function matrix $[N]$ can be expressed as [170]

$$[N] = \begin{bmatrix} N_i & 0 & 0 & 0 & 0 \\ 0 & N_i & 0 & 0 & 0 \\ 0 & 0 & N_i & 0 & 0 \\ 0 & 0 & 0 & N_i & 0 \\ 0 & 0 & 0 & 0 & N_i \end{bmatrix}_{i=1,2,3,\ldots,5} \tag{2.33}$$

Subsequently, the mid-plane strain vector $\{\varepsilon^0\}$ can be expressed in term of nodal displacement parameter vector as [170]

$$\{\varepsilon^0\} = [B]\{\delta_e\} \tag{2.34}$$

where $[B]$ denotes the strain-displacement matrix given as

$$[B] = \sum_{i=1}^{8} \begin{bmatrix} N_{i,x} & 0 & N_i/r_x & 0 & 0 \\ 0 & N_{i,y} & N_i/r_y & 0 & 0 \\ N_{i,y} & N_{i,x} & 2N_i/r_{xy} & 0 & 0 \\ 0 & 0 & 0 & 0 & N_{i,x} \\ 0 & 0 & 0 & -N_{i,y} & 0 \\ 0 & 0 & 0 & -N_{i,x} & -N_{i,y} \\ 0 & 0 & -N_{i,x} & N_i & 0 \\ 0 & 0 & -N_{i,y} & 0 & N_i \end{bmatrix} \tag{2.35}$$

2.5 Generalized Dynamic Equilibrium Equation

2.5.1 Rotating conical shell

Two reference systems $\mathcal{R}_0(X, Y, Z)$ and $\mathcal{R}_1(x, y, z)$ are considered in order to formulate the general dynamic equilibrium of a rotating conical shell as shown in **Fig. 2.5**. The first system refers to the inertial coordinate system with the unit vectors $(\mathbf{i}_X, \mathbf{i}_Y, \mathbf{i}_Z)$ which is assumed to be fixed to any arbitrary point on the axis of hub on which the blade is fitted. The second system refers to the local coordinate system and denoted with the help of unit vectors $(\mathbf{i}_x, \mathbf{i}_y, \mathbf{i}_z)$ in the shell coordinate system. The vector $\mathbf{r_0} = \{X_0, \quad Y_0, \quad Z_0\}$ signifies the translational offsets of shell coordinate system with reference to the inertial reference system. [74]

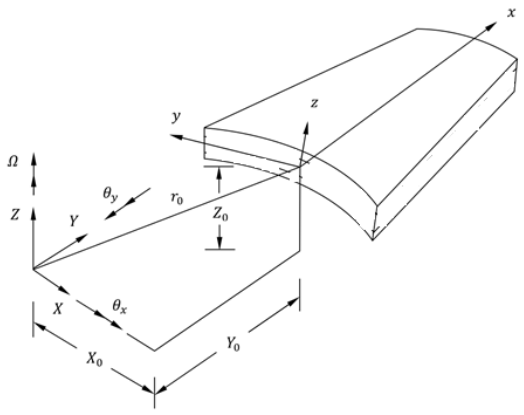

Fig. 2.5 Rotating conical shell represented in both inertial and local reference system

The kinetic energy of the rotating conical shell may be defined as

$$T_{KE} = \frac{1}{2}\int_{vol} \rho \mathbf{V}.\mathbf{V}\, d(vol) \tag{2.36}$$

where ρ symbolizes the mass density of the shell and $\mathbf{V}$ indicates the absolute velocity of an arbitrary point on the conical shell in $\mathcal{R}_0(X,Y,Z)$ reference system. The conical shell is assumed to rotate about the $\mathcal{R}_0(X,Y,Z)$ reference system with an angular velocity $\boldsymbol{\Omega} = \Omega \mathbf{i_Z}$

The angular velocity in the $\mathcal{R}_1(x,y,z)$ system may be defined in terms of its components as below, [74]

$$\{\Omega_x,\ \Omega_x,\ \Omega_x\} = \{0,\quad 0,\quad \Omega\}\left[T_{\theta y}\right]^T [T_{\theta x}]^T \tag{2.37}$$

where

$$[T_{\theta x}]^T = \begin{bmatrix} 1 & 0 & 0 \\ 0 & \cos\theta_x & -\sin\theta_x \\ 0 & \sin\theta_x & \cos\theta_x \end{bmatrix} \tag{2.38}$$

$$\left[T_{\theta y}\right]^T = \begin{bmatrix} \cos\theta_y & 0 & -\sin\theta_y \\ 0 & 1 & 0 \\ \sin\theta_y & 0 & \cos\theta_y \end{bmatrix} \tag{2.39}$$

where Ω symbolizes the rotational speed of the conical shell about Z axis of the $\mathcal{R}_0(X,Y,Z)$ system, θ_x indicates skew angle and θ_y signifies the precone angle. The order of rotations is θ_x and θ_y.

The translational offsets expressed with reference to shell coordinate system may be expressed as [74]

$$\left\{l_x,\ l_y,\ l_z\right\} = \{X_0,\quad Y_0,\quad Z_0\}\left[T_{\theta y}\right]^T [T_{\theta x}]^T \tag{2.40}$$

Base on the Chasle's theorem,

$$\mathbf{V} = \frac{d\mathbf{r}}{dt} + \boldsymbol{\Omega} \times \mathbf{r} \tag{2.41}$$

where $\boldsymbol{r}$ indicates the position vector of the arbitrary point on the conical shell after deformation from the origin of the inertial reference frame and is given by [74]

$$\mathbf{r} = (l_x + x + u)\mathbf{i_x} + \left(l_y + y + v\right)\mathbf{i_y} + (l_z + z + w)\mathbf{i_z} \tag{2.42}$$

where (x,y,z) are the coordinates of any point in the shell coordinate system (local coordinate axes) while $\left(l_x, l_y, l_z\right)$ are the fixed translational offsets of the shell coordinate axes from the

inertial axes system expressed with reference to the shell coordinate system, (u, v, w) are the displacements of a point on the shell.

The angular velocity vector $\boldsymbol{\Omega}$ in **Eq. (2.41)** is given by

$$\boldsymbol{\Omega} = \Omega \mathbf{k_Z} = \Omega_x \mathbf{i}_x + \Omega_y \mathbf{i}_y + \Omega_z \mathbf{i}_z \tag{2.43}$$

where $(\Omega_x, \Omega_y, \Omega_z)$ are the components of angular velocity in the shell coordinate system.

Substituting the expressions of $\mathbf{r}$ and $\boldsymbol{\Omega}$ into **Eq. 2.41**, the absolute velocity $\mathbf{V}$ can be derived as

$$\begin{aligned} \boldsymbol{V} = &\left[\dot{u} + \Omega_y(\dot{l_z} + z + w) - \Omega_z(l_y + y + v)\right]\mathbf{i}_x \\ &+ \left[\dot{v} + \Omega_z(\dot{l_x} + x + u) - \Omega_x(l_z + z + w)\right]\mathbf{i}_y \\ &+ \left[\dot{w} + \Omega_x(\dot{l_y} + y + v) - \Omega_y(l_x + x + u)\right]\mathbf{i}_z \end{aligned} \tag{2.44}$$

Computing $|\mathbf{V}|^2$and cancelling the terms that have no contribution when Lagrange's equation of motion is applied and substituting the result in kinetic energy expression, we have, [74]

$$\begin{aligned} T_{KE} = &\frac{1}{2}\int_{vol} \rho \begin{Bmatrix} \dot{u} \\ \dot{v} \\ \dot{w} \end{Bmatrix}^T \begin{Bmatrix} \dot{u} \\ \dot{v} \\ \dot{w} \end{Bmatrix} d(vol) + \frac{1}{2}\int_{vol} \rho \begin{Bmatrix} \dot{u} \\ \dot{v} \\ \dot{w} \end{Bmatrix}^T [A_1] \begin{Bmatrix} u \\ v \\ w \end{Bmatrix} d(vol) \\ &+ \frac{1}{2}\int_{vol} \rho \begin{Bmatrix} u \\ v \\ w \end{Bmatrix}^T [A_2] \begin{Bmatrix} u \\ v \\ w \end{Bmatrix} d(vol) \\ &+ \frac{1}{2}\int_{vol} \rho \begin{Bmatrix} l_x + x \\ l_y + y \\ l_z + z \end{Bmatrix}^T [A_2] \begin{Bmatrix} u \\ v \\ w \end{Bmatrix} d(vol) \end{aligned} \tag{2.45}$$

where the matrices $[A_1]$ and $[A_2]$ are given by

$$[A_1] = \begin{bmatrix} 0 & -2\Omega_z & 2\Omega_y \\ 2\Omega_z & 0 & -2\Omega_x \\ -2\Omega_y & 2\Omega_x & 0 \end{bmatrix} \tag{2.46}$$

$$[A_2] = \begin{bmatrix} \Omega_y^2 + \Omega_z^2 & -\Omega_x\Omega_y & -\Omega_x\Omega_z \\ -\Omega_x\Omega_y & \Omega_x^2 + \Omega_z^2 & -\Omega_y\Omega_z \\ -\Omega_x\Omega_z & -\Omega_y\Omega_z & \Omega_x^2 + \Omega_y^2 \end{bmatrix} \tag{2.47}$$

Substituting $[u, \quad v, \quad w]^T = [\bar{Z}]\{\delta\}$ into Eq. 2.45, the kinetic energy becomes [74]

$$T_{KE} = \frac{1}{2}\int_{vol} \{\dot{\delta}\}^T [\bar{Z}]^T \rho\, [\bar{Z}]\{\dot{\delta}\}\, d(vol) + \frac{1}{2}\int_{vol} \{\dot{\delta}\}^T [\bar{Z}]^T \rho [A_1]\, [\bar{Z}]\{\delta\}\, d(vol) \tag{2.48}$$

$$+\frac{1}{2}\int_{vol}[\delta]^T[\bar{Z}]^T\rho[A_2]\,[\bar{Z}]\{\delta\}\,d(vol)+\int_{vol}\rho\begin{Bmatrix}l_x+x\\l_y+y\\l_z+z\end{Bmatrix}^T[A_2][\bar{Z}]\{\delta\}d(vol)$$

where $[m_I]=\int_{-h/2}^{h/2}[\bar{Z}]^T\rho\,[\bar{Z}]\,dz$ refers the matrix of inertia per unit area.

Further, putting $\{\delta\}=[N]\{\delta_e\}$ into **Eq. 2.48** is expressed in the following form

$$T_{KE}=\frac{1}{2}\{\dot{\delta}_e\}^T[M_e]\{\dot{\delta}_e\}+\frac{1}{2}\{\dot{\delta}_e\}^T[C_e]\{\delta_e\}+\frac{1}{2}\{\delta_e\}^T[K_{Re}]\{\delta_e\}+\{\delta_e\}^T\{F_{ce}\} \tag{2.49}$$

where $[M_e]$, $[C_e]$, $[K_{Re}]$, and $\{F_{\Omega e}\}$ denote the mass matrix, Coriolis matrix (skew symmetric), centrifugal stiffness matrix (symmetric and positive definite), and rotational force vector for the shell element, and are defined as below,

$$[M_e]=\int_{-1}^{1}\int_{-1}^{1}[N]^T[m_I]\,[N]|J|d\xi d\eta \tag{2.50}$$

$$[C_e]=\rho\int_{vol}[N]^T[\bar{Z}]^T[A_1][\bar{Z}][N]\,d(vol) \tag{2.51}$$

$$[K_{Re}]=\rho\int_{vol}[N]^T[\bar{Z}]^T[A_2][\bar{Z}][N]\,d(vol) \tag{2.52}$$

$$\{F_{\Omega e}\}=\rho\int_{vol}[N]^T[\bar{Z}][A_2]\begin{Bmatrix}l_x+x\\l_y+y\\l_z+z\end{Bmatrix}^T d(vol) \tag{2.53}$$

Substituting the expression of the transformation matrix $[\bar{Z}]$ into $[m_I]$ the inertia matrix becomes [170]

$$[P']=\begin{bmatrix}I_t&0&0&0&0\\0&I_t&0&0&0\\0&0&I_t&0&0\\0&0&0&I_r&0\\0&0&0&0&I_r\end{bmatrix} \tag{2.54}$$

where I_r and I_t denote the rotary and translatory inertia terms, respectively and can be expressed as below

$$I_t=\frac{1}{h}\sum_{k=1}^{n}\int_{z_k}^{z_{k+1}}\rho_k dz,\qquad I_r=\frac{1}{h}\sum_{k=1}^{n}\int_{z_k}^{z_{k+1}}\rho_k z^2 dz \tag{2.55}$$

where ρ_k is the mass density of the k^{th} layer and z_k and z_{k+1} are the top and the bottom distances of a lamina from the mid-plane of the shell, respectively.

2.5.2 Strain energy of rotating conical shell

The elastic strain energy of the conical shell element is expressed as [170]

$$U_e^E = \frac{1}{2}\int_{vol} \{\varepsilon_l\}^T \{\sigma\}\, d(vol) \tag{2.56}$$

Using $\{\varepsilon_l\} = [\bar{T}]\{\varepsilon^0\}$ and $\{F\} = [D]\{\varepsilon^0\}$, the above expression can be rewritten

$$U_e^E = \frac{1}{2}\int_{A} \{\varepsilon^0\}^T\, [D]\{\varepsilon^0\} dA \tag{2.57}$$

in which $[D] = \int_{-h/2}^{h/2} [\bar{T}]^T \left[\bar{Q}_{ij}\right][\bar{T}] dz$ is the elasticity matrix.

Substituting $\{\varepsilon^0\} = [B]\{\delta_e\}$ in **Eq. (2.57),** the elemental elastic strain energy becomes

$$U_e^E = \frac{1}{2}\int_{A} \{\delta_e\}^T\, [B]^T [D][B]\{\delta_e\} dA = \frac{1}{2}\{\delta_e\}^T [K_e]\{\delta_e\} \tag{2.58}$$

where $[K_e]$ is the elastic stiffness matrix for the shell element that can be written as [170]

$$[K_e] = \int_{-1}^{1}\int_{-1}^{1} [B]^T\, [D][B]|J| d\xi d\eta \tag{2.59}$$

The non-linear strain components according to the Green-Lagrange relations are given as [54]

$$\{\varepsilon_{nl}\} = \begin{Bmatrix} \varepsilon_{xx} \\ \varepsilon_{yy} \\ \gamma_{xy} \\ \gamma_{xz} \\ \gamma_{yz} \end{Bmatrix}_{nl} = \frac{1}{2}\begin{Bmatrix} (u_{,x})^2 + (v_{,x} + w/r_{xy})^2 + (w_{,x})^2 \\ (u_{,y} + w/r_{xy})^2 + (v_{,y} + w/r_y)^2 + (w_{,y} - v/r_y)^2 \\ 2[u_{,x}(u_{,y} + w/r_{xy}) + (v_{,x} + w/r_{xy})(v_{,y} + w/r_y) + w_{,x}(w_{,y} - v/r_y)] \\ 2[u_{,z}u_{,x} + v_{,z}(v_{,x} + w/r_{xy}) + w_{,z}w_{,x}] \\ 2[u_{,z}(u_{,y} + w/r_{xy}) + v_{,z}(v_{,y} + w/r_y) + w_{,z}(w_{,y} - v/r_y)] \end{Bmatrix} \tag{2.60}$$

The expressions of the nonlinear strain components in the **Eq. (2.60)** can be written in compact form as

$$\{\varepsilon_{nl}\} = \frac{1}{2}[\Gamma][G]\{\delta_e\} \tag{2.61}$$

where $[\Gamma]$ is obvious from **Eq. (2.60)** and **Eq. (2.61),** and $[G]$ is the matrix that contains the derivatives of shape functions as given below [54]

$$[G] = \sum_{i=1}^{8} \begin{bmatrix} N_{i,x} & 0 & 0 & 0 & 0 & 0 & 0 \\ N_{i,y} & 0 & N_i/r_{xy} & 0 & 0 & 0 & 0 \\ 0 & N_{i,x} & N_i/r_{xy} & 0 & 0 & 0 & 0 \\ 0 & N_{i,y} & N_i/r_y & 0 & 0 & 0 & 0 \\ 0 & 0 & N_{i,x} & 0 & 0 & 0 & 0 \\ 0 & -N_i/r_y & N_{i,y} & 0 & 0 & 0 & 0 \\ 0 & 0 & 0 & N_{i,x} & 0 & 0 & 0 \\ 0 & 0 & 0 & N_{i,y} & 0 & 0 & 0 \\ 0 & 0 & 0 & 0 & N_{i,x} & 0 & 0 \\ 0 & 0 & 0 & 0 & N_{i,y} & 0 & 0 \\ 0 & 0 & 0 & 0 & 0 & N_{i,x} & 0 \\ 0 & 0 & 0 & 0 & 0 & N_{i,y} & 0 \\ 0 & 0 & 0 & 0 & 0 & 0 & N_{i,x} \\ 0 & 0 & 0 & 0 & 0 & 0 & N_{i,y} \\ 0 & 0 & 0 & 0 & 0 & 0 & 0 \\ 0 & 0 & 0 & 0 & -N_i/r_y & 0 & 0 \\ 0 & 0 & 0 & 0 & 0 & 0 & 0 \\ 0 & 0 & 0 & 0 & 0 & 0 & -N_i/r_y \end{bmatrix} \tag{2.62}$$

The elemental strain energy resulting from the initial stresses due to thermal and rotational loads is given as [170]

$$U_e^{IS} = \int_{vol} \{\varepsilon_{nl}\}^T \{\sigma_{0TH}\}\, d(vol) + \int_{vol} \{\varepsilon_{nl}\}^T \{\sigma_{0R}\}\, d(vol) \tag{2.63}$$

where $\{\sigma_{0TH}\}$ and $\{\sigma_{0R}\}$ are the initial stress vectors induced due to the thermal and rotational loads, respectively.

The strain energy due to initial stresses as given in **Eq. (2.63)** can be rewritten using **Eq. (2.61)** as [170]

$$U_e^{IS} = \frac{1}{2} \int_{vol} \{\delta_e\}^T [G]^T [\Gamma]^T \{\sigma_{0TH}\}\, d(vol) + \frac{1}{2} \int_{vol} \{\delta_e\}^T [G]^T [\Gamma]^T \{\sigma_{0R}\}\, d(vol) \tag{2.64}$$

Now the following integrations are obtained as [170]

$$\int_{-h/2}^{h/2} [\Gamma]^T \{\sigma_{0TH}\} dz = [S_{TH}][G]\, \{\delta_e\} \tag{2.65}$$

$$\int_{-h/2}^{h/2} [\Gamma]^T \{\sigma_{0R}\} dz = [S_R][G]\, \{\delta_e\} \tag{2.66}$$

where $[S_{TH}]$ and $[S_R]$ are the matrices consisting of in-plane stress resultants induced due to thermal and rotational effects, respectively**.**

Finally, the elemental strain energy due to initial stresses can be reduced as [170]

$$U_e^{IS} = \frac{1}{2}\{\delta_e\}^T[K_{\sigma THe}]\{\delta_e\} + \frac{1}{2}\{\delta_e\}^T[K_{\sigma Re}]\{\delta_e\} \tag{2.67}$$

in which $[K_{\sigma THe}]$ and $[K_{\sigma Re}]$ refer the element geometric stiffness matrices due to thermal and rotational effects, respectively and are given by [170]

$$[K_{\sigma THe}] = \int_{-1}^{1}\int_{-1}^{1}[G]^T[S_{TH}][G]|J|d\xi d\eta \tag{2.68}$$

$$[K_{\sigma Re}] = \int_{-1}^{1}\int_{-1}^{1}[G]^T[S_R][G]|J|d\xi d\eta \tag{2.69}$$

The total strain energy for the element of conical shell considering thermal and rotational effects is given by

$$U_e = U_e^E + U_e^{IS} = \frac{1}{2}\{\delta_e\}^T[K_e]\{\delta_e\} + \frac{1}{2}\{\delta_e\}^T[K_{\sigma THe}]\{\delta_e\} + \frac{1}{2}\{\delta_e\}^T[K_{\sigma Re}]\{\delta_e\} \tag{2.70}$$

2.6. Governing equation of motion

The governing equation for the dynamic equilibrium of the rotating composite conical panel is derived using Lagrange's equation of motion as given by [170]

$$\frac{d}{dt}\left[\frac{\partial}{\partial\dot{\delta}}(T_K - U)\right] - \frac{\partial}{\partial\delta}(T_K - U) = \{F^{out}\} \tag{2.71}$$

where $\{F^{out}\}$ is the externally applied load vector.

Substituting the expressions of T_{KE} and U_e into **Eq. (2.71),** the dynamic equilibrium equation of the conical shell element is derived as

$$[M_e]\{\ddot{\delta}_e\} + [C_e]\{\dot{\delta}_e\} + ([K_e] + [K_{\sigma THe}] + [K_{\sigma Re}] - [K_{Re}])\{\delta_e\} = \{F_{\Omega e}\} + \{P_e^{TH}\} + \{F_e\} \tag{2.72}$$

In the case of moderate rotating speed for which the matrices $[C_e]$ and $[K_{Re}]$ are ignored, the dynamic equilibrium equation of the conical shell element is reduced to

$$[M_e]\{\ddot{\delta}_e\} + ([K_e] + [K_{\sigma THe}] + [K_{\sigma Re}])\{\delta_e\} = \{F_{\Omega e}\} + \{P_e^{TH}\} + \{F_e\} \tag{2.73}$$

where $[M_e]$, $[K_e]$, $[K_{\sigma THe}]$, $[K_{\sigma Re}]$, and $\{P_e^{TH}\}$ represent the elemental mass matrix, elemental elastic stiffness matrix, elemental geometric stiffness matrix due to thermal load, elemental

geometric stiffness matrix due to rotational load, and elemental thermal load vector, respectively, and are defined as

$$[M_e] = \int_{-1}^{1}\int_{-1}^{1} [N]^T [m_l] [N] |J| d\xi d\eta \tag{2.74}$$

$$[K_e] = \int_{-1}^{1}\int_{-1}^{1} [B]^T [D][B] |J| d\xi d\eta \tag{2.75}$$

$$[K_{\sigma THe}] = \int_{-1}^{1}\int_{-1}^{1} [G]^T [S_{TH}][G] |J| d\xi d\eta \tag{2.76}$$

$$[K_{\sigma Re}] = \int_{-1}^{1}\int_{-1}^{1} [G]^T [S_R][G] |J| d\xi d\eta \tag{2.77}$$

$$\{P_e^{TH}\} = \int_{-1}^{1}\int_{-1}^{1} [B]^T [F^{TH}] |J| d\xi d\eta \tag{2.78}$$

The integrals in the above expressions are numerically solved by using (2X2) Gaussian quadrature. The dynamic equilibrium equation is obtained by assembling all the elemental matrices and force vectors in the global form as below,

$$[M]\{\ddot{\delta}\} + ([K] + [K_\sigma]_{Th} + [K_\sigma]_{Rot})\{\delta\} = \{F(\Omega^2)\} + \{P^{TH}\} + \{F\} \tag{2.79}$$

where $[M], [K], [K_{\sigma TH}]$, and $[K_{\sigma R}]$ indicate the global mass matrix, global elastic stiffness matrix, global geometric stiffness matrices due to thermal and rotational loads, respectively, $\{\delta\}$ represents the global displacement vector, $F(\Omega^2)$ is the nodal equivalent centrifugal load vector, $\{F\}$ denotes the global externally applied load vector, and $\{P^{TH}\}$ is the global thermal load vector. In the case of moderate rotating speed for which the matrices $[C]$ and $[K_\sigma]_R$ may be neglected, the expression of the dynamic equilibrium is reduced to [54]

$$[M]\{\ddot{\delta}\} + ([K] + [K_\sigma]_{Th} + [K_\sigma]_{Rot})\{\delta\} = \{F(\Omega^2)\} + \{P^{TH}\} + \{F\} \tag{2.80}$$

The matrix $[K_{\sigma R}]$ depends on initial stress distribution due to rotational load and is estimated by iterative procedure [34] upon solving: [54]

$$([K] + [K_\sigma]_{Th} + [K_\sigma]_{Rot})\{\delta\} = \{F(\Omega^2)\} \tag{2.81}$$

First, stresses due to rotational load are converged to zero and the above equation becomes [54]

$$([K] + [K_\sigma]_{Th})\{\delta\} = \{F(\Omega^2)\} \tag{2.82}$$

Solving **Eq. (2.82)** gives the first set of stress distribution, then **Eq. (81)** becomes [54]

$$([K] + [K_\sigma]_{Th}) + [K_{\sigma R}]_1)\{\delta\} = \{F(\Omega^2)\} \tag{2.83}$$

The solution of the above equation gives a new set stress distribution in the form of displacement $\{\delta\}$, and the stresses may be found after convergence (generally within two iterations).

2.7 Boundary conditions

In finite element analysis, the boundary conditions are imposed by considering or vanishing the generalized displacements $u, v, w, \beta_x, \beta_y$ at the different nodes of the discretized structure.

The essential boundary conditions of the cantilevered conical shell are:

$$u = v = w = \theta_x = \theta_y = 0 \ ; \ x = 0 \tag{2.84}$$

2.8 Formulating free vibration problem

The natural frequencies and eigenvectors are obtained by solving the equations of motion. Initially, the initial strains developed owing to the thermal and the rotational effects are evaluated upon solving for δ_{static} considering both the thermal and centrifugal loadings as below, [56]

$$([K] + [K_\sigma]_{Th} + [K_\sigma]_{Rot})\{\delta_{static}\} = \{F\}_{Thermal} + \{F\}_{Centrifugal} \tag{2.85}$$

where δ_{static} is the static equilibrium solution as a result of the combined effects of thermal and centrifugal loads.

In case of the dynamic analyses, both the static as well as the time-dependent components are considered where the displacement vector $\{\delta\}$ is expressed as the sum of a static and a dynamic term. Thus, [56]

$$\{\delta\} = \{\delta_{static}\} + \{\delta_p\} \tag{2.86}$$

where $\{\delta_p\}$ is a small linear time-dependent perturbation about the static deflected position $\{\delta_{static}\}$.

The equation of motion for free vibration is given by

$$[M]\{\ddot{\delta}\} + ([K] + [K_\sigma]_{Th} + [K_\sigma]_{Rot})\{\delta\} = 0 \tag{2.87}$$

Assuming harmonic vibrations, $\{\delta\} = \{\delta\}\exp(i\omega_n t)$ we have

$$\left[([K] + [K_\sigma]_{Th} + [K_\sigma]_{Rot}) - \omega_n^2[M]\right]\{\delta\} = 0 \tag{2.88}$$

This is a standard eigenvalue problem, and is solved for the eigenvalues and eigenvectors by the QR iteration algorithm [36].

$$[\mathcal{A}]\{\delta\} = \lambda\{\delta\} \tag{2.89}$$

where $[\mathcal{A}] = ([K] + [K_\sigma]_{TH} + [K_\sigma]_{Rot})^{-1}[M]$, and $\lambda = 1/\omega_n^2$

2.9 Low velocity impact problem

In the impact problem, the composite conical shell is subjected to impact with a solid spherical mass (m_{imp}) and radius r_{imp} moving with an initial velocity of V_0.

Taking into account the contact force vector $\{F_C\}$ resulting from the low-velocity impact phenomenon, the dynamic equilibrium equation can be expressed as [142]

$$[M]\{\ddot{\delta}\} + ([K] + [K_{\sigma TH}] + [K_{\sigma R}])\{\delta\} = \{F(\Omega^2)\} + \{P^{TH}\} + \{F_C\} \tag{2.90}$$

where $\{F_C\}$ signifies the contact force vector resulted from impact on the "i^{th}" node expressed as [142]

$$\{F_C\} = \{0 \quad 0 \quad 0 \ldots F_{ci} \ldots 0 \quad 0 \quad 0\} \tag{2.91}$$

where F_{ci} denotes the contact force at the i^{th} node where impacted occurs.

The dynamic equilibrium equation of the impactor can be expressed as [142]

$$m_{imp}\ddot{w}_{imp} + F_c = 0 \tag{2.92}$$

where m_{imp} and $\ddot{w}_{imp}$ are the mass and acceleration of the impactor, respectively.

The contact force is evaluated based on the Hertzian contact law that relates the contact force with the indentation. The local indentation $a(t)$ at the impact location on the composite conical shell target is defined as [142]

$$a(t) = w_{imp} - w_s \cos\psi \tag{2.93}$$

where w_{imp} denotes the impactor displacement and w_s indicates the mid-surface shell displacement.

According to modified Hertzian contact law [130], the contact force during loading cycle of impact is estimated as [142]

$$F_C = k_c a^{1.5} \quad 0 < a \leq a_m \tag{2.94}$$

where a_m denotes the maximum contact force and indentation during loading cycle and k_c the modified contact stiffness for the impact phenomenon.

The modified contact stiffness (k_c) is given by [142]

$$k_c(T) = \frac{4}{3}\frac{\left[\frac{1}{r_{imp}} + \frac{1}{2r_y(L/2,0)}\right]^{-1/2}}{\left[\frac{1-\nu_{imp}^2}{E_{imp}} + \frac{1}{E_{22}(T)}\right]} \tag{2.95}$$

where the terms E_{imp}, and ν_{imp} Young's modulus and Poisson's ratio of the spherical impactor, while $E_{22}(T)$ and r_y denotes Young's modulus in transverse direction and radius of curvature in $y-$ direction of the target composite conical shell.

It is assumed that permanent indentation occurs even at comparatively lower values of impact load, and the unloading phase of the impact process differs notably from the loading phase. The reloading curve is different from the unloading curve during subsequent reloading. The contact force upon unloading and reloading can be given as [142]

$$F_C = F_m\left(\frac{a-a_p}{a_m-a_p}\right)^{2.5} \text{ for loading cycle} \tag{2.96}$$

$$F_C = F_m\left(\frac{a-a_p}{a_m-a_p}\right)^{1.5} \text{ for reloading cycle} \tag{2.97}$$

where F_m is the maximum contact force at the commencement of the unloading cycle and a_p indicate the permanent indentation during contact period and is estimated from the following expression [142]

$$a_p = \begin{cases} 0 & \text{if } a_m < a_{cr} \\ \beta_c(a_m - a_{cr}) & \text{if } a_m \geq a_{cr} \end{cases} \tag{2.98}$$

where $\beta_c = 0.094$ and $a_{cr} = 1.667\times10^{-1}$ mm

The dynamic equilibrium equations of the rotating composite conical shell and the impactor include the time-dependent contact force F_c. These equations can be treated as a system of ordinary differential equations with constant coefficients and are made to be satisfied at discrete time intervals Δt apart. Newmark's direct integration scheme [129, 130] is used to obtain the approximate time derivatives and solution of the forced vibration equations. Accordingly, the dynamic equilibrium equations can be written at the time $(t+\Delta t)$ as, [142]

$$[M]\{\ddot{\delta}\}^{t+\Delta t} + ([K] + [K_\sigma]_{TH})\{\delta\}^{t+\Delta t} = \{F_c\}^{t+\Delta t} \tag{2.99}$$

$$m_{imp}\{\ddot{w}_{imp}\}^{t+\Delta t} + \{F_c\}^{t+\Delta t} = 0 \tag{2.100}$$

The Eq. (2.99) can be rewritten in the following form [36]

$$\left[\hat{K}\right]\{\delta\}^{t+\Delta t} = \{F_c\}^{t+\Delta t} + \left\{\hat{R}\right\}^{t+\Delta t} \tag{2.101}$$

where the effective stiffness matrix $\left[\hat{K}\right]$ and effective load vector $\left\{\hat{R}\right\}$ for the target panel are determined as

$$\left[\hat{K}\right] = a_0[M] + [K] + [K_\sigma]_{TH} \tag{2.102}$$

$$\left\{\hat{R}\right\}^{t+\Delta t} = [M](a_0\{\delta\}^t + a_2\left\{\dot{\delta}\right\}^t + a_3\left\{\ddot{\delta}\right\}^t) \tag{2.103}$$

Similarly, the **Eq. (2.100)** is rearranged as

$$\hat{k}_{imp}{w_{imp}}^{t+\Delta t} = {\hat{f}_{imp}}^{t+\Delta t} \tag{2.104}$$

where the effective stiffness $\hat{k}_{imp}$ and effective load vector $\hat{f}_{imp}$ for the impactor are expressed as

$$\hat{k}_{imp} = a_0 m_{imp} \tag{2.105}$$

$${\hat{f}_{imp}}^{t+\Delta t} = m_{imp}\left(a_0{w_{imp}}^t + a_2{\dot{w}_{imp}}^t + a_3{\ddot{w}_{imp}}^t\right) - F_C^t \tag{2.106}$$

For each time step, the acceleration and the velocity of the target panel are obtained from the following expressions

$$\left\{\ddot{\delta}\right\}^{t+\Delta t} = a_0(\{\delta\}^{t+\Delta t} - \{\delta\}^t) - a_2\left\{\dot{\delta}\right\}^t - a_3\left\{\ddot{\delta}\right\}^t \tag{2.107}$$

$$\left\{\dot{\delta}\right\}^{t+\Delta t} = \{\delta\}^t + a_6\left\{\ddot{\delta}\right\}^t + a_7\left\{\ddot{\delta}\right\}^{t+\Delta t} \tag{2.108}$$

Similarly, the acceleration and the velocities of the impactor are obtained as

$$\left\{\ddot{w}_{imp}\right\}^{t+\Delta t} = a_0\left(\left\{w_{imp}\right\}^{t+\Delta t} - \left\{w_{imp}\right\}^t\right) - a_2\left\{\dot{w}_{imp}\right\}^t - a_3\left\{\ddot{w}_{imp}\right\}^t \tag{2.109}$$

$$\left\{\dot{w}_{imp}\right\}^{t+\Delta t} = \left\{w_{imp}\right\}^t + a_6\left\{\ddot{w}_{imp}\right\}^t + a_7\left\{\ddot{w}_{imp}\right\}^{t+\Delta t} \tag{2.110}$$

The following initial conditions are considered in the present analysis

$$\{\delta\}_{t=0} = \left\{\dot{\delta}\right\}_{t=0} = \left\{\ddot{\delta}\right\}_{t=0} = 0 \tag{2.111}$$

$$\left(w_{imp}\right)_{t=0} = \left(\ddot{w}_{imp}\right)_{t=0} = 0; \qquad \left(\dot{w}_{imp}\right)_{t=0} = V_0 \tag{2.112}$$

The integration constants a_i $(i = 1,2,3,4,5,6,7)$ used in **Eqs. (2.102) is** expressed as [36]

$$a_0 = \frac{1}{\alpha_n \Delta t^2}; \quad a_1 = \frac{\beta_n}{\alpha_n \Delta t}; \quad a_2 = \frac{1}{\alpha_n \Delta t}; \quad a_3 = \frac{1}{2\alpha_n} - 1; \tag{2.113}$$

$$a_4 = \frac{\beta_n}{\alpha_n} - 1; \quad a_5 = \frac{\Delta t}{2}\left(\frac{\beta_n}{\alpha_n} - 2\right); \quad a_6 = \Delta t(1 - \beta_n); \quad a_7 = \beta_n \Delta t$$

where the values $\alpha_n = 0.25$ and $\beta_n = 0.5$ are adopted based on the constant average acceleration method. The Eq. (61) is solved by the Gauss elimination technique, and the dynamic stresses are obtained at each time step. The time step for each impact case is chosen to satisfy the convergence of the time-based responses.

2.10 Multi Point Constraint Algorithm for Delamination

The mid plane delamination (*d*) is assumed to occur alongside of the span. The resultant forces and moments at delamination region are mathematically modeled [20] using shell element 1. For the undelaminated region element 2 and element 3 are detached by the delamination in the delaminated zone **(Fig. 2.6**). Nodal displacements of element 2 and element 3 are given by [53,54]

$$u_i = u_i' - (z - z_i)\theta_{xi},$$
$$v_i = v_i' - (z - z_i)\theta_{yi},$$
$$w_i = w_i'$$

(2.114)

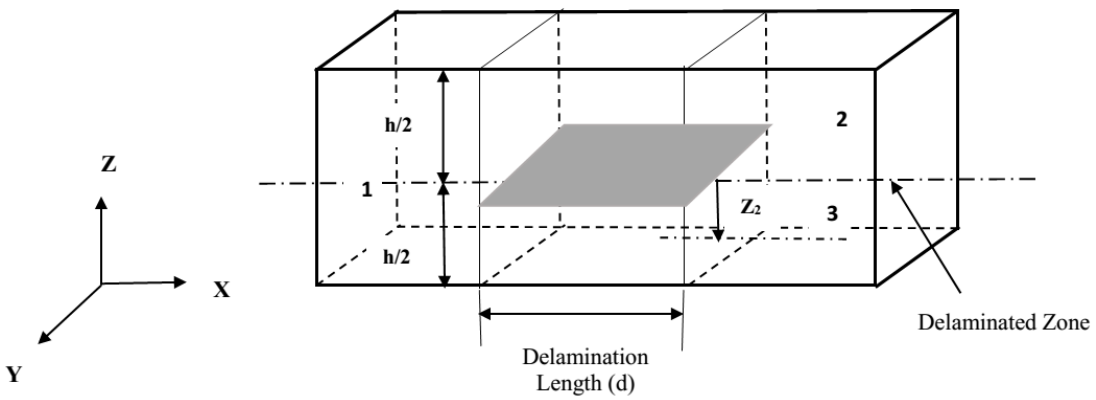

Fig. 2.6 Delamination Model

The mid plane displacements are u'_i, v_i', w_i'. At shared node the transverse displacements and rotations of all three shell elements are likewise in values and are given by [53,54]

$$w_1 = w_2 = w_3 = w,$$

$$\theta_{x1} = \theta_{x2} = \theta_{x3} = \theta_x,$$
$$\theta_{y1} = \theta_{y2} = \theta_{y3} = \theta_y$$

(2.115)

The in-plane displacements at the delamination region of all three elements are [53,54]

$$u_2' = u_1' - z_2'\theta_{x,}$$
$$u_3' = u_1' - z_3'\theta_{x,}$$
$$v_2' = v_1' - z_2'\theta_y,$$
$$v_3' = v_1' - z_3'\theta_y$$

(2.116)

For elements 1, 2, and 3 the strains vector from mid-plane are connected as [37,53,54]

$$\{\varepsilon_s'\}_j = \{\varepsilon_s'\}_1 + z_j'\{k\}$$

(2.117)

where $\{\varepsilon_s'\}$ is the strain vector and{k} is the curvature vector at the delamination zone for all the three elements.

where, $\{\varepsilon'\}\ and\ \{\kappa\}$ represents strain vector and the curvatures vector being identical at the crack tip for elements 1, 2 and 3. This equation can be considered as a special case for element 1 where z_1' is equal to zero. The in-plane stress resultants $\{N\}$ and the moment resultants $\{M\}$ of elements 2 and 3 considering the thermal effects can be expressed as [53,54]

$$\{N\}_j = [A]_j\{\varepsilon'\}_1 + \left(z'_j[A]_j + [B]_j\right)\{\kappa\} - \{F_e^N\} \qquad (j = 2, 3)$$

(2.118)

$$\{M\}_j = [B]_j\{\varepsilon'\}_1 + \left(z'_j[B]_j + [D]_j\right)\{\kappa\} - \{F_e^N\} \qquad (j = 2, 3)$$

(2.119)

where, $[A]$, $[B]$ and $[D]$ are the extension, bending-extension coupling and bending stiffness coefficients of the composite laminate, respectively. The resultant forces and moments at the delamination front for the elements 1, 2 and 3 satisfy the following equilibrium conditions [37]

$$\{N\} = \{N\}_1 = \{N\}_2 + \{N\}_3$$

$$\{M\} = \{M\}_1 = \{M\}_2 + \{M\}_3 + \bar{z}_2\{N\}_2 + \bar{z}_3\{N\}_3$$

$$\{Q\} = \{Q\}_1 = \{Q\}_2 + \{Q\}_3$$

(2.120)

where $\{Q\}$ denotes the transverse shear resultants.

2.11 First Ply Failure Criterion

The general criterion of failure for composite materials is the tensor polynomial criterion [104,105]

$$F_i\sigma_i + F_{ij}\sigma_i\sigma_j + F_{ijk}\sigma_i\sigma_j\sigma_k + \cdots \geq 1$$

(2.121)

where σ_i are the stress components along the material coordinates, while F_i, $F_{ij}$and F_{ijk} are the strength components along the principal material directions.

Maximum Stress Criterion (Independent)

The failure initiates when any one of the following criteria is satisfied, [104,105]

$$|\sigma_1| \geq X_T \text{ or } X_C; \quad |\sigma_2| \geq Y_T \text{ or } Y_C; \quad \sigma_4 \geq R; \quad \sigma_5 \geq S; \quad \sigma_6 \geq T$$

(2.122)

where σ_1 and σ_2 are the normal stress components while σ_4, σ_5 and σ_6 are the shear stress components. The normal strengths of the lamina along the 1 and 2 directions are (X_T, X_C) and (Y_T, Y_C), respectively, while *R*, *S*and *T* are the shear strengths of the lamina along the 2-3, 1-3, and 1-2 planes, respectively. The normal characteristics of stresses are compared with the corresponding tensile or compressive strengths.

Maximum Strain Criterion (Independent)

Failure of ply occurs if any of the following conditions are met, [104,105]

$$|\varepsilon_1| \geq X_{\varepsilon T} \text{ or } X_{\varepsilon C}; \quad |\varepsilon_2| \geq Y_{\varepsilon T} \text{ or } Y_{\varepsilon C}; \quad \varepsilon_4 \geq R_\varepsilon; \quad \varepsilon_5 \geq S_\varepsilon; \quad \varepsilon_6 \geq T_\varepsilon$$

(2.123)

where ε_1 and ε_2 are the normal strain components, while ε_4, ε_5, and ε_6 are the shear strain components; ($X_{\varepsilon T}$, $X_{\varepsilon C}$) and ($Y_{\varepsilon T}$, $Y_{\varepsilon C}$) are the lamina normal strain strengths, while R_ε, S_ε, and T_ε are the shear strain strengths of the lamina along the 2-3, 1-3 and 1-2 planes, respectively.

Maximum Stress Criterion (Polynomial)

The polynomial type maximum stress criterion is [104,105]

$$(\sigma_1-X_T)(\sigma_1+X_C)(\sigma_2-Y_T)(\sigma_2+Y_C)(\sigma_4-R)(\sigma_4+R)(\sigma_5-S)(\sigma_5+S)(\sigma_6-T)(\sigma_6+T)=0$$

(2.124)

Hoffmann Criterion

The mathematical expression of failure for this criterion is [104,105]

$$\frac{1}{2}\left(\frac{1}{X_TX_C}-\frac{1}{Y_TY_C}\right)\sigma_1^2+\frac{1}{2}\left(\frac{1}{Y_TY_C}-\frac{1}{X_TX_C}\right)\sigma_2^2 + \frac{1}{2}\left(\frac{1}{X_TX_C}+\frac{1}{Y_TY_C}\right)(\sigma_1-\sigma_2)^2+\left(\frac{1}{X_T}-\frac{1}{X_C}\right)\sigma_1+\left(\frac{\sigma_6}{S}\right)^2\geq 1$$

(2.125)

Tsai-Hill Criterion

Ply-failure initiates if the following criterion is, [104,105]

$$\left(\frac{\sigma_1}{X}\right)^2+\left(\frac{\sigma_2}{Y}\right)^2-\left(\frac{1}{X^2}+\frac{1}{Y^2}\right)\sigma_1\sigma_2+\left(\frac{\sigma_6}{S}\right)^2\geq 1$$

(2.126)

Tsai-Wu Criterion

In present FE analysis Tsai-Wu failure criterion is also selected. The mathematical relation for this criterion is [104,105]

$$\left(\frac{1}{X_T}-\frac{1}{X_C}\right)\sigma_1+\left(\frac{1}{Y_T}-\frac{1}{Y_C}\right)\sigma_2+\frac{1}{X_TX_C}\sigma_1^2+\frac{1}{Y_TY_C}\sigma_2^2-\frac{1}{2}\sqrt{X_TX_CY_TY_C}\sigma_1\sigma_2+\left(\frac{\sigma_6}{S}\right)^2\geq 1$$

(2.127)

CHAPTER 3:

First Ply Failure of Pre-twisted Delaminated Rotating Composite Conical Shells

3.1 Overview

Computer codes are established based on the present FE formulation and used to investigate the FPF loads in delaminated pre-twisted composite conical shells. The analyses involve determination of the FPF loads of delaminated graphite-epoxy composite pre-twisted conical shells having single or multiple delaminations for a range of rotational speeds. Appendix includes a flowchart of the steps involved in the computation of the FPF loads. At first, the convergence and the validation study of the present FE formulation are presented. Afterward, the analysis is are carried out considering the effects of pre-twist angle, location and presence of delamination, rotational speed, and stacking sequence of the conical shell laminates on the FPF loads. The pre-twisted conical shells are assumed to be subjected to a transverse central point load, and the FPF loads are evaluated based on the well-established failure-criterions namely, maximum strain, maximum stress (Independent and polynomial based), Hoffmann, Tsai-Hill, and Tsai-Wu criteria. The failure locations on the conical shell surface (*x-y* plane) and the failed-ply location are recognized in terms of the element number and the first-failed ply number at which the failure initiates. The ply numbers are sequentially started from the top to the bottom of the laminate. At first ply failure load principal stress (σ_1 & σ_2) and plane stress (τ_{12}) at are plotted.

3.2 *System Capabilities*

The entire analysis is done using FORTRAN based FEM codes on i5 processor based system with clock speed of 4.1 GHz with 16GB RAM. For 6X6 mesh size analysis it takes around 10 minutes. And for 8X8 mesh size it takes around 15 minutes. For transient analysis it takes around 40 minutes for each analysis. The surface plot of different stresses are done on MATLAB and graphs are plotted using ORIGIN software.

3.3 *Parametric Study*

The FPF loads are computed for the laminates in respect of different pre-twist angles (0° and 30°), delamination locations (d_1/L=0.25, 0.50, and 0.75), delamination sizes (d/L=0.00, 0.25and

0.50)and non-dimensional rotational speeds ($\Omega = \frac{\omega_z}{\omega_0} = 0.00, 0.25, 0.50, 0.75$ and 1.00). The relevant geometrical dimensions of the conical shell assumed are s=0.4 m, L/s=0.7, s/h=100, θ_0=20° and θ_v=20°. The material properties and corresponding strength parameters of the graphite-epoxy composite lamina adopted in the present analysis are given below [104]:

E_1=142.5 GPa, E_2=9.79 GPa, G_{12}=G_{13}=4.72 GPa, G_{23}=1.192 GPa, v_{12}=0.27,X_T=2193.50 MPa, X_C=2457.0 MPa, Y_T=41.30 MPa, Y_C=206.80 MPa, R=61.28 MPa, S=T=78.78 MPa, $X_{\varepsilon T}$=0.015393, $X_{\varepsilon C}$=0.017242, $Y_{\varepsilon T}$=0.004128, $Y_{\varepsilon C}$=0.021124, R_ε=0.051409, S_ε=T_ε=0.016691

3.4 Convergence and Validation

For the convergence study, the FPF loads [**Table 3.1(a) and 3.1(b)**] of both untwisted and pre-twisted laminated composite[$(0/90/0/90/0)_s$ and $(45/-45/90/0/45/90/-45/0)_s$] conical shell subjected to a centrally applied point load (F_P) are obtained for different mesh sizes of (6×6), (8×8) and (10×10). The FPF loads converged at a mesh size of (8×8), as evident from both **Tables 3.1(a)** and **3.1(b)**. Considering the ease of computations, a converged mesh size of (8×8) with 225 nodes (**Fig. 3.1**) is used in the whole analysis. Assuming five degrees of freedom at each node, the total number of degrees of freedom (DOFs) is given by 1040 (225*5-17*5=1040) for the cantilever boundary condition with the 17 nodes on the left edge are fixed. The validation of the model of the shallow conical shell for FE analysis is compared with Liew et al. [1] for its vibration behavior in **Table 3.2.** The effect of delamination length on the natural frequencies of the delaminated cantilever composite plates is compared with those of Zak et al. [53], as shown in **Fig. 3.2.** **Table 3.3** compares the FPF loads predicted by the present codes and compared with Kam et al. [104]. The good close agreement between the present FEM results with established literature confirms the validity of the developed codes to carry out the present analyses.

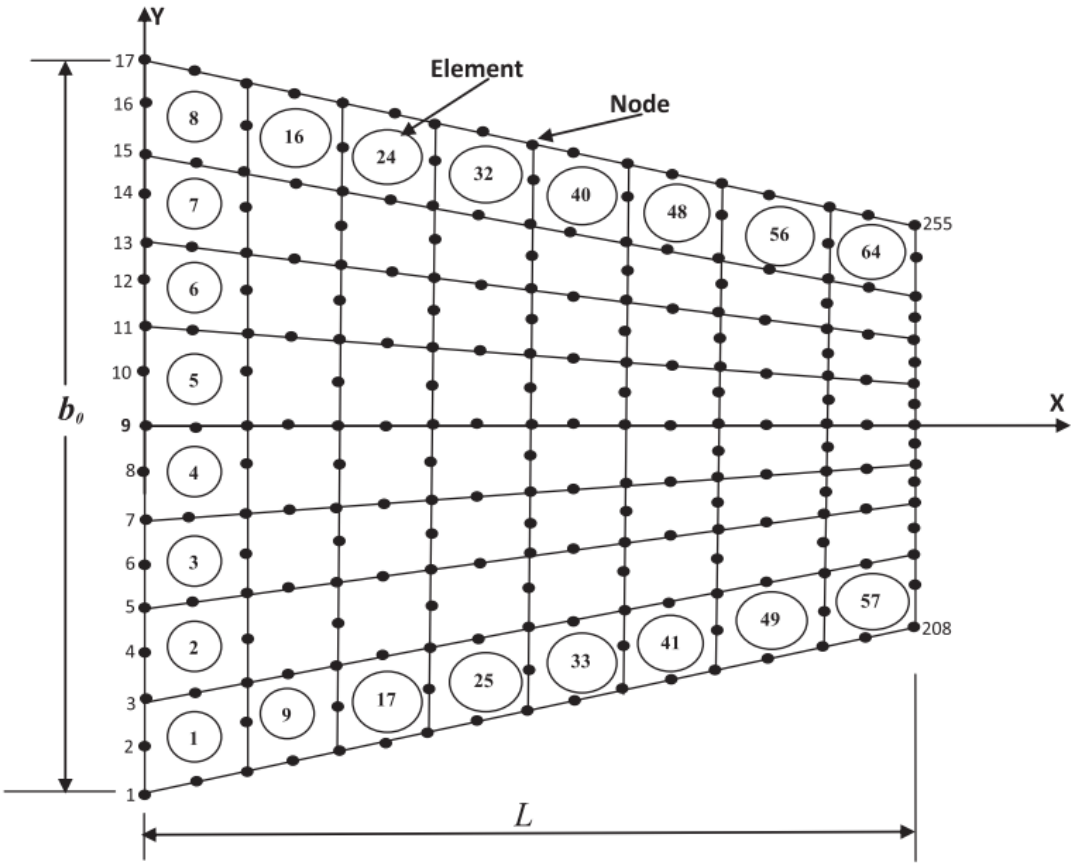

Fig. 3.1 Finite Element Mesh representation of the plan form of the conical shell

Table 3.1(a): Convergence of the FPF loads (N) for non-rotating (Ω=0.0) laminated composite $[(0/90/0/90/0)_s]$ conical shell subjected to a centrally applied point load (F_P) for different mesh sizes of (6×6), (8×8) and (10×10) [(†Failed Element, ‡Failed-ply from the bottom)]

Failure Criterion	**Untwisted Conical Shell (ψ=0°)**			**Pre-twisted Conical Shell (ψ=30°)**		
	(6×6)	**(8×8)**	**(10×10)**	**(6×6)**	**(8×8)**	**(10×10)**
Max. Strain	224.19 (1†,9‡)	220.08 (1,9)	218.65 (1,9)	219.38 (1,9)	214.74 (1,9)	212.95 (1,9)
Max. Stress (Independent)	230.54 (1,9)	226.20 (1,9)	224.67 (1,9)	225.71 (1,9)	220.79 (1,9)	218.87 (1,9)

Max. Stress (Polynomial)	230.34 (1,9)	226.04 (1,9)	224.54 (1,9)	225.61 (1,9)	220.68 (1,9)	218.76 (1,9)
Hoffmann	230.44 (1,9)	226.14 (1,9)	224.62 (1,9)	225.72 (1,9)	220.78 (1,9)	218.86 (1,9)
Tsai-Hill	230.40 (1,9)	226.09 (1,9)	224.58 (1,9)	225.64 (1,9)	220.72 (1,9)	218.79 (1,9)
Tsai-Wu	229.96 (1,9)	225.68 (1,9)	224.18 (1,9)	225.19 (1,9)	220.31 (1,9)	218.61 (1,9)

Table 3.1(b): Convergence of the FPF loads (N) for non-rotating (Ω=0.0) laminated composite [(45/-45/90/0/45/90/-45/0)$_s$] conical shell subjected to a centrally applied point load (F_P) for different mesh sizes of (6×6), (8×8) and (10×10) [(†Failed Element, ‡Failed-ply from the bottom)]

Failure Criterion	**Untwisted Conical Shell (ψ=0°)**			**Pre-twisted Conical Shell (ψ=30°)**		
	(6×6)	**(8×8)**	**(10×10)**	**(6×6)**	**(8×8)**	**(10×10)**
Max. Strain	101.63 ($1^{\dagger}$,$14^{\ddagger}$)	99.28 (1,14)	98.03 (1,14)	100.15 (1,14)	97.94 (1,14)	96.91 (1,14)
Max. Stress (Independent)	111.49 (1,14)	109.11 (1,14)	107.94 (1,14)	111.33 (1,14)	108.71 (1,14)	107.66 (1,14)
Max. Stress (Polynomial)	110.77 (1,14)	108.07 (1,14)	107.21 (1,14)	109.68 (1,14)	107.09 (1,14)	105.97 (1,14)
Hoffmann	112.30 (1,14)	109.91 (1,14)	108.89 (1,14)	111.27 (1,14)	108.55 (1,14)	107.40 (1,14)
Tsai-Hill	110.94 (1,14)	108.31 (1,14)	107.26 (1,14)	109.74 (1,14)	107.16 (1,14)	105.99 (1,14)
Tsai-Wu	108.69 (1,14)	106.48 (1,14)	105.32 (1,14)	107.97 (1,14)	105.44 (1,14)	104.31 (1,14)

Table 3.2. Non-dimensional fundamental frequencies ($\lambda = \omega_n b_0^2\sqrt{\rho h/D}$), $D = Eh^3/12(1-\nu^2)$ of pre-twisted shallow conical shell [1]

Pre-twist Angle (ψ)	Aspect Ratio (*L*/s)	Present (4×4)	Present (6×6)	Present (8×8)	Present (10×10)	Liew et al. [1]	% Variation with (10X10) mesh size
30°	0.6	0.28387	0.28103	0.27855	0.27801	0.28828	3.56%
	0.7	0.25426	0.25125	0.25077	0.25054	0.25752	2.71%
	0.8	0.23896	0.23657	0.23642	0.23630	0.24179	2.27%

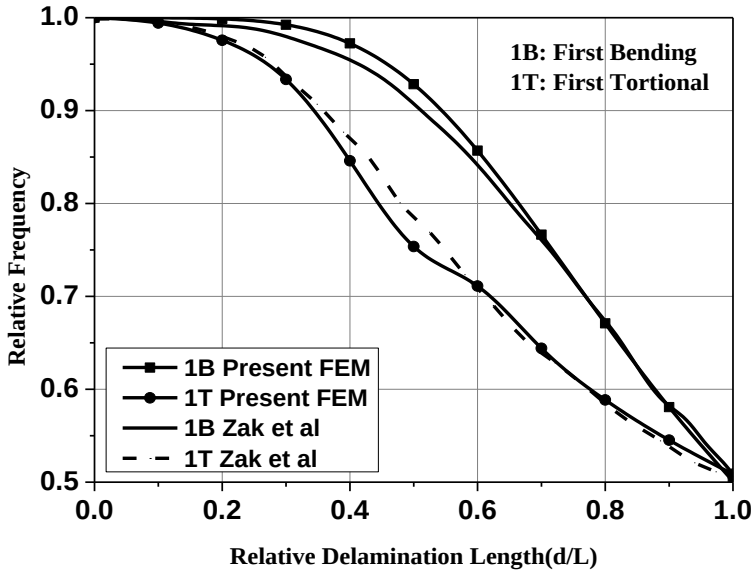

Fig. 3.2. The variation of relative frequencies of graphite-epoxy composite plate $[(\pm 45°)_4]$ clamped at one side with relative delamination length. [53]

Table 3.3. FPF loads for the partially clamped laminated plate under centrally applied transverse point load [104]

Failure criterion	$(0/90)_s$		$(0_2/90)_s$		$(0_2/90_2)_s$		(0/90/0/90)s	
	Kam et al.	Present FEM	Kam et al.	Present FEM	Kam et al.	Present FEM	Kam et al.	Present FEM
Max. Strain	76.04	78.40	122.86	116.41	267.55	260.38	355.47	353.81
Max. Stress	64.94	68.67	108.26	105.46	229.11	229.09	290.12	296.06
Max. Stress (polynomial)	63.52	67.11	106.34	103.55	222.43	222.19	278.12	281.22
Hoffmann	63.60	66.46	106.45	102.74	222.69	220.13	278.53	278.01
Tsai-Hill	64.03	67.76	107.06	104.36	224.19	224.97	280.81	286.92
Tsai-Wu	68.30	69.91	112.77	106.96	238.60	230.99	304.13	295.26

3.5 Result and Discussion

3.5.1 Effect of Delamination size and Aspect ratio of the Untwisted Conical Shell

The FPF failure loads of both intact and single-delaminated 16-layered composite pre-twisted laminated conical shells(I) {$[(45/-45/90/0/45/90/-45/0)_s]$,(II) $[(45/0/-45/0/-45/90/0/45)_s]$ and(III) $[(45/-45/0/90/45/0/-45/90)_s]$} under centrally applied point load are presented in **Table 3.4(a)-(c),** for different aspect ratio(L/s=0.6, 0.7 and 0.8), pre-twist angles ($\psi=0^0$ and 30^0) and different delamination sizes (25% and 50% mid-plane delamination). A decrease in the FPF loads are predicted by all the failure theories, with an increase in the aspect ratio in both undelaminated and delaminated composite conical shells for all the laminate configurations (I, II, and III). There is an increase in the flexibility of the cantilevered conical shell with an increase in its span length. The percentage drop in the FPF loads are drastic for an increase in the delamination size from 25% to 50%, suggesting that delamination plays a pivotal role in the failure initiation of delaminated shells. This is corroborated by the failure initiation zone being close to the delamination line near the fixed end (**Fig. 3.4**), as is evident with the failed elements being (25,32) for 25% delaminated and (17,24) for 50% delaminated conical shells. However, the failed element in an intact conical shell is located near the edge of the fixed element (Element No. 1) at all aspect ratios, as predicted

by all the failure theories. For intact shells, the fixed ends are prone to failure initiation because the maximum bending moments develop there. The failed lamina is located at the outermost layers (the 13th, 14thand 16thply) since the highest bending stresses always develop near the outer layers of the point-loaded conical shell. In general, the highest first-ply failure loads are observed for laminate (II) compared to laminates (I) and (III), indicating that the failure loads are highly dependent on the choice of the stacking sequence of the laminates. The spatial distribution of the stresses (σ_1, σ_2 and τ_{12}) and deflection for laminate (II) and aspect ratio L/s=0.7 of untwisted intact laminated (d/L =0.00) and delaminated (d/L =0.50 and d_1/L=0.50) composite conical shell subjected to the respective failure centrally point loads are illustrated in **Figs. 3.5** and **3.6**, respectively. From **Fig. 3.4**, σ_1 values are much higher near the fixed end in comparison of σ_2 and (σ_1, σ_2 and σ_6) values are always tensile for undelaminated composite conical shells. Since, the laminates have lower X_T and Y_T values, σ_1 plays the predominant role in the tensile failure of the laminates. This is evident from **Table 3.4(b)** where the failed elements are near the fixed end (Element no 1 or 8) where σ_1 is maximum. However, from **Fig. 3.3**, it is observed that a zone of high compressive stress (σ_1, σ_2 and σ_6) is developed near the centrally located delaminated zone, as indicated by the blue-colored contour lines. Since the delaminated zone has much lower strength than the rest of the laminate, the failure initiates at delaminated, zone. It can be clearly correlated from **Table 3.4(b)** where the failure initiates near the delaminated zone (Element No: 17, 24, 25, and 32) for both 25% and 50% delaminated conical shells in general.

Table 3.4(a): FPF loads (N) for laminate (I) $[(45/-45/90/0/45/90/-45/0)_s]$with centrally located delamination sizes (d/L =0.00, 0.25 and 0.50; d_1/L=0.50) of the untwisted conical shell (ψ=0^0) for different aspect ratios (L/s) of the conical shell and delamination sizes subjected to a point load (F_P). [(†Failed Element, ‡Failed-ply from the bottom)]

Failure Criterion	***L*/s=0.6**			***L*/s=0.7**			***L*/s=0.8**		
	Intact Shell	**25% Delam**	**50% Delam**	**Intact Shell**	**25% Delam**	**50% Delam**	**Intact Shell**	**25% Delam**	**50% Delam**
Max. Strain	113.38 (1†,14‡)	106.17 (25,14)	50.37 (17,14)	99.28 (1,14)	89.37 (25,14)	43.15 (17,14)	88.31 (1,14)	77.57 (25,14)	37.31 (17,14)
Max. Stress (Independent)	124.29 (1,14)	121.33 (25,14)	58.62 (17,14)	109.11 (1,14)	101.93 (25,14)	49.37 (17,14)	98.89 (1,14)	88.29 (25,14)	43.04 (17,14)

Max. Stress (Polynomial)	123.14 (1,14)	120.54 (25,14)	57.29 (17,14)	108.07 (1,14)	100.21 (25,14)	48.96 (17,14)	99.21 (1,14)	87.44 (32,14)	44.64 (17,14)
Hoffmann	124.09 (1,14)	121.29 (25,14)	58.12 (17,14)	109.91 (1,14)	101.37 (25,14)	49.54 (17,14)	98.34 (1,14)	88.29 (25,14)	43.78 (17,14)
Tsai-Hill	125.26 (1,14)	120.84 (25,14)	57.94 (17,14)	108.31 (1,14)	101.91 (25,14)	50.08 (17,14)	98.68 (1,14)	87.37 (25,14)	43.91 (17,14)
Tsai-Wu	120.35 (1,14)	116.37 (25,14)	55.47 (17,14)	106.48 (1,14)	97.16 (25,14)	47.36 (17,14)	95.91 (1,14)	85.14 (25,14)	41.22 (17,14)

Table 3.4(b): FPF loads (N) for laminate (II) $[(45/0/-45/0/-45/90/0/45)_s]$having centrally located delamination sizes (d/L =0.00, 0.25 and 0.50; d_1/L=0.50) of the untwisted conical shell ($\psi=0^0$) for different aspect ratios (L/s) of the conical shell and delamination sizes subjected to a point load (F_P)

Failure Criterion	***L*/s=0.6**			***L*/s=0.7**			***L*/s=0.8**		
	Intact Shell	**25% Delam**	**50% Delam**	**Intact Shell**	**25% Delam**	**50% Delam**	**Intact Shell**	**25% Delam**	**50% Delam**
Max. Strain	309.11 (1,11)	306.28 (1,11)	119.38 (24,2)	265.59 (1,11)	253.31 (32,11)	101.34 (24,2)	237.34 (1,11)	214.39 (32,11)	85.14 (23,2)
Max. Stress (Independent)	335.39 (8,16)	330.16 (8,16)	148.25 (24,2)	**269.71 (8,16)**	236.69 (25,16)	**111.65 (17,16)**	273.97 (1,16)	258.74 (25,16)	107.98 (24,2)
Max. Stress (Polynomial)	245.41 (8,16)	243.37 (8,16)	127.09 (24,16)	188.34 (8,16)	187.35 (32,16)	92.98 (24,16)	199.26 (8,16)	193.53 (8,16)	96.25 (24,16)
Hoffmann	243.38 (8,16)	241.49 (8,16)	126.14 (24,16)	188.91 (8,16)	187.21 (32,16)	92.72 (24,16)	197.15 (8,16)	192.37 (8,16)	97.37 (24,16)
Tsai-Hill	265.35 (8,16)	263.13 (8,16)	141.67 (24,16)	209.37 (8,16)	208.94 (32,16)	102.37 (24,16)	219.38 (8,16)	211.61 (8,16)	106.16 (24,16)
Tsai-Wu	249.07 (8,16)	244.07 (8,16)	127.29 (24,16)	189.74 (8,16)	187.67 (32,16)	91.68 (24,16)	196.73 (8,16)	191.28 (8,16)	96.83 (24,16)

Table 3.4(c): FPF loads (N) for laminate (III)[(45/-45/0/90/45/0/-45/90)$_s$] having centrally located delamination sizes (d/L=0.00, 0.25 and 0.50; d_1/L=0.50) of the untwisted conical shell (ψ=0^0) for different aspect ratios (L/s) of the conical shell and delamination sizes subjected to a point load (F_P)

Failure Criterion	***L*/s=0.6**			***L*/s=0.7**			***L*/s=0.8**		
	Intact Shell	**25% Delam**	**50% Delam**	**Intact Shell**	**25% Delam**	**50% Delam**	**Intact Shell**	**25% Delam**	**50% Delam**
Max. Strain	158.37 (1,13)	148.33 (25,13)	71.36 (17,13)	138.21 (1,13)	122.14 (25,13)	61.39 (17,13)	123.38 (1,13)	104.05 (25,12)	52.21 (17,13)
Max. Stress (Independent)	177.51 (1,13)	173.67 (25,13)	84.79 (17,13)	156.34 (1,13)	143.27 (32,13)	71.84 (17,13)	139.07 (1,13)	122.19 (32,13)	63.35 (17,13)
Max. Stress (Polynomial)	176.35 (1,13)	169.72 (32,13)	82.44 (24,16)	140.25 (8,16)	123.58 (32,16)	61.25 (24,16)	138.96 (1,13)	120.37 (32,13)	61.71 (17,13)
Hoffmann	175.61 (8,16)	170.34 (32,16)	81.05 (24,16)	139.34 (8,16)	123.27 (32,16)	61.37 (24,16)	140.61 (1,13)	121.45 (32,13)	62.96 (24,16)
Tsai-Hill	177.38 (1,13)	169.67 (25,13)	84.18 (17,13)	154.89 (8,16)	138.29 (32,16)	68.17 (24,16)	138.58 (1,13)	120.87 (32,13)	61.87 (17,13)
Tsai-Wu	171.93 (1,13)	163.28 (25,13)	79.62 (17,13)	141.08 (8,16)	124.61 (32,16)	61.52 (24,16)	134.73 (1,13)	116.34 (25,13)	59.23 (17,13)

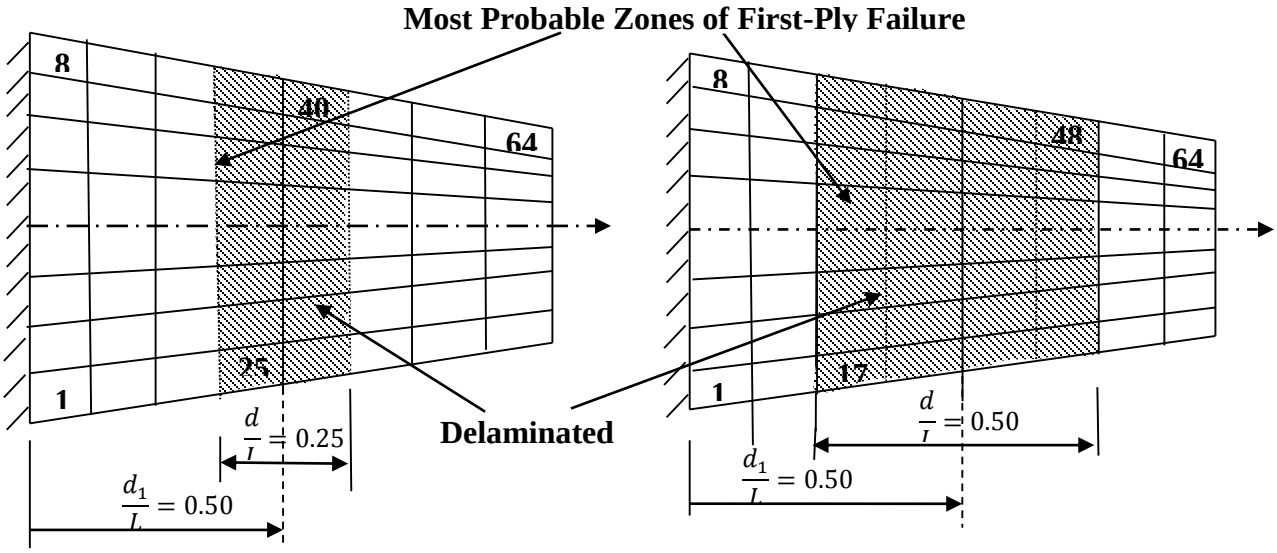

Fig. 3.3 Location of delaminated zone and most probable zones of failure initiation in 25% ($\frac{d}{L}$ = 0.25) and 50% ($\frac{d}{L}$ = 0.50) mid-delaminated ($\frac{d_1}{L}$ = 0.50) composite conical shell

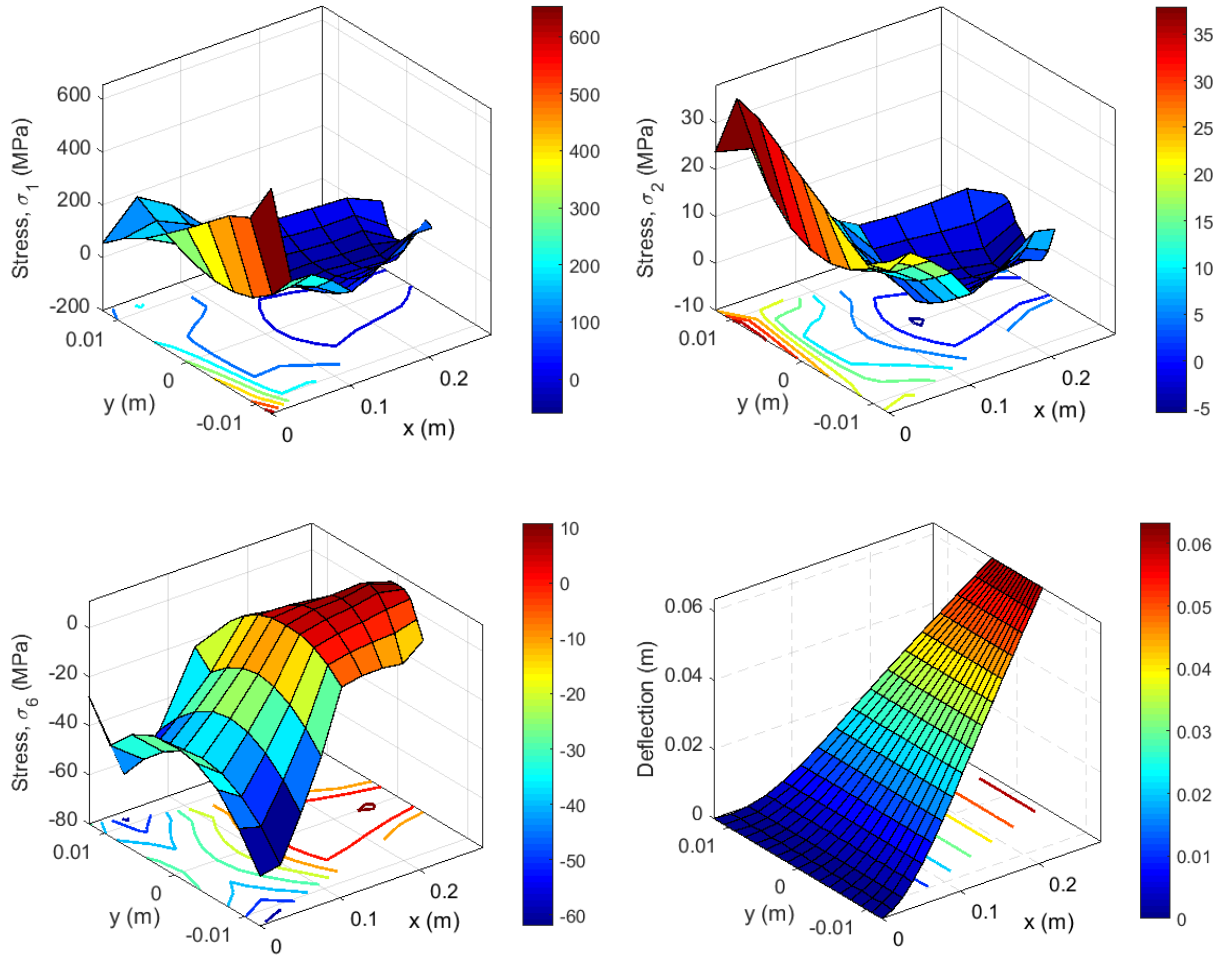

Fig. 3.4 Spatial distribution of stresses and deflection for laminate (II) $[(45/0/-45/0/-45/90/0/45)_s]$ and aspect ratio L/s=0.7 of the untwisted (ψ=0^0) intact laminated composite conical shell subjected to a failure point load F_P=269.71N as predicted by maximum stress (independent) theory (marked in bold in **Table 4(b)**).

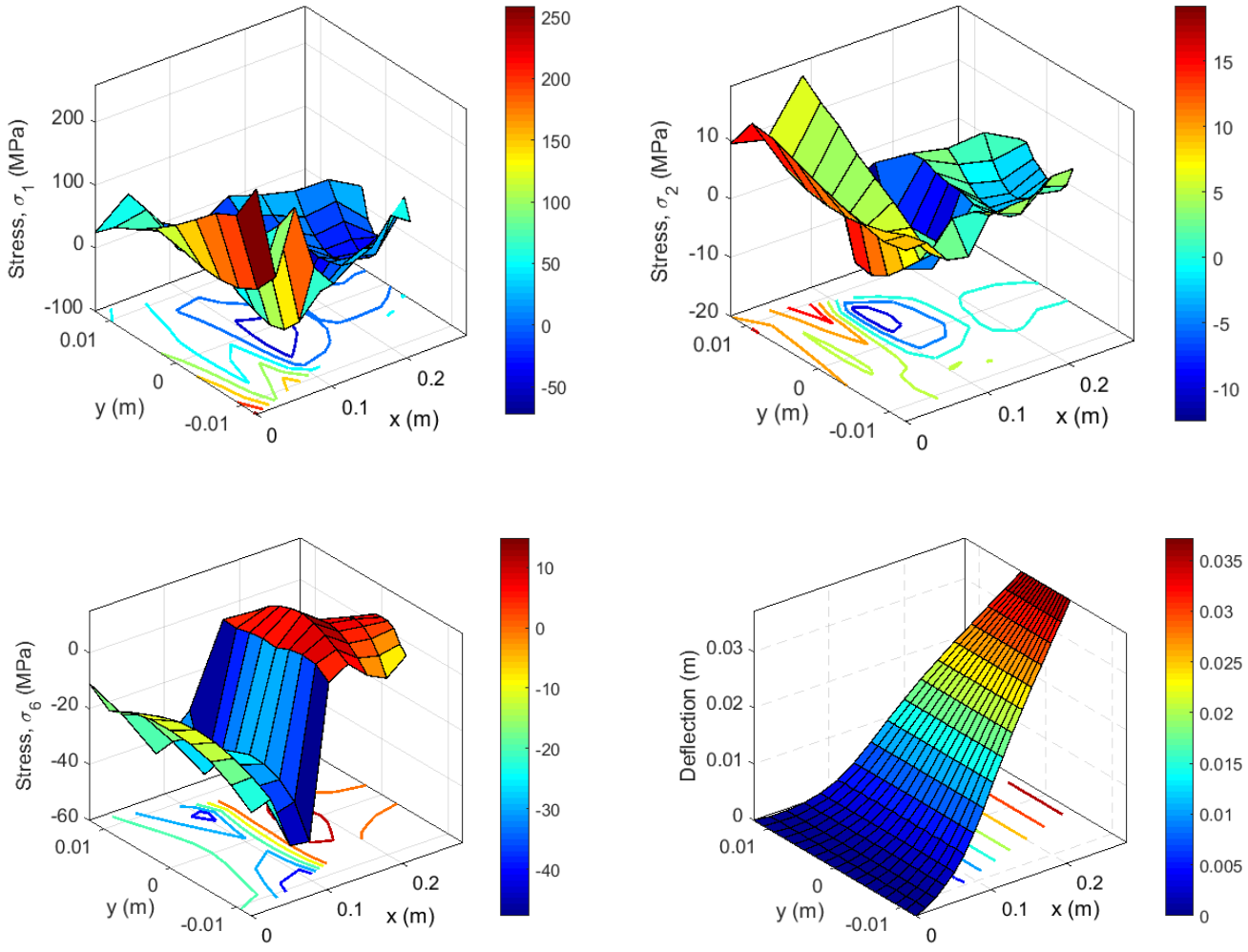

Fig. 3.5 Spatial distribution of stresses and deflection for laminate (II) [(45/0/-45/0/-45/90/0/45)$_s$]having centrally located delamination (d/L= 0.50 and d_1/L=0.50) and aspect ratio(L/s=0.7) of the untwisted (ψ=0^0)composite conical shell subjected to a failure point load (F_P=111.65 N) predicted by the maximum stress (independent) theory (marked in bold in **Table 4(b)**).

3.5.2 Effect of pre-twist angle and Delamination Size

The FPF loads for both undelaminated and single centrally delaminated ten-ply (0/90/0/90/0)$_s$ laminated composite conical shells with different pre-twist angles of ψ=0^0, 15^0, $30^0$and $45^0$are presented in **Table 3.5,** under central point load. Under both conditions, a reduction in the FPF

loads with the pre-twist angle and the presence of delamination under all failure criteria is considered. The relative drops in the FPF loads are comparable for different pre-twist angle ($\psi=0^0$ to 45^0) for all the failure theories considered. In general, the failure loads predicted by the stress-based failure theories (maximum stress, Hoffmann, Tsai-Hill, and Tsai-Wu) are always predicted higher compared to the maximum strain theory, irrespective of the pre-twist angle and delamination. In intact shells, the failure location is at the corner of the fixed end (Element No.: 1) due to point loading for all the failure criteria is observed. However, for delaminated composite conical shells, the failed elements are at the edge of the delaminated zone near the fixed end (Element No.: 17). The failed ply location is situated in the penultimate top layer (ply-location=9) under point loading for both undelaminated and delaminated composite conical shells at all pre-twist angles.

Table 3.5: FPF loads (N) for centrally delaminated (d_1/L=0.50) ten-layered $(0/90/0/90/0)_s$ transversely loaded laminates subjected to a center point transverse load (†Failed Element, ‡Failed layer from bottom) [$(0/90/0/90/0)_s$, d_1/L=0.50, d/L=0.50]

Failure Criterion	**No Delamination**				**50% Delamination**			
	$\psi=0^0$	**$\psi=15^0$**	**$\psi=30^0$**	**$\psi=45^0$**	**$\psi=0^0$**	**$\psi=15^0$**	**$\psi=30^0$**	**$\psi=45^0$**
Max. Strain	220.08 ($1^{\dagger}$,$9^{\ddagger}$)	217.38 (1,9)	214.74 (1,9)	211.99 (1,9)	136.98 (17,9)	134.95 (17,9)	132.94 (17,9)	130.85 (17,9)
Max. Stress (Independent)	226.20 (1,9)	223.46 (1,9)	220.79 (1,9)	218.02 (1,9)	141.53 (17,9)	139.45 (17,9)	137.47 (17,9)	135.38 (17,9)
Max. Stress (Polynomial)	226.04 (1,9)	223.34 (1,9)	220.68 (1,9)	217.93 (1,9)	141.49 (17,9)	139.48 (17,9)	137.44 (17,9)	135.19 (17,9)
Hoffmann	226.14 (1,9)	223.13 (1,9)	220.78 (1,9)	218.03 (1,9)	141.61 (17,9)	139.61 (17,9)	137.56 (17,9)	135.31 (17,9)
Tsai-Hill	226.09 (1,9)	223.37 (1,9)	220.72 (1,9)	217.95 (1,9)	141.50 (17,9)	139.47 (17,9)	137.44 (17,9)	135.25 (17,9)
Tsai-Wu	225.68 (1,9)	222.96 (1,9)	220.31 (1,9)	217.54 (1,9)	141.06 (17,9)	139.04 (17,9)	136.98 (17,9)	134.72 (17,9)

3.5.3 Effect of Rotation

The FPF loads of 4-layered cross-ply (0/90/90/0) laminates loaded centrally at different non-dimensional rotational speeds (Ω) are presented in **Table 3.6** and **Table 3.7** for pre-twist angles of ψ=0^0 and 30^0, respectively. The predicted FPF loads increase under different failure theories with an increase in the non-dimensional rotational speeds in both undelmainated and delaminated conical shells due to centrifugal stiffening. For point loading, the failed element is at the corner of the fixed end (Element No. 1 or 8) in undelmainated conical shells, while it is at the center of the delaminated elements (Element No. 44) near the free end of the conical shell. The percentage increase in the FPF loads with rotational speeds is higher in the case of undelmainated composite conical shells compared to the delaminated ones, as observed in all the failure theories, irrespective of the pre-twist angle. For all the pre-twist angles considered, the failed layer is located at the penultimate bottom layer (3^{rd} layer) in undelmainated conical shells. While it is at the bottommost layer (4^{th} layer) for delaminated conical shells as predicted by all the failure theories due to point loading. The spatial distribution of the stresses in the material directions(σ_1, σ_2 and σ_6) and deflections of both the non-rotating (Ω=0.0) and rotating (Ω=1.0) pre-twisted (ψ=30^0) un-delaminated (d/L= 0.0) composite conical shell subjected to central point loads at failure are illustrated in **Figs. 3.6** and **3.7,** respectively. As evident from the figures, the stresses (σ_1, σ_2andσ_6) developed near the fixed end (Element No. 1 or 8) of the non-rotating (Ω=0.0), as well as rotating (Ω=1.0) pre-twisted conical shell, are comparatively higher than the free end. From the deflection plots at the prescribed failure load, the maximum deflection occur at the free end is relatively higher in the non-rotating conical shell than the rotating one owing to centrifugal stiffening. As a result, the stresses (σ_1, σ_2 and σ_6) developed in the rotating (Ω=1.0) conical shell corresponding to the central failure point load ($F_p = 775.23\ N$) are lower than those of non-rotating (Ω=0.0) conical shell corresponding to the central failure point load ($F_p = 506.66\ N$). This additional stiffness induction due to rotation results in higher values of the first ply failure loads in rotating conical shells, which in turn is observed in **Tables 3.6** and **Table 3.7**.

Table 3.6: FPF loads (N) for (0/90/90/0) untwisted laminates ($\psi=0^0$) subjected to a center point transverse load for different non-dimensional rotational speeds (Ω)

Failure Criterion	**Pre-twist Angle ($\psi=0^0$)**									
	No Delamination ω_0=658.90 rad/s					**50% mid-plane Delamination ω_0=539.31 rad/s**				
Ω	**0.0**	**0.25**	**0.50**	**0.75**	**1.00**	**0.0**	**0.25**	**0.50**	**0.75**	**1.00**
ω_0 (rad/s)	0	164.72	329.45	494.17	658.90	0	134.83	269.66	404.48	539.31
Max. Strain	496.12 (1,3)	518.71 (1,3)	580.90 (1,3)	670.32 (1,3)	774.17 (1,3)	229.38 (44,4)	236.46 (44,4)	255.10 (44,4)	279.90 (44,4)	307.24 (44,4)
Max. Stress (Independent)	512.09 (1,3)	535.43 (1,3)	599.75 (1,3)	692.11 (1,3)	799.60 (1,3)	243.70 (44,4)	251.31 (44,4)	271.30 (44,4)	297.44 (44,4)	325.13 (44,4)
Max. Stress (Polynomial)	511.48 (1,3)	535.38 (1,3)	598.64 (1,3)	691.24 (1,3)	796.23 (1,3)	244.58 (44,4)	253.64 (44,4)	270.31 (44,4)	298.66 (44,4)	323.89 (44,4)
Hoffmann	511.50 (1,3)	534.76 (1,3)	598.82 (1,3)	690.72 (1,3)	797.51 (1,3)	243.75 (44,4)	251.46 (44,4)	271.47 (44,4)	297.62 (44,4)	321.80 (44,4)
Tsai-Hill	511.46 (1,3)	534.74 (1,3)	598.87 (1,3)	690.90 (1,3)	797.92 (1,3)	243.19 (44,4)	250.88 (44,4)	270.82 (44,4)	296.93 (44,4)	324.63 (44,4)
Tsai-Wu	509.69 (1,3)	532.87 (1,3)	596.7 (1,3)	688.30 (1,3)	794.74 (1,3)	240.43 (44,4)	247.97 (44,4)	267.60 (44,4)	293.49 (44,4)	321.25 (44,4)

Table 3.7: FPF load (N) for (0/90/90/0) pre-twisted laminates ($\psi=30^0$) subjected to a center point transverse load for different non-dimensional rotational speeds (Ω)

Failure Criterion	**Failure Loads (N)**									
	No Delamination ω_0=625.04rad/s					**50% mid-plane Delamination ω_0=515.50rad/s**				
Ω	**0.0**	**0.25**	**0.50**	**0.75**	**1.00**	**0.0**	**0.25**	**0.50**	**0.75**	**1.00**
ω_0 (rad/s)	0.0	156.26	312.52	468.78	625.04	0.0	128.87	257.75	386.62	515.50
Max. Strain	490.65 (1,3)	518.79 (1,3)	586.70 (8,3)	665.38 (8,3)	751.28 (8,3)	230.16 (44,4)	237.48 (44,4)	256.49 (44,4)	281.50 (44,4)	308.42 (44,4)
Max. Stress (Independent)	**506.66 (1,3)**	535.76 (1,3)	605.35 (8,3)	686.52 (8,3)	**775.23 (8,3)**	244.56 (44,4)	252.52 (44.4)	272.99 (44,4)	299.30 (44,4)	326.49 (44,4)
Max. Stress (Polynomial)	506.94 (1,3)	533.67 (1,3)	604.91 (8,3)	686.04 (8,3)	774.98 (8,3)	244.56 (44,4)	252.34 (44.4)	272.13 (44.4)	299.64 (44.4)	321.69 (44.4)

Hoffmann	505.97 (1,3)	534.95 (1,3)	604.49 (8,3)	685.39 (8,3)	773.79 (8,3)	244.46 (44,4)	252.43 (44,4)	272.93 (44,4)	299.27 (44,4)	322.04 (44,4)
Tsai-Hill	505.96 (1,3)	534.97 (1,3)	604.52 (8,3)	685.50 (8,3)	773.89 (8,3)	243.99 (44,4)	251.93 (44,4)	272.36 (44,4)	298.65 (44,4)	325.97 (44,4)
Tsai-Wu	504.10 (1,3)	532.97 (1,3)	602.46 (8,3)	683.16 (8,3)	771.29 (8,3)	241.09 (44,4)	248.89 (44,4)	269.00 (44,4)	295.06 (44,4)	322.50 (44,4)

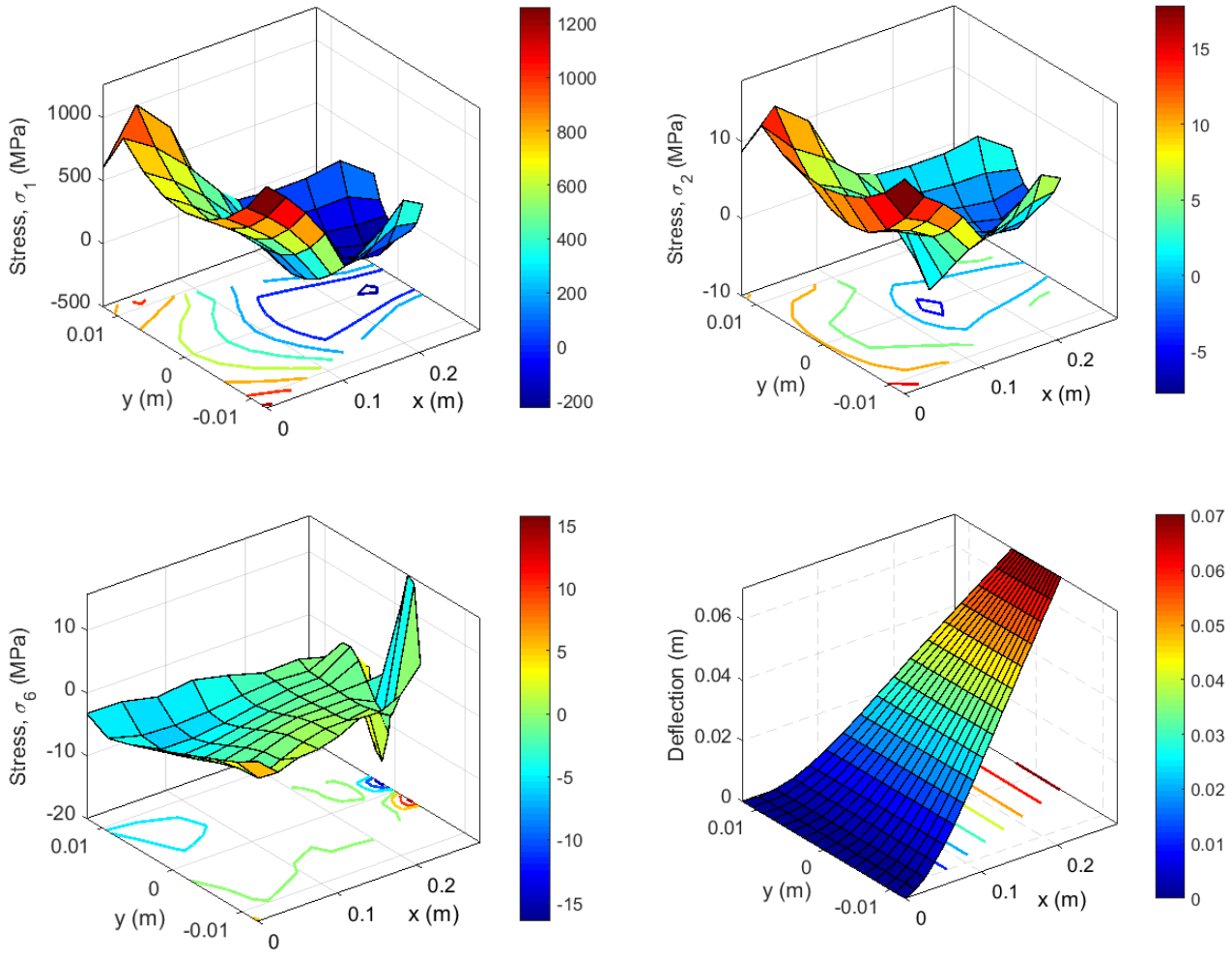

Fig. 3.6 Spatial distribution of stresses and deflection of pre-twisted (ψ=30^0) non-rotating (Ω=0.0) intact composite conical shell (0/90/90/0) under centrally applied failure point load F_P=506.66 N (marked in bold in **Table 7**) as predicted by maximum stress (independent) theory.

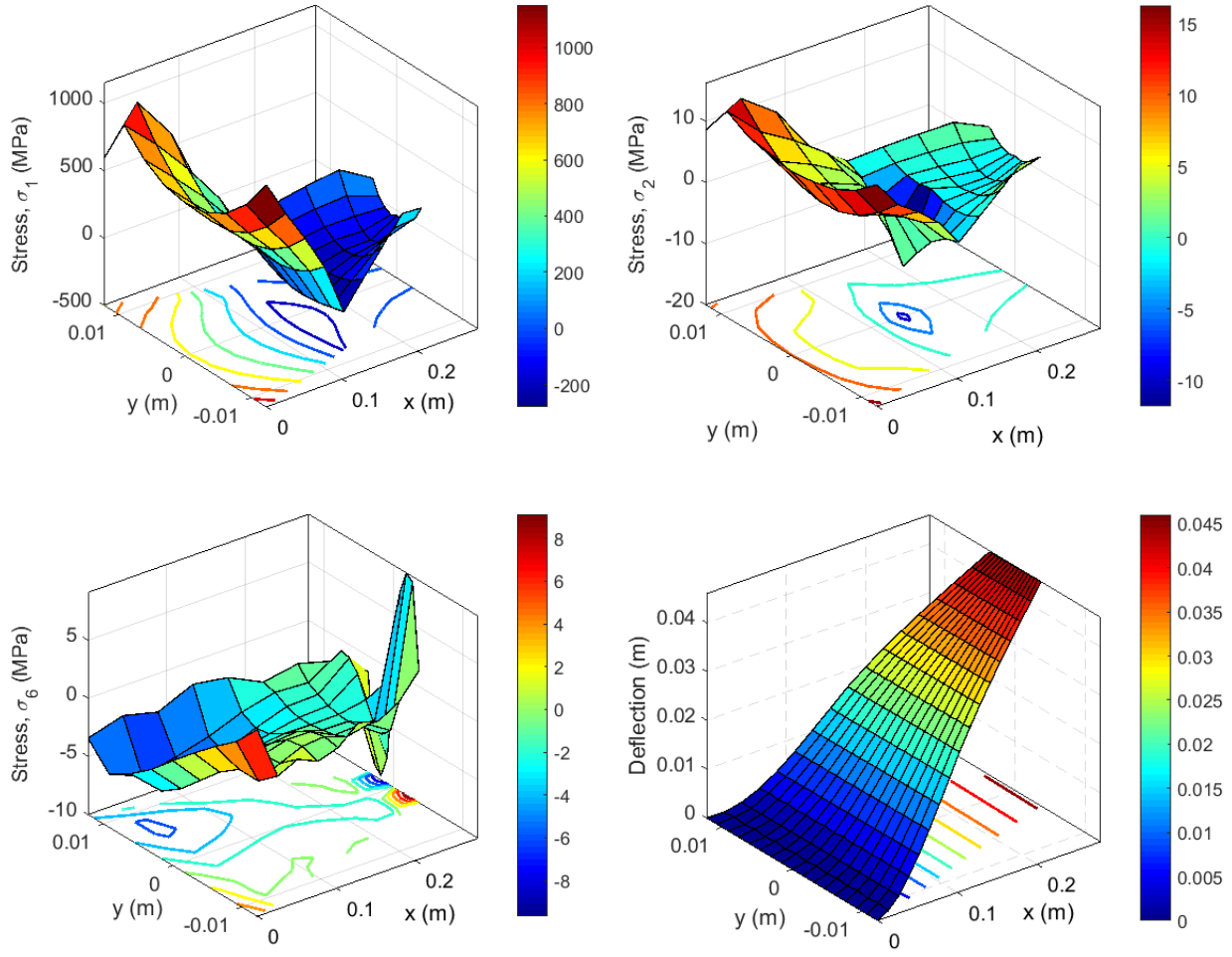

Fig. 3.7 Spatial distribution of stresses and deflection of pre-twisted (ψ=30^0) rotating (Ω=1.0) intact composite conical shell (0/90/90/0) under centrally applied failure point load F_P=775.23N (marked in bold in **Table 7**) as predicted by maximum stress (independent) theory.

3.5.4 Effect of Location of Delamination

The FPF loads for conical shells containing blind, central and an open cracks along with undelmainated conical shells are presented in **Table 3.8** for torsion-stiff $(45/-45/-45/45)_s$ conical shell laminates. The failure loads for conical shells having a blind-crack (d_1/L=0.25, d/L=0.50) adjoining the fixed end display a much lower FPF load compared to a centrally-located (d_1/L=0.50, d/L=0.50) crack or an open-end crack (d_1/L=0.75, d/L=0.50); with an open-ended crack capable of bearing the highest failure load. The reason is that the highest bending stress is invariably occur

near the fixed end of the conical shell, making a blind crack prone to drastic failure. An open-end crack is comparatively less constrained and hence able to nullify the effects of the induced bending stresses, thereby capable of carrying the higher load. There is an increase in the FPF loads with an increase in the rotational speed in both undelmainated and delaminated conical shells. The FPF loads in case of an open crack are very close to that of an undelmainated conical shell laminate. In addition, the failed element is mostly located near the fixed end (Element No: 8) except in the case of a centrally located crack where the failed element is at the edge of the delaminated zone (Element No: 17) as predicted by the maximum stress and maximum strain theories. The failed layer is at the bottommost layer in all the cases considered. It is evident that the FPF behavior of delaminated composite conical shells is largely dependent on the position of the mid-plane delamination along the span (x-axis) of the conical shell. The FPF loads of delaminated conical shells for various locations of the single delamination along the thickness of the conical shell $\left(\frac{h_{Del}}{h}\right)$ are presented in **Table 3.9** for transversely applied concentrated load at ψ=30°. The delaminated ply location (h_{Del}) is always measured from the bottom of the conical shell laminate. The FPF loads are the lowest for mid-plane delamination, while they increase for delamination presence near the outer layers of the conical shell. The failure loads for delamination presence on either side of the mid-plane of the conical shell are identical mirror images of each other. For the point load considered, the failed element is near the delaminated zone (Element No. 17) for delamination presence near the mid-plane, while it is near the fixed end (Element No: 1) for delamination presence near the outer layers of the delaminated conical shell. The failed layer is the penultimate bottom layer (9th layer).

Table 3.8: FPF loads for 8-layered $(45/-45/-45/45)_s$ angle-ply transversely point-loaded laminates (d/L=0.50) for varying locations of the delamination along the span of the conical shell ($\psi=30^0$)

Failure Criterion	**No Delamination**		**d_1/L=0.25 (Blind Crack)**		**d_1/L=0.50 (Central Crack)**		**d_1/L=0.75 (Open Crack)**	
	ω_0=246.21rad/s		ω_0=148.23/s		ω_0=189.09rad/s		ω_0=231.87	
	Ω=0.0	**Ω=0.50**	**Ω=0.0**	**Ω=0.50**	**Ω=0.0**	**Ω=0.50**	**Ω=0.0**	**Ω=0.50**
Max. Strain	84.89 (8,8)	101.71 (8,8)	27.29 (8,8)	32.94 (8,8)	46.89 (17,8)	58.71 (17,8)	82.29 (8,8)	99.94 (8,8)
Max. Stress (Independent)	84.01 (8,8)	102.10 (8,8)	28.23 (8,8)	33.64 (8,8)	46.01 (17,8)	58.10 (17,8)	83.23 (8,8)	99.64 (8,8)

Max. Stress (Polynomial)	72.58 (8,8)	89.34 (16,8)	19.81 (8,8)	23.35 (8,8)	32.64 (24,8)	40.69 (24,8)	71.33 (16,8)	84.31 (16,8)
Hoffmann	73.19 (16,8)	88.28 (16,8)	19.92 (8,8)	23.30 (8,8)	32.34 (24,8)	39.80 (24.8)	71.02 (16,8)	85.55 (16,8)
Tsai-Hill	81.50 (8,8)	98.36 (16,8)	21.81 (8,8)	26.58 (8,8)	35.50 (24,8)	44.72 (24,8)	80.47 (16,8)	95.26 (16,8)
Tsai-Wu	72.76 (16,8)	88.36 (16,8)	19.95 (8,8)	23.37 (8,8)	32.37 (24,8)	40.85 (24,8)	71.10 (16,8)	86.66 (16,8)

Table 3.9: FPF loads for $(0/90/0/90/0)_s$ transversely loaded untwisted conical shell subjected to a center point transverse load(d_1/L=0.50, d/L=0.50, $\psi=30^0$) for different locations of the delamination along the thickness of the conical shell laminated $\left(\frac{h_{Del}}{h}\right)$

$\left(\frac{h_{Del}}{h}\right)$	**Max. Strain**	**Max. Stress (Independent)**	**Max. Stress (Polynomial)**	**Hoffmann**	**Tsai-Hill**	**Tsai-Wu**
0.1	212.34 (1,9)	218.19 (1,9)	219.23 (1,9)	219.81 (1,9)	218.64 (1,9)	215.35 (1,9)
0.2	203.07 (1,9)	203.21 (1,9)	202.57 (1,9)	201.19 (1,9)	202.34 (1,9)	203.16 (1,9)
0.3	153.24 (17,9)	158.67 (17,9)	157.44 (1,9)	158.47 (17,9)	157.34 (17,9)	157.48 (17,9)
0.4	149.57 (17,9)	154.11 (17,9)	154.79 (1,9)	154.33 (17,9)	153.67 (17,9)	154.68 (17,9)
0.5 (Mid-plane delamination)	132.94 (17,9)	137.47 (17,9)	137.44 (17,9)	137.56 (17,9)	137.44 (17,9)	137.98 (17,9)
0.6	149.27 (17,9)	154.29 (17,9)	154.22 (1,9)	154.78 (17,9)	153.24 (17,9)	153.12 (17,9)
0.7	153.28 (17,9)	158.79 (17,9)	158.21 (1,9)	158.43 (17,9)	157.84 (17,9)	157.24 (17,9)
0.8	203.57 (1,9)	203.57 (1,9)	202.59 (1,9)	201.27 (1,9)	202.31 (1,9)	203.34 (1,9)
0.9	212.39 (1,9)	218.98 (1,9)	218.97 (1,9)	219.56 (1,9)	217.89 (1,9)	215.67 (1,9)

3.5.5 Multiple Delaminations

The first-ply failure behavior of multiple-delaminated composite conical shells is analyzed for delaminations located both symmetrically and unsymmetrically across the mid-plane of the laminate. The number of delaminations (n_d) and the thickness-wise locations of the multiple-delaminations are indicated by their respective positions along the lamina interfaces from the bottom (**Fig. 3.8)**. The FPF loads of multiple-delaminated (d_1/L=0.25, d/L=0.50 and ψ=30^0) cross-ply composite $(0/90/0/90/0)_s$ pre-twisted conical shells(**Fig. 3.8**) are presented in **Tables 10** for a centrally applied transverse point load. A comparison of **Table 3.1(a) and Table 3.10** suggests that a drastic reduction in the failure loads is predicted by all the failure theories due to the presence of multiple delaminations in comparison to a single-delaminated shell for the non-rotating twisted (ψ=30^0) conical shell. The failed element for n_d=2 is near the centerline of the delaminated zone (Element No. 28), while it is located near the edge of the delaminated zone (Element No. 17) for n_d=4. The failed layer is at the bottommost layer (1^{st} layer) for n_d=2 and the penultimate top layer (9^{th} layer) for n_d=4. An increase in the FPF loads is found with an increase in the rotational speed (**Ω**), although the failed element and the failed-ply are the same as the stationary case.

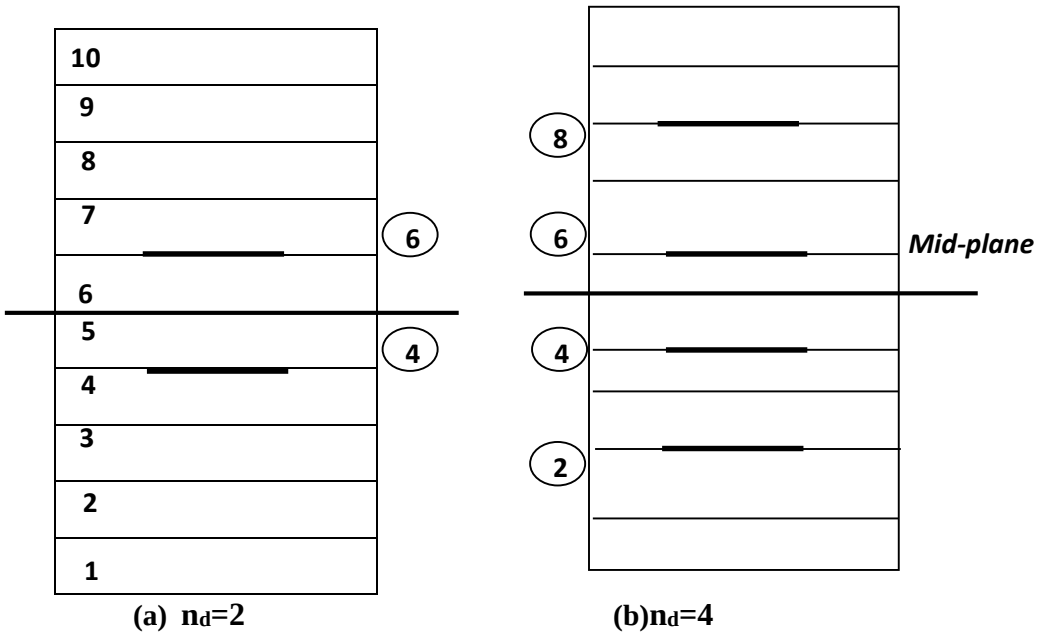

Fig .3.8 Location of the multiple delaminations (d_1/L=0.50, d/L=0.50)*w.r.t* to the mid-plane of the multiple-delaminated composite conical shell, **a)** Delamination at 4^{th} and 6^{th} interface from the bottom; **b)** Delamination at 2^{nd}, 4^{th}, $6^{th}$and 8^{th} interface from bottom

Table 3.10: FPF loads (N) for $(0/90/0/90/0)_s$ transversely loaded pre-twisted conical shell subjected to a centrally applied transverse load (d_1/L=0.50, d/L=0.50, and ψ=30^0)containing two and four symmetrically placed delaminations (n_d=2 and 4)

Failure Criterion	**n_d=2 (4th and 6th interface from bottom) ω_0=424.10rad/s**			**n_d=4 (2nd, 4th, 6thand 8th interface from bottom) ω_0=384.75rad/s**		
	Ω=0.0	**Ω=0.50**	**Ω=1.0**	**Ω=0.0**	**Ω=0.50**	**Ω=1.0**
Max. Strain	72.19 (28,1)	81.15 (28,1)	92.13 (28,1)	65.12 (17,9)	81.19 (17,9)	81.87 (17,9)
Max. Stress (Independent)	74.93 (28,1)	81.23 (28,1)	89.41 (28,1)	66.25 (17,9)	82.14 (17,9)	82.54 (17,9)
Max. Stress (Polynomial)	75.12 (28,1)	80.68 (28,1)	89.23 (28,1)	65.98 (17,9)	82.33 (17,9)	82.56 (17,9)
Hoffmann	74.84 (28,1)	81.11 (28,1)	89.24 (28,1)	65.19 (17,9)	82.17 (17,9)	83.14 (17,9)
Tsai-Hill	74.59 (28,1)	81.26 (28,1)	90.45 (28,1)	66.23 (17,9)	82.94 (17,9)	83.86 (17,9)
Tsai-Wu	74.21 (28,1)	82.94 (28,1)	89.78 (28,1)	65.11 (17,9)	82.34 (17,9)	82.78 (17,9)

The circular frequencies (rad/s) for both single and multiple delaminated untwisted composite four-layered untwisted conical shells ([0/θ/0/θ]) are plotted in **Fig. 3.9** while the FPF loads considering the Hoffman failure criterion, are plotted in **Fig.3.9(b), 3.9(c) and 3.9(d)**for non-dimensional rotational speeds of Ω=0.0, 0.5 and 1.0, respectively. For the intact shell, the fundamental frequency values are the highest, while the lowest values of the fundamental frequencies are for 50% multiple delamination. At θ=15^0, the slope of both the frequency and FPF curves at all rotational speeds are very steep but becomes asymptotic when θ approaches 90^0. Further on increasing the non-dimensional spinning speed from Ω=0.0 to 1.0, the FPF loads are increased in both single and multiple delaminated composite conical shells due to the centrifugal stiffening effect. The FPF load is found lower for 50% multiple delamination compared to 25% multiple delamination. For all the non-dimensional rotational speeds considered (Ω=0.0, 0.5, and

1.0), 50% multiple delamination gives the lowest value of FPF load at θ=90^0 while the highest FPF is observed for intact shell at the same fiber orientation angle (θ=90^0).

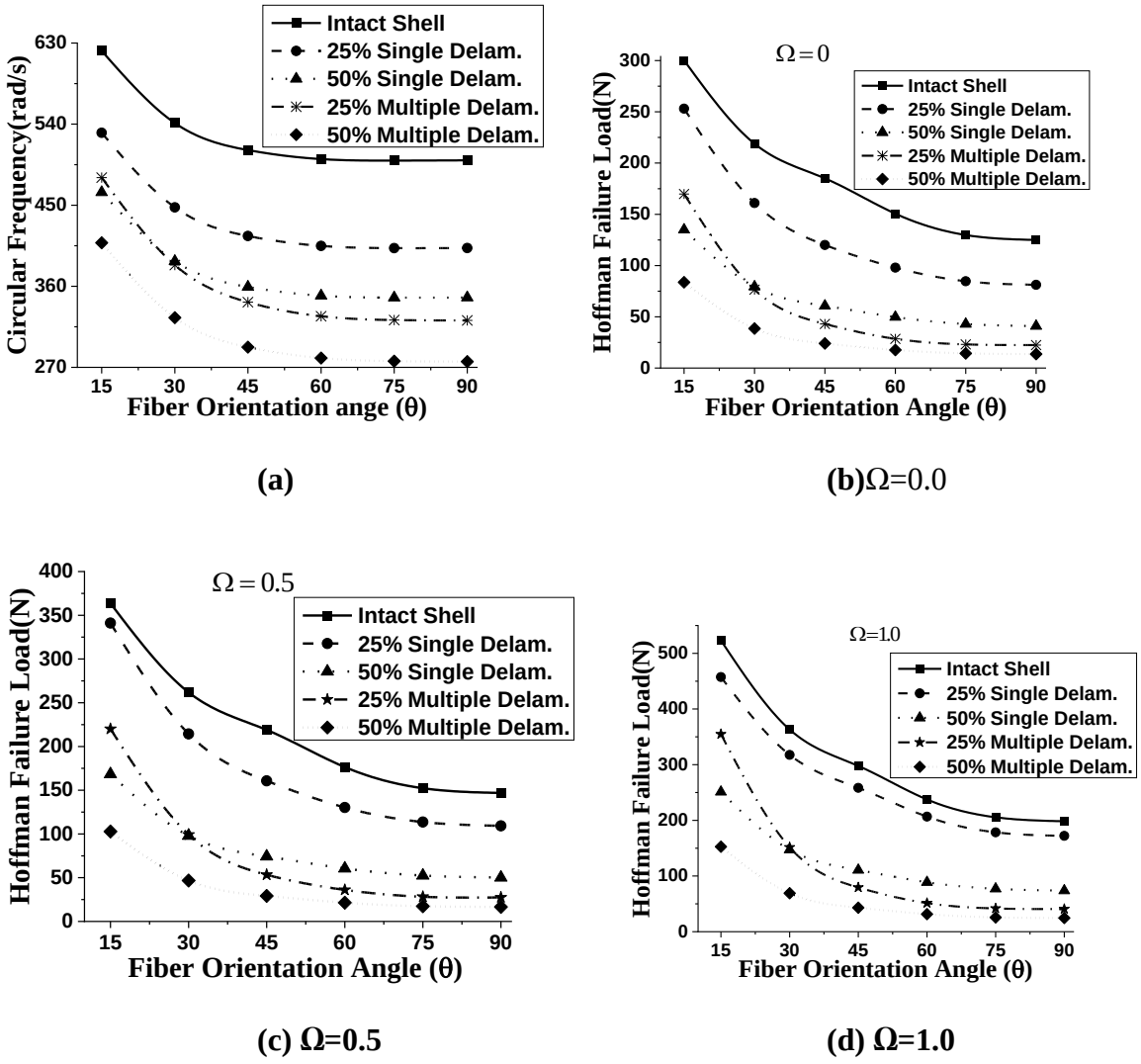

Fig 3.9. Variation of fundamental frequency (Hz) and Hoffman first-ply failure load (N)with fiber orientation angle (θ) for both single and multiple delaminated untwisted composite four-layered (0/θ/0/θ) composite conical shells at different rotational speeds (Ω)

The variations of FPF loads considering the Tsai-Hill failure criterion for intact as well as single and multiple delaminated untwisted (0/90/0/90) composite conical shells at different aspect ratios (*L*/*s*) of the conical shell are plotted in **Fig. 3.10**. With the increase in aspect ratio (*L*/*s*) from 0.2 to

0.9, the FPF loads decreases monotonically until it becomes asymptotic as the aspect ratio (L/s) approaches 0.9. At lower value of aspect ratios (0.2 to 0.4), the percentage reduction in the FPF values are drastic though it becomes much less at higher aspect ratios. With an increase of aspect ratio (L/s) there is a reduction of structural stiffness of the composite conical shell, which causes a reduction in the FPF loads. In addition, the FPF values decrease as the size of delamination and the number of delaminations increase thereby predicting lesser structural strengths due to the presence and size of delamination.

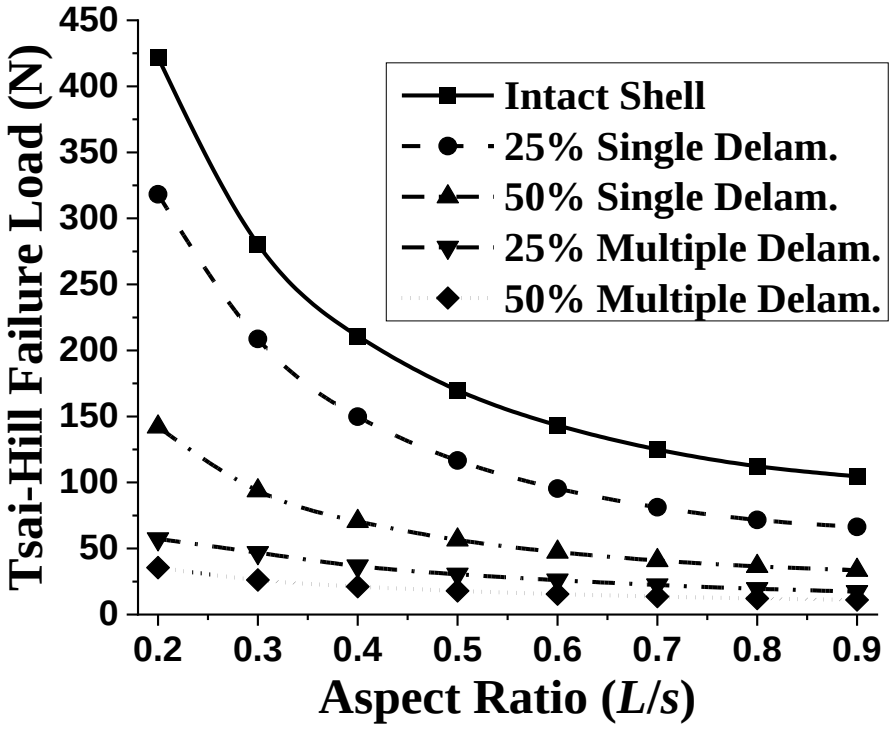

Fig 3.10. Tsai-Hill Failure Load (N) with Aspect Ratio (L/s) for intact, single & multiple delaminated untwisted ($\psi=0^0$) composite (0/90/0/90) conical shells with different delamination size located from the mid-plane

The FPF loads of delaminated $(0/90/0/90/0)_s$ pre-twisted ($d_1/L=0.50$, $d/L=0.50$ and $\psi=30^0$) composite conical shell are presented in **Table 3.11** for different arbitrary locations [(I)-(VIII)] of the unsymmetrically placed multiple delaminations ($n_d=2$). The assumed centrally applied point load act at the mid-point of the top surface of the composite conical shell. A reduction in the FPF

loads is found as the distance between the two delaminations increases, as evident from the delamination presence at the interfaces mentioned in (I)-(VI). However, an increase in the FPF loads at the interface (VII) owing to the presence of delaminations close to symmetrically opposite locations across the mid-plane of the composite conical shell, though the value again decreases as one of the delaminations reaches close to the point of application of the centrally applied point load as indicated by the interfaces in (VIII).

Table 3.11 FPF loads (N) for $(0/90/0/90/0)_s$ transversely loaded pre-twisted non-rotating (Ω=0.0) conical shell subjected to a centrally applied transverse load (d_1/L=0.50, d/L=0.50 and ψ=30^0) containing two arbitrary unsymmetric delaminations (n_d=2) located at(I) 1st and 2nd interface from the bottom,(II)1st and 3rd interface from bottom, (III)1st and 4th interface from bottom, (IV) 1st and 5th interface from bottom, (V) 1st and 6th interface from bottom,(VI) 1st and 7th interface from bottom, (VII) 1st and 8th interface from bottom, (VIII) 1st and 9th interface from bottom (symmetric)

Failure Criterion	**I**	**II**	**III**	**IV**	**V**	**VI**	**VII**	**VIII**
Max. Strain	216.36 (17,9)	134.56 (17,9)	115.69 (17,9)	84.97 (17,9)	83.01 (17,9)	73.73 (17,9)	134.29 (17,9)	128.56 (17,9)
Max. Stress (Independent)	223.74 (17,9)	138.41 (17,9)	119.21 (17,9)	87.37 (17,9)	87.31 (17,9)	75.33 (17,9)	138.52 (17,9)	131.54 (17,9)
Max. Stress (Polynomial)	222.64 (17,9)	137.38 (17,9)	118.68 (17,9)	86.96 (17,9)	85.34 (17,9)	75.35 (17,9)	138.51 (17,9)	131.26 (17,9)
Hoffmann	223.56 (17,9)	136.49 (17,9)	119.35 (17,9)	87.21 (17,9)	86.97 (17,9)	74.98 (17,9)	137.64 (17,9)	130.28 (17,9)
Tsai-Hill	223.11 (17,9)	137.73 (17,9)	118.79 (17,9)	86.34 (17,9)	85.11 (17,9)	74.35 (17,9)	138.42 (17,9)	131.87 (17,9)
Tsai-Wu	222.78 (17,9)	136.98 (17,9)	119.66 (17,9)	87.09 (17,9)	86.78 (17,9)	73.97 (17,9)	137.35 (17,9)	130.58 (17,9)

3.6 Effect of Twist angle and Aspect ratio

A FE investigation is done to predict the effect of some vital parameters such as aspect ratio, pre-twist angle and size of the delamination on the FPF load. The failure analysis is done for a graphite-epoxy cross-ply $[(0^0/90^0)_{2S}]$ lamina. An 8×8 mesh division is employed for discretisation and the conical shell is subjected to a centre point transverse load. The FPF loads of intact and delaminated shell for untwisted and different pre-twist angle at different aspect ratio (L/s) 0.6, 0.7, 0.8 are represented in **Table 3.12**, **Table 3.13, Table 3.14** and **Table 3.15.**

Table 3.12: FPF failure load of Intact & Delaminated untwisted ($\psi=0^0$) Conical Shell $(0/90)_{2S}$ for different aspect ratios (L/s)

Failure Criterion	***L*/s=0.60**		***L*/s=0.70**		***L*/s=0.8**	
	Intact Shell	**50% Delam.**	**Intact Shell**	**50% Delam.**	**Intact Shell**	**50% Delam.**
Max. Strain	281.98 (1^*,$7^\#$)	182.69 (17,7)	244.16 (1,7)	154.35 (17,7)	217.42 (1,7)	134.52 (17,7)
Max. Stress	289.80 (1,7)	189.42 (17,7)	250.99 (1,7)	160.08 (17,7)	223.56 (1,7)	139.55 (17,7)
Max. Stress (Polynomial)	289.70 (1,7)	189.36 (17,7)	250.90 (1,7)	160.03 (17,7)	223.45 (1,7)	139.51 (17,7)
Hoffmann	289.73 (1,7)	189.56 (17,7)	250.97 (1,7)	160.21 (17,7)	223.55 (1,7)	139.66 (17,7)
Tsai-Hill	289.67 (1,7)	189.35 (17,7)	250.89 (1,7)	160.03 (17,7)	223.48 (1,7)	139.50 (17,7)
Tsai-Wu	289.15 (1,7)	188.58 (17,7)	250.44 (1,7)	159.37 (17,7)	223.06 (1,7)	138.91 (17,7)

* Failed Element, # Failed Layer

Table 3.13: FPF failure load of Intact & Delaminated twisted ($\psi=15^0$) Conical Shell $(0/90)_{2S}$ for different aspect ratios (L/s)

Failure Criterion	L/s=0.60		L/s=0.70		L/s=0.8	
	Intact Shell	50% Delam.	Intact Shell	50% Delam.	Intact Shell	50% Delam.
Max. Strain	278.65 (1^*,$7^\#$)	180.02 (17,7)	241.75 (1,7)	152.53 (17,7)	215.19 (1,7)	133.25 (17,7)
Max. Stress	286.42 (1,7)	186.72 (17,7)	248.56 (1,7)	158.25 (17,7)	221.72 (1,7)	138.26 (17,7)
Max. Stress (Polynomial)	286.23 (1,7)	186.68 (17,7)	248.43 (1,7)	158.22 (17,7)	221.70 (1,7)	138.25 (17,7)
Hoffmann	286.35 (1,7)	186.89 (17,7)	248.54 (1,7)	158.39 (17,7)	221.73 (1,7)	138.39 (17,7)
Tsai-Hill	286.29 (1,7)	186.67 (17,7)	248.50 (1,7)	158.21 (17,7)	221.65 (1,7)	138.23 (17,7)
Tsai-Wu	285.76 (1,7)	185.89 (17,7)	247.99 (1,7)	157.55 (17,7)	221.23 (1,7)	137.65 (17,7)

* Failed Element, # Failed Layer

Table 3.14: FPF failure load of Intact & Delaminated twisted ($\psi=30^0$) Conical Shell$(0/90)_{2S}$ different aspect ratios (L/s)

Failure Criterion	*L*/s=0.60		*L*/s=0.70		*L*/s=0.8	
	Intact Shell	50% Delam.	Intact Shell	50% Delam.	Intact Shell	50% Delam.
Max. Strain	275.58 (1^*,$7^\#$)	177.63 (17,7)	239.47 (1,7)	150.83 (17,7)	213.85 (1,7)	132.03 (17,7)
Max. Stress	283.31 (1,7)	184.33 (17,7)	246.25 (1,7)	156.55 (17,7)	219.96 (1,7)	137.05 (17,7)

Max. Stress (Polynomial)	283.11 (1,7)	184.27 (17,7)	246.12 (1,7)	156.50 (17,7)	219.86 (1,7)	137.03 (17,7)
Hoffmann	283.24 (1,7)	184.47 (17,7)	245.63 (1,7)	156.69 (17,7)	219.96 (1,7)	137.19 (17,7)
Tsai-Hill	283.18 (1,7)	184.26 (17,7)	246.16 (1,7)	156.49 (17,7)	219.89 (1,7)	137.02 (17,7)
Tsai-Wu	282.63 (1,7)	183.47 (17,7)	245.69 (1,7)	155.83 (17,7)	219.46 (1,7)	136.42 (17,7)

* Failed Element, # Failed Layer

Table 3.15: FPF failure load of Intact & Delaminated twisted ($\psi=45^0$) Conical Shell $(0/90)_{2S}$ for different aspect ratios (L/s)

Failure Criterion	***L*/s=0.60**		***L*/s=0.70**		***L*/s=0.8**	
	Intact Shell	**50% Delam.**	**Intact Shell**	**50% Delam.**	**Intact Shell**	**50% Delam.**
Max. Strain	272.73 (1^*,$7^\#$)	175.64 (17,7)	237.24 (1,7)	149.25 (17,7)	212.07 (1,7)	130.82 (17,7)
Max. Stress	280.45 (1,7)	182.37 (17,7)	244.02 (1,7)	154.98 (17,7)	218.18 (1,7)	135.86 (17,7)
Max. Stress (Polynomial)	280.21 (1,7)	182.20 (17,7)	243.85 (1,7)	154.88 (17,7)	218.07 (1,7)	135.79 (17,7)
Hoffmann	280.33 (1,7)	182.41 (17,7)	243.97 (1,7)	155.07 (17,7)	218.17 (1,7)	135.96 (17,7)
Tsai-Hill	280.29 (1,7)	182.24 (17,7)	243.89 (1,7)	154.89 (17,7)	218.09 (1,7)	135.79 (17,7)
Tsai-Wu	279.71 (1,7)	182.38 (17,7)	243.41 (1,7)	154.18 (1,7)	217.65 (1,7)	135.18 (17,7)

* Failed Element, # Failed Layer

3.7 Effect of Delamination and Rotation

The effect of some vital parameters such as aspect ratio, size of the delamination, effect of rotation and fiber orientation angle(θ) on the FPF load are predicted. An 8×8 mesh division is selected and a centre point transverse load acted on the graphite-epoxy angel-ply laminate. FPF loads of untwisted static shell for various delamination length at various aspect ratio (L/s= 0.6, 0.7 and 0.8) are presented in **Table 3.16.** **Table 3.17** represents the FPF loads at various delamination size of different non-dimensional rotational speeds.

Table 3.16: FPF loads (N) for laminate $[(45/-45)_2]$ with central delamination sizes (d/L = 0.00, 0.25 & 0.50) of a cantilever conical shell for different aspect ratios (L/s) subjected to a centre point transverse load

Failure Criterion	L/s=0.6			L/s=0.7			L/s=0.8		
	Intact Shell	25% Delam.	50% Delam.	Intact Shell	25% Delam.	50% Delam.	Intact Shell	25% Delam.	50% Delam.
Max Strain	109.80 (1*,4#)	97.88 (25,4)	47.06 (17,4)	92.26 (1,4)	80.59 (25,4)	40.40 (17,4)	80.10 (1,4)	69.53 (25,4)	35.93 (17,4)
Max Stress	109.12 (1,4)	96.49 (25,4)	46.79 (17,4)	92.06 (1,4)	79.91 (25,4)	40.21 (17,4)	80.09 (1,4)	69.31 (25,4)	35.78 (17,4)
Max Stress (poly.)	88.04 (1,4)	69.87 (25,4)	33.94 (17,4)	76.79 (1,4)	58.02 (25,4)	28.92 (17,4)	68.11 (1,4)	50.17 (25,4)	25.48 (17,4)
Hoffmann	88.03 (1,4)	69.79 (25,4)	33.99 (17,4)	76.73 (1,4)	57.99 (25,4)	28.89 (17,4)	68.08 (1,4)	50.13 (25,4)	25.46 (17,4)
Tsai-Hill	97.40 (1,4)	76.28 (25,4)	37.04 (17,4)	85.19 (1,4)	63.31 (25,4)	31.60 (17,4)	75.78 (1,4)	54.76 (25,4)	27.88 (17,4)
Tsai-Wu	88.09 (1,4)	70.18 (25,4)	34.06 (17,4)	76.80 (1,4)	58.23 (25,4)	29.01 (17,4)	68.19 (1,4)	50.33 (25.4)	25.56 (17,4)

*****Failed Element, **#** Failed Layer

The combined effects of rotational speed and delamination size and location are discussed as presented in **Table 3.17.** It is observed that with an increase in the delamination size a drastic reduction in the FPF value is observed. However this effect is compensated by the fact that corresponding increase in the FPF values may be noted with an increase in non-dimensional

rotational speeds. The designer must take into account the effects of centrifugal loading and delamination presence to accurately predict their failure load in service condition.

Table 3.17 FPF loads (N) for $[(45/-45)_2]$ laminate with different delamination sizes for different non-dimensional speeds (Ω) for aspect ratio (L/s) 0.7 subjected to a center point transverse load

Failure Criterion	Failure Loads (N)								
	Intact Shell (No Delamination) ω_0=256.28 rad/s			25% mid-plane Delamination ω_0=219.34rad/s			50% mid-plane Delamination ω_0=191.78rad/s		
Ω	0.0	0.5	1.0	0.0	0.5	1.0	0.0	0.5	1.0
ω (rad/s)	0.0	128.14	256.28	0.0	109.67	219.34	0.0	95.89	191.78
Max. Strain	92.26 (1*, 4#)	110.20 (1,4)	155.09 (1,4)	80.59 (25,4)	105.89 (25,4)	137.51 (25,4)	40.40 (17,4)	49.53 (17,4)	72.67 (17,4)
Max. Stress (Independent)	92.06 (1,4)	109.17 (1,4)	155.01 (1,4)	79.91 (25,4)	105.62 (25,4)	137.49 (25,4)	40.21 (17,4)	49.26 (17,4)	72.25 (17,4)
Max. Stress (Polynomial)	76.79 (1,4)	90.06 (1,4)	121.17 (1,4)	58.02 (25,4)	81.54 (25,4)	109.05 (25,4)	28.92 (17,4)	35.55 (17,4)	52.59 (17,4)
Hoffmann	76.73 (1,4)	90.04 (1,4)	121.14 (1,4)	57.99 (25,4)	81.46 (25,4)	109.03 (25,4)	28.89 (17,4)	35.52 (17,4)	52.49 (17,4)
Tsai-Hill	85.19 (1,4)	99.99 (1,4)	134.54 (1,4)	63.31 (25,4)	88.81 (25,4)	121.20 (25,4)	31.60 (17,4)	38.82 (17,4)	57.32 (17,4)
Tsai-Wu	76.80 (1,4)	90.13 (1,4)	121.27 (1,4)	58.23 (25,4)	81.88 (25,4)	109.14 (25,4)	29.01 (17,4)	35.69 (17,4)	52.72 (17,4)

*Failed Element, # Failed Layer

3.8 Variation of Tsai-Wu Failure Load with Aspect Ratio and Fiber Orientation Angle

The variation of Tsai-Wu first-ply failure load with aspect ratio and fibre orientation angle for intact and delaminated shell are given below (**Fig. 3.11 & Fig. 3.12**). It is found that on increase of aspect ratio and fibre orientation angle Tsai-Wu failure load decreases asymptotically.

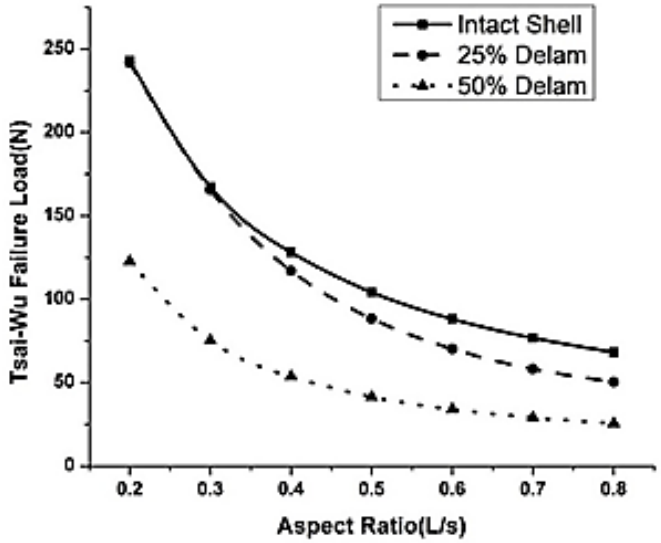

Fig. 3.11 Deviation of Tsai-Wu Failure Load with Aspect Ratio (L/s)

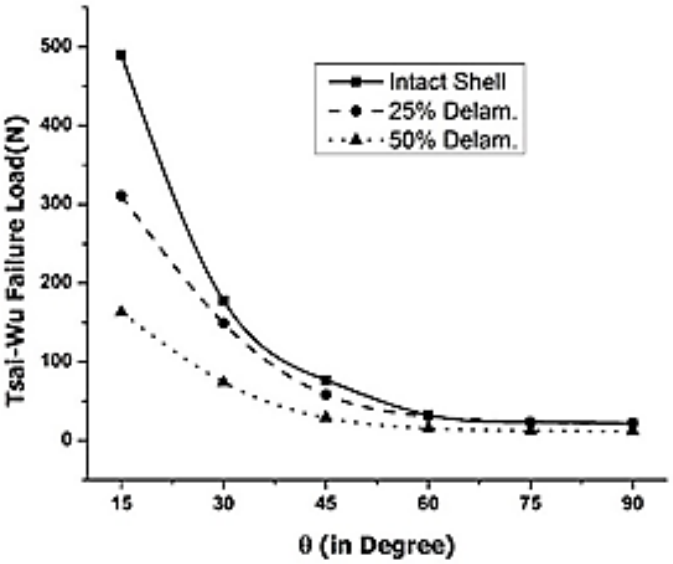

Fig. 3.12 Deviation of Tsai-Wu Failure Load with Fibre orientation angle (θ)

CHAPTER 4:

Impact Induced First Ply Failure of Delaminated Composite Conical Shells

4.1 Overview

The present chapter describes the impact induced first ply failure of delaminated composite conical shells. At first, the computer codes developed are validated with available benchmark results related to the impact phenomenon and convergence results of both the mesh and time-steps are performed and are found to be in good agreement with established benchmark results. The Tsai-Wu failure criterion is employed to predict impact induced first ply failure because it is most general for biaxial stress and results are much accurate than other theories. Initially critical velocity of impact is found at which first-ply failure starts for different aspect ratio of intact and delaminated shells. Then variation of contact force, shell deflection, impactor displacement, impactor velocity and Tsai-Wu polynomials with time are found for different aspect ratio, intact and delaminated shell. The transient response of said parameter for blind, open and central crack are found. Also varying impactor location transient response are recorded. For each case principal stress (σ_1 and σ_2) and plane stress (τ_{12}) at critical velocity of impact are plotted.

4.2 Consideration and Validation

At first the present FE formulation is validated with benchmark results from the available literatures. **Table 4.1** represents the validation of Tsai-Wu criterion for FPF theory for different laminates. The existing results are very close to available literature [104].**Table 4.2** represents the validation of cantilever conical shell with different aspect ratio (L/s = 0.6, 0.7 and 0.8) for different non-dimensional fundamental frequencies (NDFF) and the results for each aspect ratio converges on increasing of mesh division from 4X4 to 10X10. **Fig. 4.1** represents the validation of relative frequencies of graphite-epoxy composite plate $[(\pm 45°)_4]$ clamped at one side with relative delamination length. **Fig. 4.2** and **Fig. 4.3** represents the validation of contact force and shell deflection during impact of a cross ply $[0/90/0/90/0]_s$ composite laminated plate with the following properties [129]. FE results for impact validation are in good agreement with Sun et al. [129].

a=20cm, b=20cm, h=0.269cm, E_1=120GPa, E_2=7.9GPa, $G_{12}=G_{23}=G_{13}$=5.5GPa, ν_{12}=0.30, ρ=1.58X10-5N-sec^2/cm^4.

Table 4.1: FPF loads under different failure criterion [104]

Failure Criterion	$(0/90)_s$		$(0_2/90)_s$		$(0_2/90_2)_s$		(0/90/0/90)s	
	Kam et al.	Present FEM	Kam et al.	Present FEM	Kam et al.	Present FEM	Kam et al.	Present FEM
Tsai-Wu	68.30	69.91	112.77	106.96	238.60	230.99	304.13	295.26

Table 4.2: Non-dimensional fundamental frequencies ($\lambda = \omega_n b_0^2\sqrt{\rho h/D}$, flexural rigidity $D = Eh^3/12(1-\nu^2)$ of untwisted shallow cantilever conical shell (ν=0.3, s/*h*=1000, θ_o=30°,θ_v=15°, E=138GPa, G= 53.08GPa, ρ=16000 kg/m^3) [1]

Aspect Ratio (*L*/s)	**Present (4×4)**	**Present (6×6)**	**Present (8×8)**	**Present (10×10)**	**Liew et al.**[1]
0.6	0.34250	0.34240	0.34237	0.34235	0.35997
0.7	0.29418	0.29412	0.29410	0.29409	0.30608
0.8	0.26919	0.26914	0.26913	0.26913	0.27832

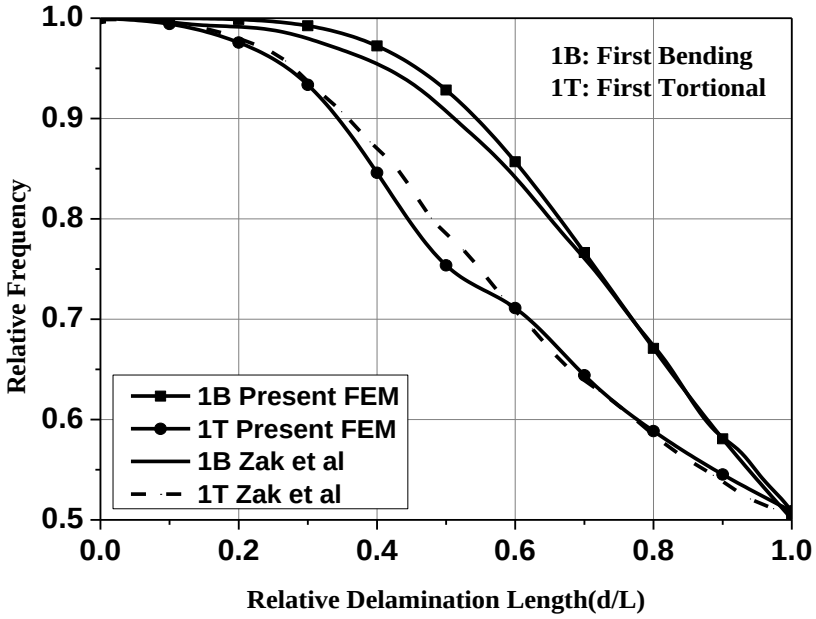

Fig. 4.1 Deviation of relative frequencies with relative delamination length [53]

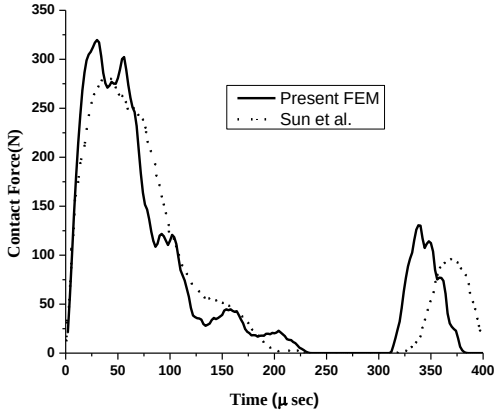

Fig.4.2 Validation of Contact Force [129]

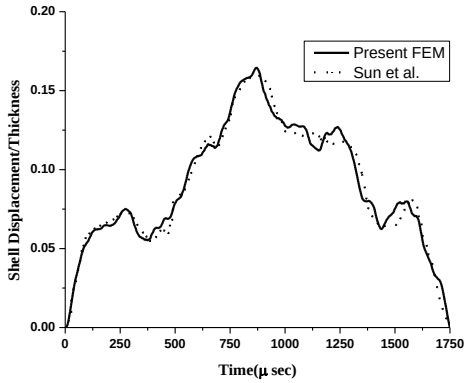

Fig.4.3 Validation of shell deflection [129]

The geometrical dimensions of the composite conical shell are taken as s=0.4 m, L/s=0.7, s/h=100, θ_0=20°, and θ_v=20°. The material properties and corresponding strength properties of the graphite-epoxy angle ply composite shell $[0°/90°]_2$ employed for present analysis are given below [104]:

E_1=142.5 GPa, E_2=9.79 GPa, G_{12}=G_{13}=4.72 GPa, G_{23}=1.192 GPa, ν_{12}=0.27,X_T=2193.50 MPa, X_C=2457.0 MPa, Y_T=41.30 MPa, Y_C=206.80 MPa, R=61.28 MPa, S=T=78.78 MPa, $X_{\varepsilon T}$=0.015393, $X_{\varepsilon C}$=0.017242, $Y_{\varepsilon T}$=0.004128, $Y_{\varepsilon C}$=0.021124, R_ε=0.051409, S_ε=T_ε=0.016691

4.3 Convergence Study

The present FE formulation is also verified for both mesh and time convergence. For mesh convergence different mesh sizes of (4X4), (6X6), (8X8) and (10X10) are selected at a time step of $2\mu s$. It is found that on increase of mesh size contact force converges (**Fig.4.4**) and Tsai-Wu tensor polynomial [18] approaches close to 1 when the size of mesh division increased (**Fig.4.5**). So a converged mesh division of (8X8) is selected for present analysis.

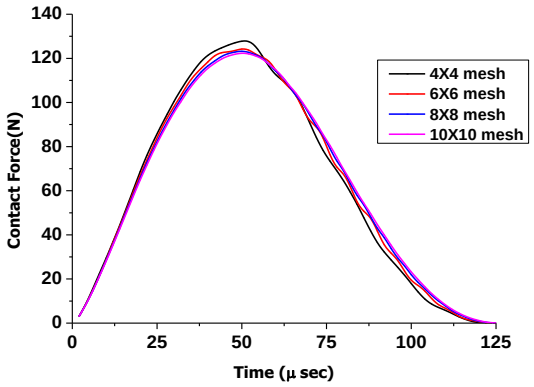

Fig. 4.4 Convergence of Contact Force

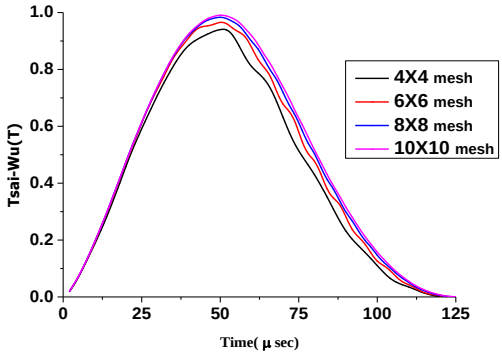

Fig. 4.5 Convergence of Tsai-Wu Tensor

For time convergence the different time steps of Δt=0.5 μs, 2.0 μs, 4.0 μs and 6.0 μs are employed for the converged mesh size of (8X8) obtained from the previous analysis. On increasing time step gradually from Δt= 0.5 μs to 6.0 μs the value of contact force and Tsai-Wu tensor increases (**Fig. 4.6 and Fig. 4.7**). Also the results with higher time step (Δt= 4.0μs and 6.0 μs) indicates initiation of FPF with the Tsai-Wu tensor polynomial value crosses more than 1.0. So a time step of Δt= 2.0μs is employed for present analysisin the subsequent analyses.

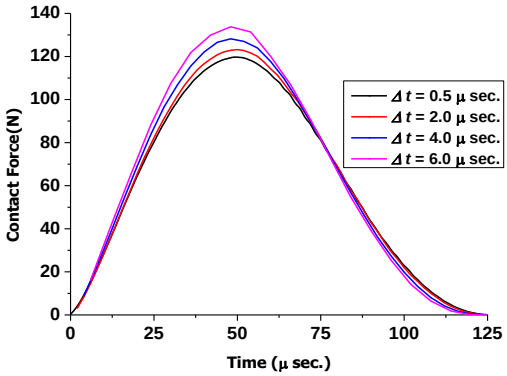

Fig. 4.6 Convergence of Contact Force

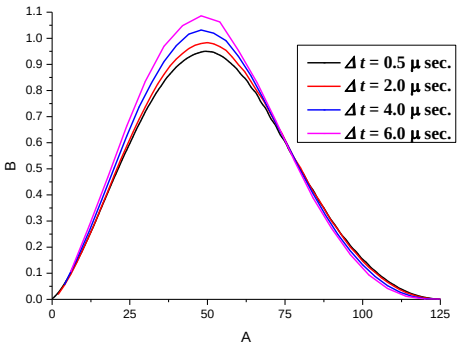

Fig. 4.7 Convergence of Tsai-Wu Tensor

4.4 Results from the Present FEM

4.4.1 *Critical Velocity and Transient Response of Single Delaminated Shell*

On increasing of velocity of impact (VOI) gradually contact force increases. For present analysis Tsai-Wu failure criterion is selected for FPF of cross ply [0°/90°/0°/90°] laminate due to impact as it is polynomial in nature. Initially VOI is gradually increased to find critical velocity of impact at which FPF will initiates which depends on delamination size and location as well as aspect ratio. **Fig. 4.8** shows the variation of critical velocity of impact with aspect ratio for intact shell, 25% and 50% centrally located delamination about mid plane. It is found that the critical velocity for first-ply failure initiation decreases with an increase in the delamination size though the slope of the critical velocity curve is highly dependent on the aspect ratio of the conical shell. At lower aspect ratios (0.2 to 0.4) difference in critical velocity of intact shell and 25% delaminated shell are found close to each other while for higher aspect ratios (0.5 to 0.9) the difference is found to be considerable. Also at low aspect ratios, the critical velocity curve is very steep in nature but it is found to be less steep for higher aspect ratios of the conical shell. This may be attributed to the gradual decrease in the structural stiffness of the conical shell with an increase in the aspect ratio which contributes directly to the first-ply failure initiation. **Fig. 4.9.a, 4.9.b** and **4.9.c** represents the variation of contact force with time (in μs) for intact, 25% delaminated and 50% mid-plane delaminated conical shell for different aspect ratios (L/s= 0.6, 0.7 and 0.8). It is found that on increasing the aspect ratio and delamination size, the contact force reduces considerably. The contact force reduces to zero at around 125μs for all the cases and as the delamination increases though it takes slightly higher time to diminish. The variation of shell displacement/thickness with time are represented in **Fig. 4.10.a, Fig. 4.10.b** and **Fig. 4.10.c** indicates that the displacements are gradually increase with time. For intact shell (**Fig. 4.10.a)** displacements are close to each other irrespective of aspect ratio but for aspect ratio 0.6 it suddenly starts decreasing around t=750μs. For 25% delaminated shell (**Fig. 4.10.b)** displacements are close to each other for aspect ratio 0.7 and 0.8 while the displacements at aspect ratio 0.6 have considerable amount of difference with the other two. The magnitude of displacements for 50% delaminated shell (**Fig. 4.10.c)** are comparatively lower than intact and 25% delaminated shell and all the displacements are close to each other with different aspect ratios. The magnitude of the impactor displacements (**Fig.4.11.a, Fig. 4.11.b** and **Fig. 4.11.c)** gradually reduces on increasing length of delamination.

For intact shell its magnitude is low for an aspect ratio 0.6 compared with 0.7 and 0.8. For 25% delaminated shell impactor displacements at an aspect ratio 0.6 is slightly higher than 0.7 and 0.8. For 50% delaminated shell all the values of impactor displacements with different aspect ratio are very close to each other. The impactor velocity found to be decreasing significantly on increase of delamination size (**Fig. 4.12a, Fig. 4.12.b** and **Fig. 4.12.c)**. On increase of aspect ratio from 0.6 to 0.8 there is a gradual reduction of impactor velocity. In all the cases i.e. intact shell, 25% delamination and 50% delamination impactor velocity reduces drastically upto t=100μs, after that it becomes constant.

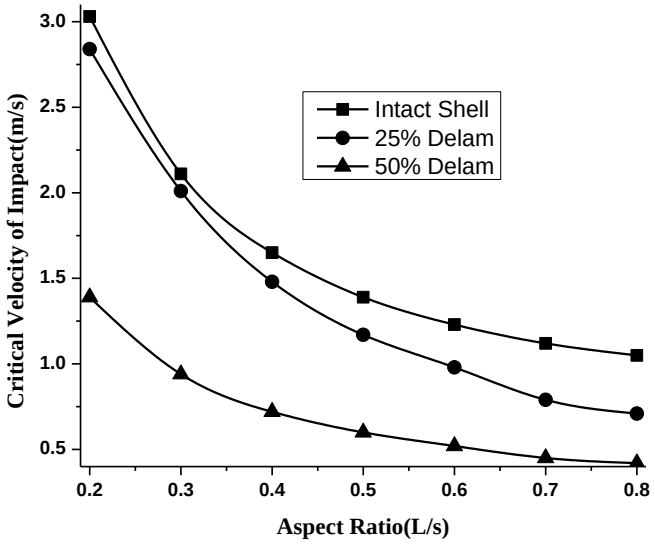

Fig. 4.8 Variation of the critical velocity of Impact with different aspect ratios (L/s) of the conical shell and delamination sizes (Intact, 25% & 50% Delamination) for [0/90/0/90] cross ply laminates

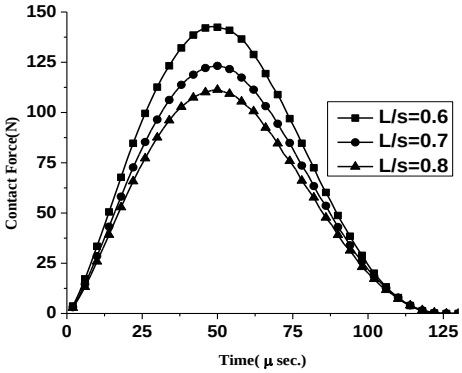

Fig. 4.9.a Variation of Contact Force with time for Intact Shell

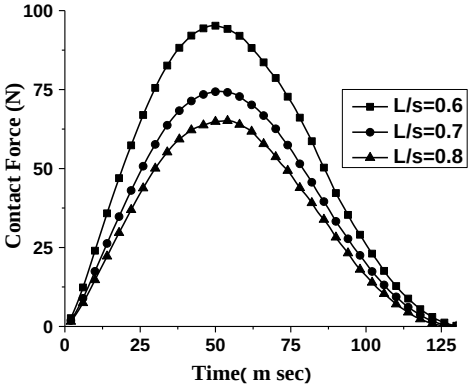

Fig. 4.9.b Variation of Contact Force with time for 25% delaminated shell

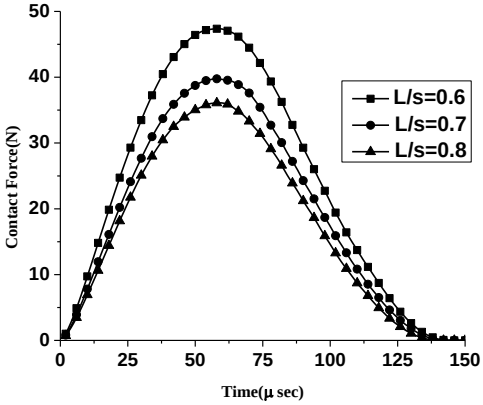

Fig. 4.9.c Variation of Contact Force with time for 50% delaminated shell

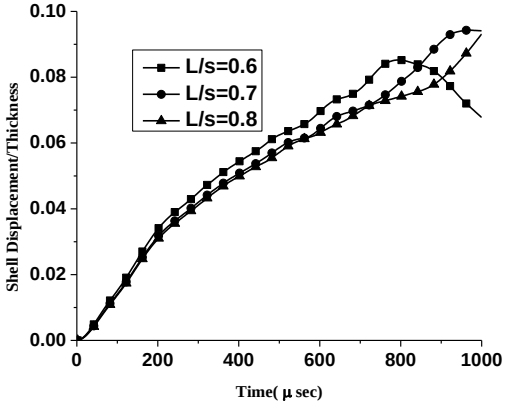

Fig. 4.10.a Variation of shell deflection with time for Intact Shell

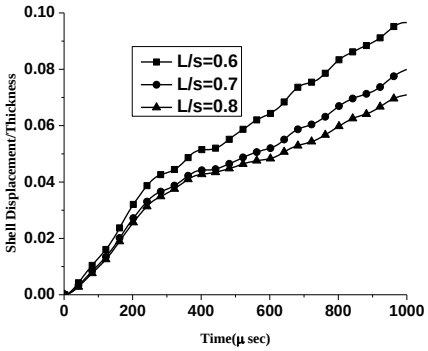

Fig. 4.10.b Variation of shell deflection with time for 25% delaminated Shell

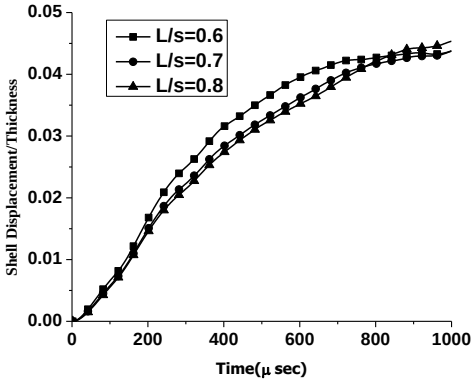

Fig. 4.10.c Variation of Shell deflection with time for 50% delaminated shell

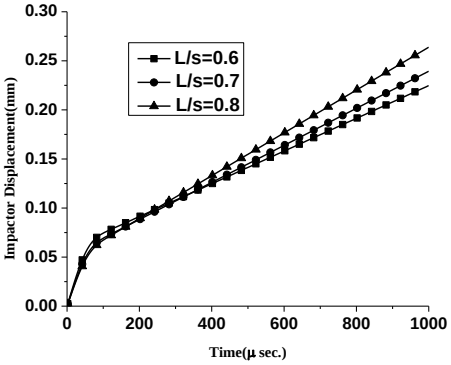

Fig. 4.11.a Variation of impactor displacements with time for intact shell

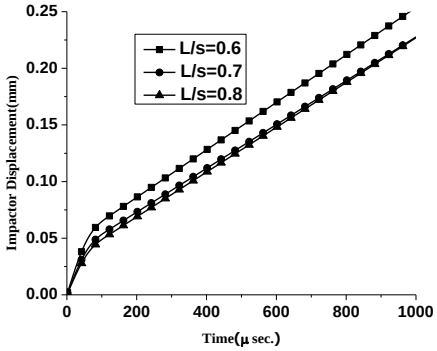

Fig. 4.11.b Variation of impactor displacements with time for 25% delaminated shell

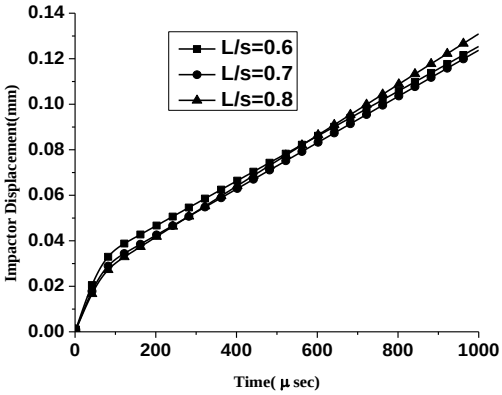

Fig. 4.11.c Variation of impactor displacements with time for 50% delaminated shell

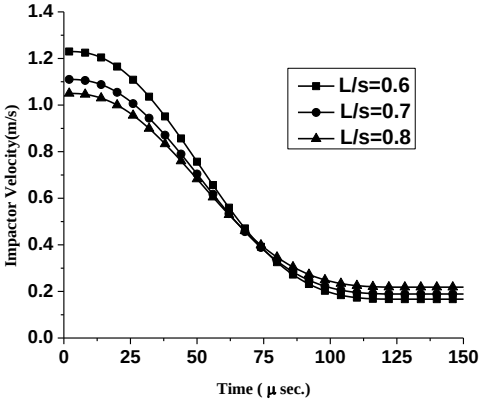

Fig. 4.12.a Variation of impactor Velocity(m/s) with time for Intact Shell

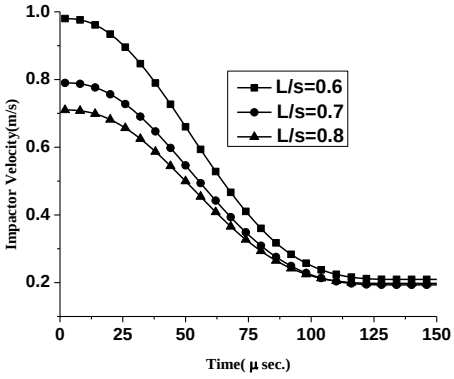

Fig. 4.12.b Variation of impactor Velocity(m/s) with time for 25% delaminated Shell

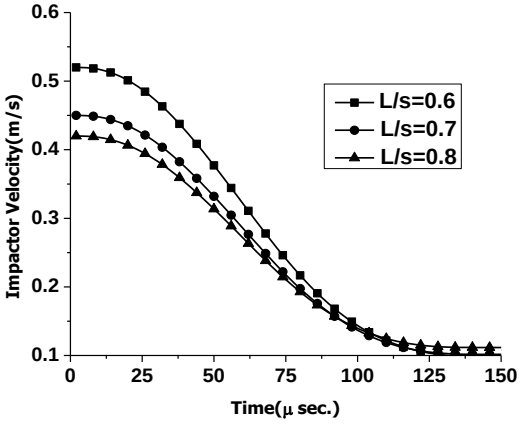

Fig. 4.12.c Variation of impactorVelocity(m/s) with time for 50% delaminated Shell

4.4.2 *Transient Response of Blind, Central and Open Crack*

The spanwise location of the single–delamination are varied to study the influence of Blind crack, central crack and open crack (**Fig. 4.13(a), Fig. 4.13(b), Fig. 4.13(c)**) on the transient response of delaminated conical shells. The delaminations are assumed to present near the fixed end in case of a blind crack, close to the centre in case of a central crack while near the free end in case of an open crack. For each the cases, the impact is assumed to occur at the centre of the cantilever shell in the transverse direction shown in the Fig. The analysis is performed considering the critical velocity of impact at which FPF is initiates.

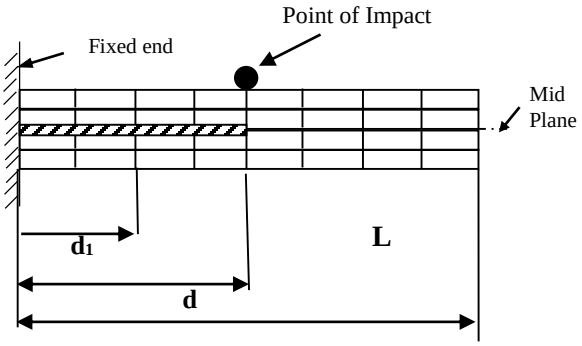

Fig. 4.13(a) Blind Crack (d/L=0.50, d_1/L=0.25)

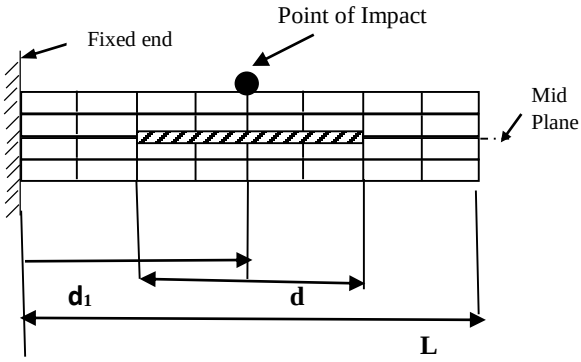

Fig. 4.13(b) Central Crack (d/L=0.50, d_1/L=0.50)

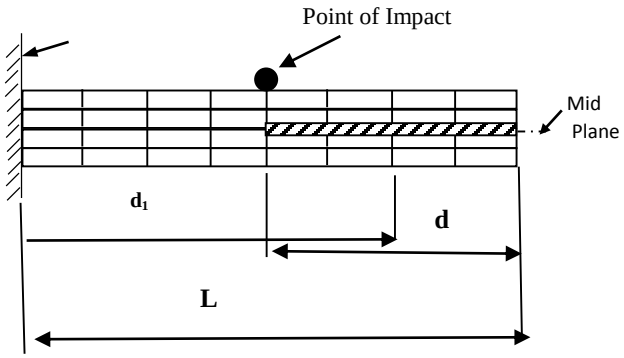

Fig. 4.13(c) Open Crack (d/L=0.50, d_1/L=0.75)

In figure (**4.13 (a** to **c)**) **d** is the length of delamination along the span, $\mathbf{d_1}$ is the location of the centreline of delamination from fixed end and **L** is total length of the shell.

The transient response of contact force and Tsai-Wu polynomial for delaminated composite conical shells are plotted for blind crack, central crack and open crack in **Fig. 4.14(a)** and **4.14(b)**, respectively. The contact force is found to be the highest in case of an open crack followed by central crack and the least contact force is found in case of a blind crack. This is due to the fact that under impact loading, the highest shell deflection is observed in case of an open crack while the least is observed for a blind crack. The Tsai-Wu tensor for open and central crack are close to each other and becomes zero around 140μs whereas for open crack it attains zero value around t=115μs.

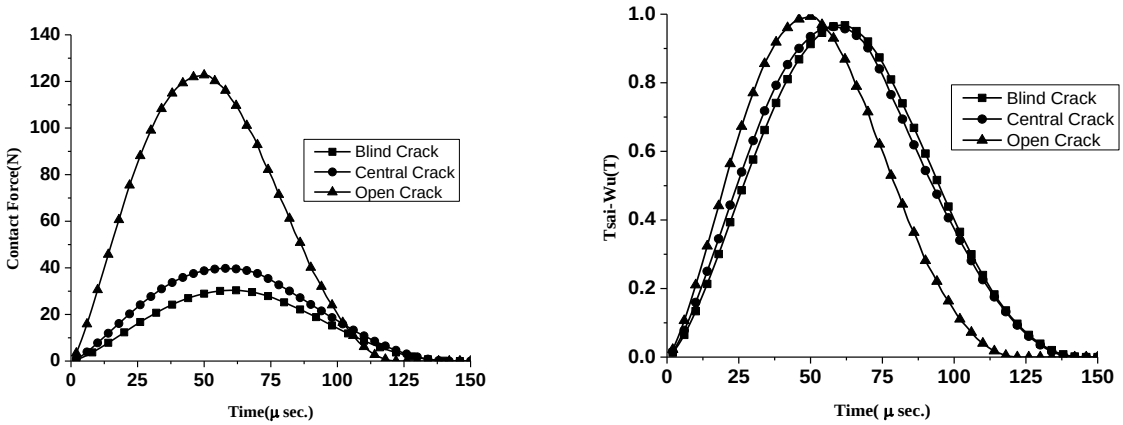

4.14. (a) **4.14. (b)**

Fig. 4.14 Time-based variations in the Contact force (N) and Tsai-Wu (**T**) polynomial for various types of crack

The variations of the contact stresses in the principal directions, σ_1, σ_2 and τ_{12}, along the contour of the conical shell plan form arising out of a central impact $\left(\frac{L}{2}, \frac{b}{2}, \frac{h}{2}\right)$ are plotted in **Fig 4.15, 4.16** and **4.17,** for blind, central and open cracks respectively. The impact velocity is taken to be the critical velocity (V_{cr}) at which the first-ply failure in the composite laminates just initiates. As expected, the contact stresses for blind, central and open crack are found to be compressive in nature. In addition, the contact stresses in the normal directions (σ_1 and σ_2) are almost comparable in magnitude though the shear stresses τ_{12} are much lesser compared to the normal stresses as such, the first-ply failure is highly dependent on the variations in the normal stresses compared to the shear stresses. For the blind crack, the stresses $\sigma_1$and $\sigma_2$are found to be highest close to the fixed end of the conical shell while they are the highest near to the mid-span of the conical shell

$(\frac{L}{2}, \frac{b}{2})$ n case of the central and the open cracks. This suggests that the first-ply failed elements are close to the cantilevered end (Element No: 4 in **Fig. 2.2**) in case of a blind crack, while they are close to the mid-span of the conical shell in case of central and the open cracks.

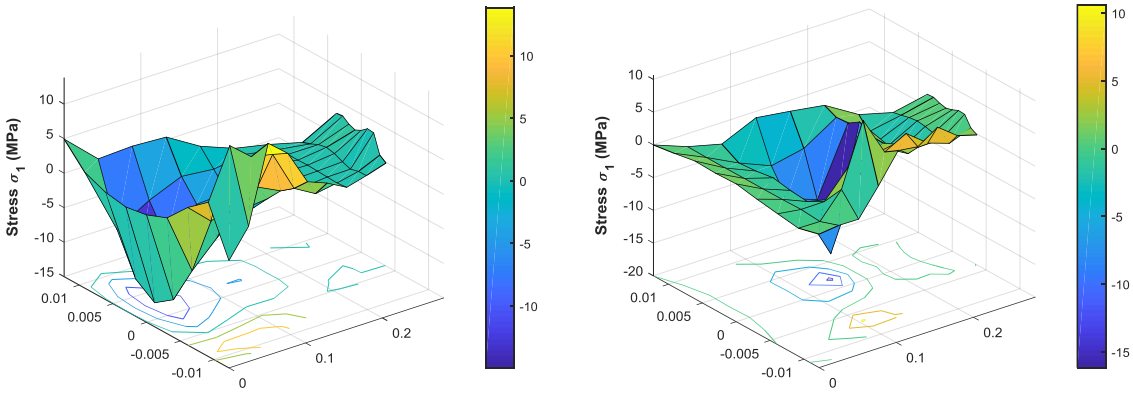

4.15.a) Blind Crack

4.15.b) Central Crack

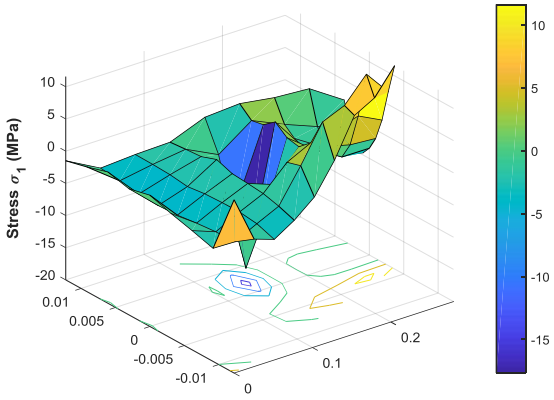

4.15.c) Open Crack

Fig.4.15 Variation of stresses (σ_1) in principal directionat critical velocity of impact for various types of crack

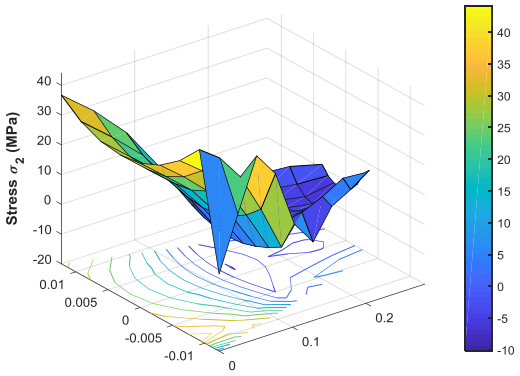

4.16.a) Blind Crack

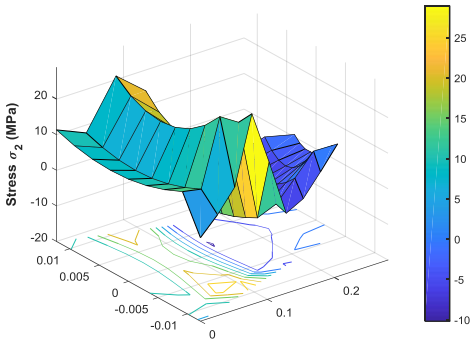

4.16.b) Central Crack

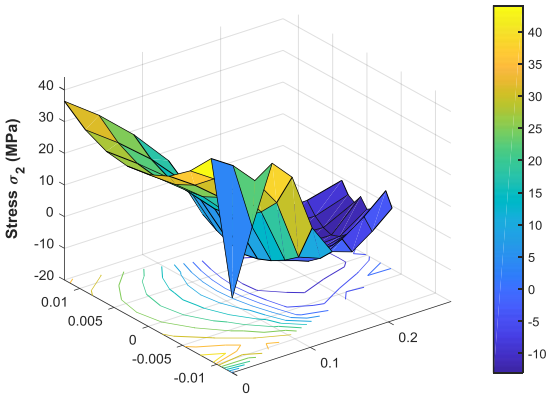

4.16. c) Open Crack

Fig.: 4.16 Variation of stresses (σ_2) in principal direction at critical velocity of impact for various types of crack

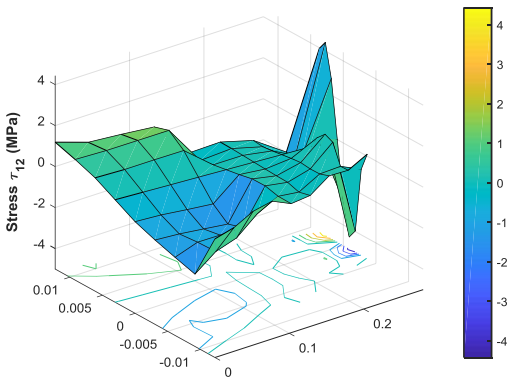

4.17.a) Blind Crack

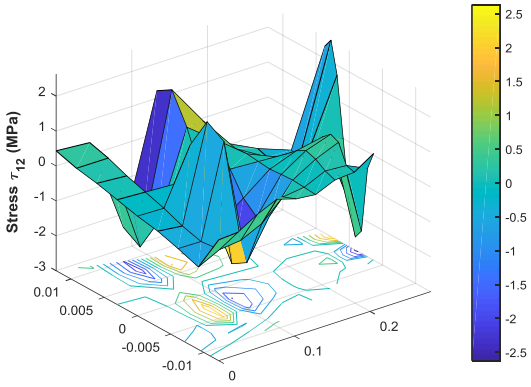

4.17.b) Central Crack

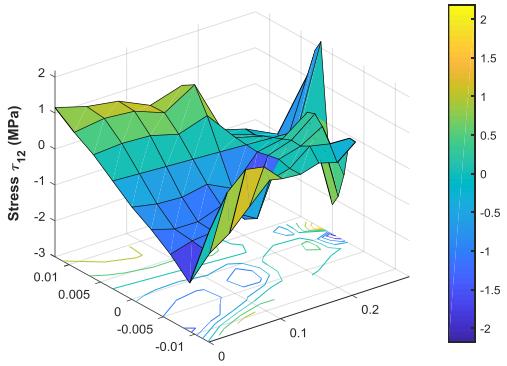

4.17.c) Open Crack

Fig. 4.17 Variation of in plane stresses (τ_{12})at critical velocity of impact for various types of crack

4.4.3 *Transient Response and contact stress of multiple delamination*

Multiple delamination occurs when more than one delamination zone are present in the composite structure. The figure below (**Fig. 4.18)** shows multiple delamination in between layer 1&2 and 3&4. In this analysis a four-layer graphite epoxy composite laminate ($[0°/90°]_2$) is selected with geometric and material properties are similar as mentioned earlier. The size of the delaminations are chosen as 25% (d/L=0.25) and 50%(d/L=0.50). Impact is assumed to occur centre point with critical velocity. The contact force due to impact is maximum for intact shell and it reduces gradually with the increase of size and no of delaminations (**Fig. 4.19**). The same tendency appears in the magnitude of shell displacement (**Fig. 4.20**), impactor velocity (**Fig. 4.21**) and impactor displacement (**Fig. 4.22**). On the increase of size and number of delamination Tsai-Wu tensor (**Fig. 4.23**) shifts towards the right hand side i.e. it takes more time to diminish.

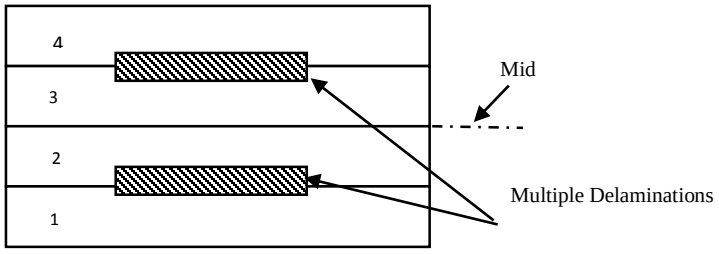

Fig. 4.18 Schematic diagram of multiple delamination

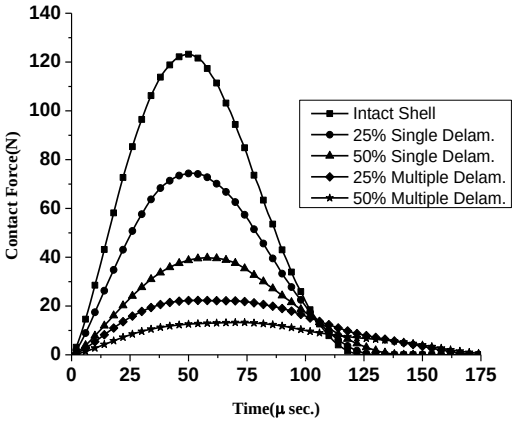

Fig. 4.19 Variation of contact force with time for multiple delamination

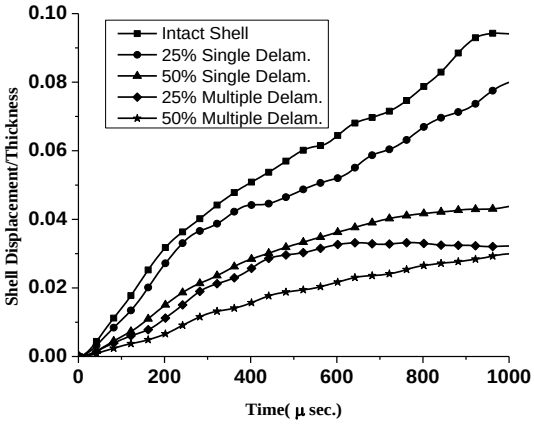

Fig. 4.20 Variation of shell displacement/thickness with time for multiple delamination

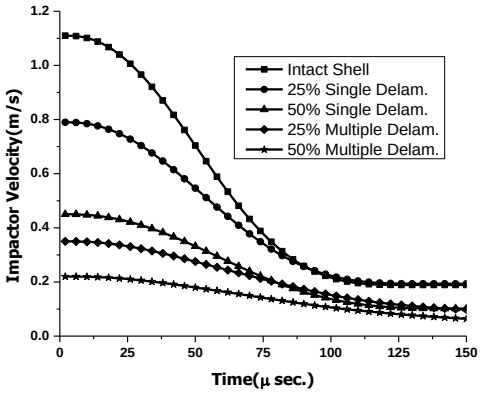

Fig. 4.21 Variation of Impactor velocity with time multiple delamination

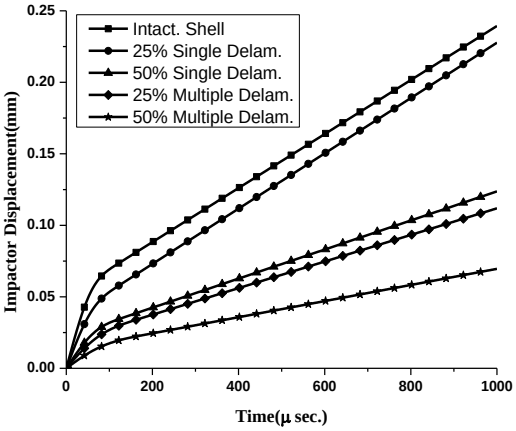

Fig. 4.22 Variation of impactor displacement with time for multiple delamination

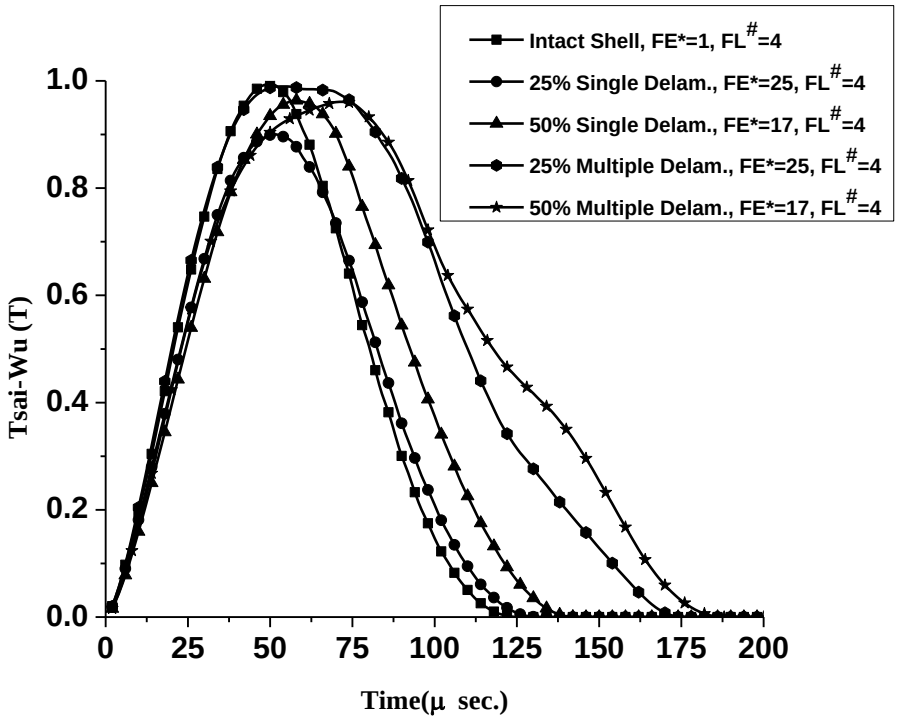

Fig. 4.23 Variation of Tsai-Wu Tensor with time **(***Failed Element, #Failed Layer)

The impact induced stresses (σ_1, σ_2 and τ_{12}) developed in both intact as well as 25% and 50% delaminated composite conical shells are plotted in **Figs. 4.24, 4.25, 4.26,** (a), (b) and (c), respectively. The composite conical shells are assumed to be impacted centrally by a spherical steel ball (impactor) moving at the critical velocity of impact resulting in first-ply failure initiation. The σ_1 values are found to be the lowest in the intact composite conical shells though they increase with an increase in the size of delamination in delaminated conical shells. However the reverse trend is observed in case of $\sigma_2$values wherein the highest value of $\sigma_2$is observed in case of the intact composite conical shell while the lowest is observed in case of 50% delaminated shells. The shear stress values (τ_{12}) are again found to be lower compared to the normal contact stresses σ_1 and σ_2. The combined effects of the impact loading and delamination size is found to be widely influenced by the critical parameters namely the critical velocity of impact (Vc). The Tsai-Wu tensor polynomials (T) tends to attain a critical value of 1.0 at a certain critical time

period which is highly dependent on a critical size of delamination.

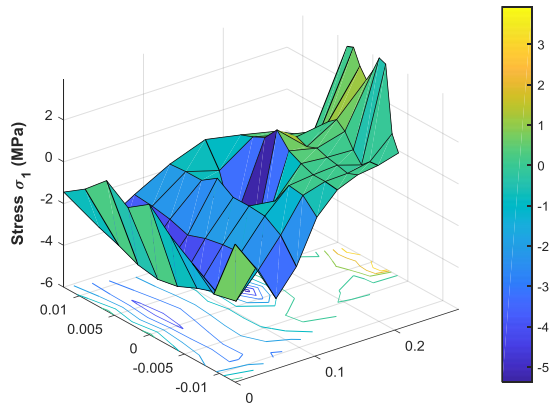

4.24.a) Intact Shell

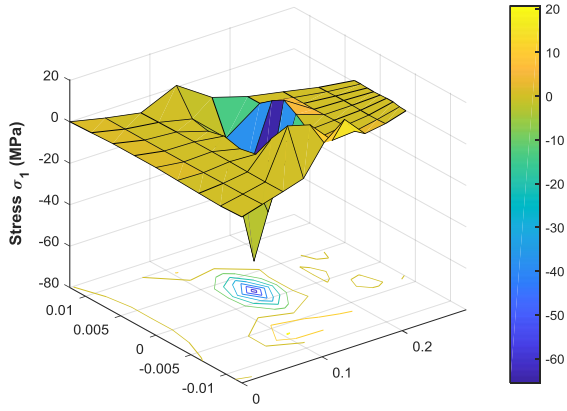

4.24.b)25% Multiple Delaminated Shell

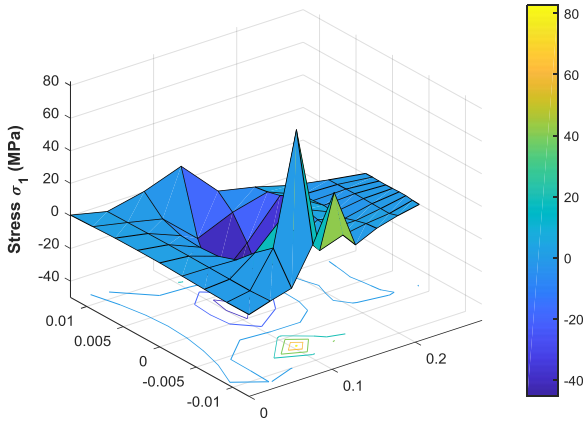

4.24.c)50% Multiple Delaminated Shell

Fig. 4.24 Variation of stresses (σ_1) in principal direction at critical velocity of impact for intact and multiple delaminated shell

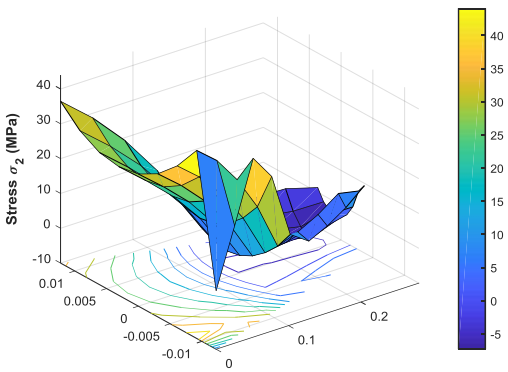

4.25.a) Intact Shell

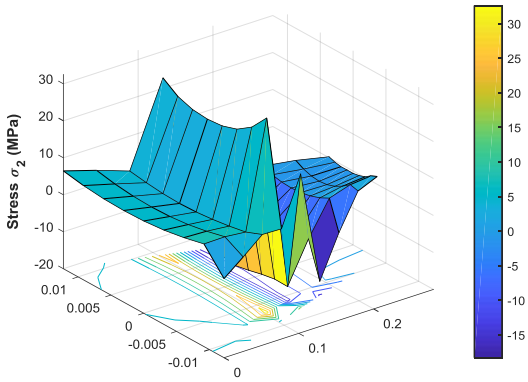

4.25.b) 25% Multiple Delaminated Shell

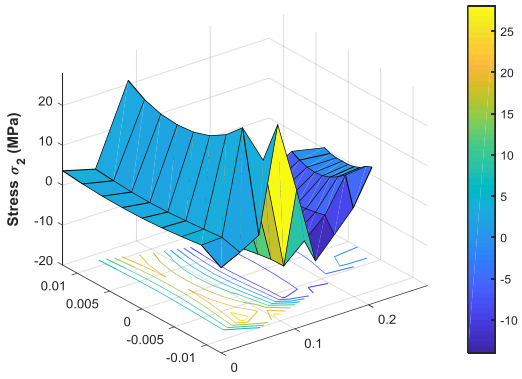

4.25.c) 50% Multiple Delaminated Shell

Fig. 4.25 Variation ofstresses (σ_2) in principal directionat critical velocityof impact for intact and multiple delaminated shell

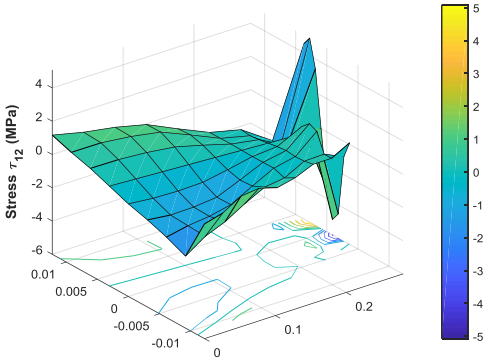

4.26.a) Intact Shell

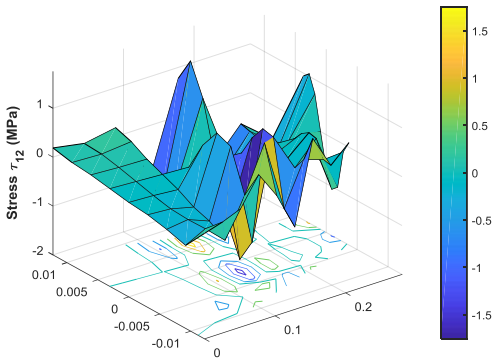

4.26.b) 25% Multiple Delaminated Shell

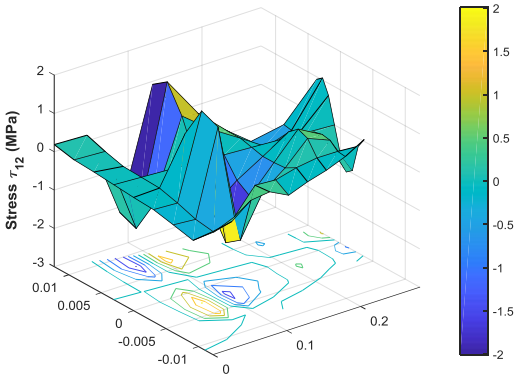

4.26.c) 50% Multiple Delaminated Shell

Fig. 4.26 Variation ofin plane stresses (τ_{12})at critical velocity of impact for intact and multiple delaminated shell

4.4.4 *Transient Response due to change in location of impact*

In the following analysis impacts are assumed in different location (**Fig. 4.27**) of the intact cantilever composite conical shell. The different location of impact are near free end (L/4), mid-point (L/2) and near fixed end (3L/4) and the FE results are compared. It is found that the contact force due to impact is maximum (**Fig. 4.28**) when the impact occurs near fixed end at critical velocity. When impact occurs near fixed end the shell displacement gradually increases and constant for a while (**Fig. 4.29**). After that shell displacement start decreasing at t=400μs. For impact at mid-point and near free end shell displacement increases gradually and close to each other. The impactor velocity drastically reduces and become constant for impact location at mid-point and near free end (**Fig. 4.30**) while for impact near fixed end impactor velocity at first reduces and constant for a while. Further it becomes negative. The impactor displacement when impact occur at mid-point and near free end gradually increases (**Fig. 4.31**). When impact occur near fixed end at first the impactor displacement increases rapidly then it continues increasing slowly and finally at t=600μs it starts decreasing.

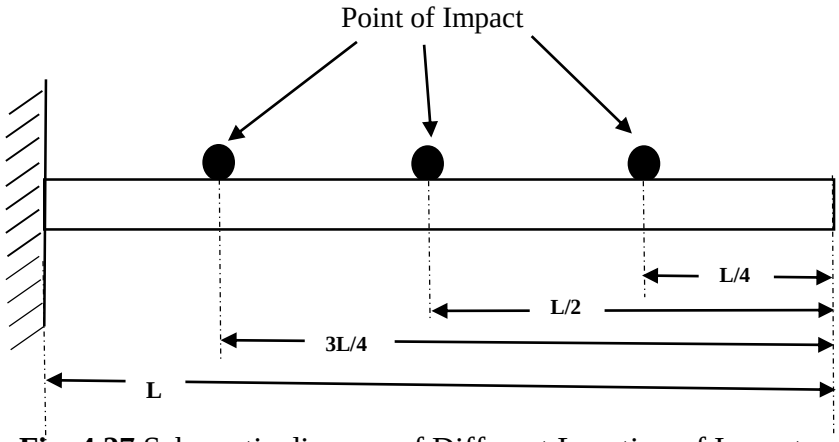

Fig. 4.27 Schematic diagram of Different Location of Impact

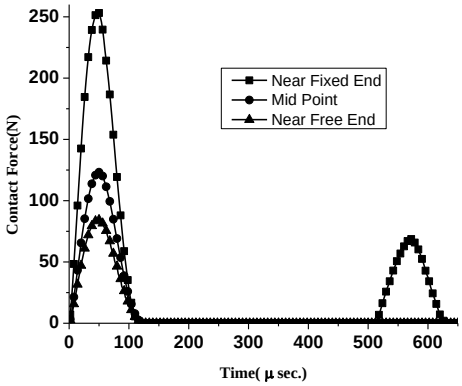

Fig. 4.28 Comparison of Contact force

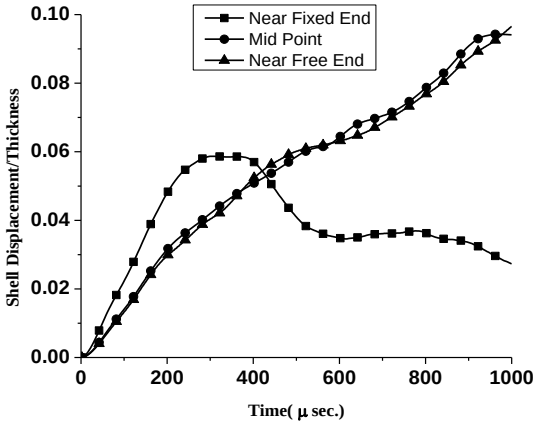

Fig. 4.29 Comparison of Shell Displacement

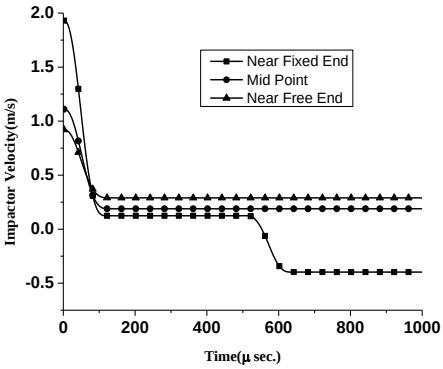

Fig. 4.30 Comparison of impactor velocity

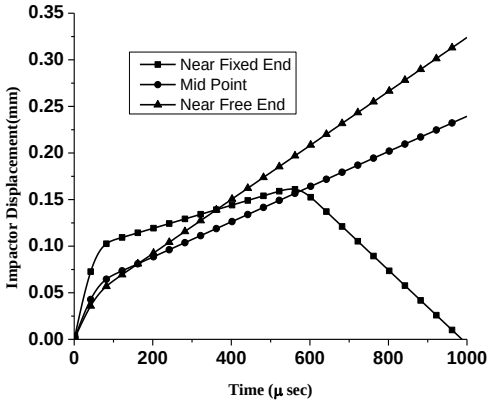

Fig. 4.31 Comparison of impactor displacement

CHAPTER 5

Summary & Conclusion

5.1 First Ply Failure of Pre-twisted Delaminated Rotating Conical Shells

The main conclusions drawn from the present analyses are:

1. A decrease in the first-ply failure strengths is predicted using different failure theories with an increase in the aspect ratio (*L/s*) in both undelaminated and delaminated composite conical shells.

2. For non-rotating conical shells, the σ_1 values are much higher near the fixed end in comparison with σ_2 and σ_6 values and are always tensile for undelaminated composite conical shells as seen from the stress variation plots.

3. Since the laminates have lower X_T and Y_T values, σ_1 plays the predominant role in the tensile failure of the laminates for undelaminated conical shells. Accordingly, the failed elements are near the fixed end (Element no 1 or 8) where $\sigma_1$is maximum.

4. The presence and location of delamination play a pivotal role in the failure initiation of delaminated composite conical shells. All the elements close to the edges of the delaminated zone near the cantilever end are most prone to experience the first-ply failure initiation under the influence of centrally applied point load. This is also corroborated by the stress-distribution plots wherein a zone of high compressive stresses (σ_1, σ_2andσ_6) is developed close to the delaminated zone. The failed laminas are mostly close to the outermost layers considering that the maximum bending stresses developed near the outermost layers.

5. The failure loads predicted using the stress-based failure theories (Maximum stress, Hoffmann, Tsai-Hill, and Tsai-Wu) are always higher than the Maximum strain theory irrespective of the pre-twist angle and delamination presence.

6. Failure loads increase with the increase in the non-dimensional rotational speed in both undelmainated and delaminated conical shells, which is due to corresponding stiffness rise owing to centrifugal stiffening.

7. Due to rotational stiffening, the stresses (σ_1, σ_2 and σ_6) developed in the rotating conical shell are lower than in non-rotating conical shell corresponding to a centrally applied point load.

8. The spanwise location of delamination center significantly influences the first-ply failure loads. It is observed that a blind crack adjoining the fixed end displays a much reduced first-ply failure load compared to a centrally-located crack or an open-end crack. This may be attributed to the high bending stresses developed close to the cantilever end of the conical shell leaving the blind-crack to be highly constrained under a centrally applied point loading.

9. The first-ply failure loads are the lowest for mid-plane delamination, while it increases for delamination presence near the outer layers of the conical shell. This is due to the highest bending stresses developed close to the outermost layers of the cantilever conical shell.

10. A drastic reduction in the failure loads is predicted using different failure theories due to the presence of multiple delamination compared to a single-delaminated shell with different rotational speeds. The FPF loads in single and multiple delaminated (0/90/0/90) composite conical shells decrease monotonically with an increase in the aspect ratio of the conical shell until they become asymptotic as the aspect ratio (*L*/*s*) approaches 0.9. A decrease in the first-ply failure loads is observed as the distance between the delamination increases in the case of multiple-delaminated $(0/90/0/90/0)_s$ conical shells.

11. The result shows that on the increase of delamination size the FPF load decreases drastically whereas on the increase of aspect ratio (L/s) FPF load decreases considerably. Further on increase of pre-twist angle (ψ), FPF load reduces gradually.

12. For intact-shell failure occurs near the fixed end (element 1) and for delaminated shell failure occur close to delamination zone (element 17). In all the situations failure occurs at layer number 7 from the bottom layer, since the bending stresses are higher at the extreme layer for cantilever shell.

13. There is the decrease in the FPF load with the increase in the size of delamination. The maximum value of FPF load is observed for intact shell and decrease significantly with rise in size of delamination. The maximum value of the FPF load is happened for maximum independent theories (strain & stress) and it is much lower for all the dependent theories.

14. With the rise in rotational speed the FPF values rises due to centrifugal stiffening effect. On rise of aspect ratio (L/s) of the conical shell FPF loads are reduced. From the slope of the FPF curve it is found that the percentage decrease in the failure load is much drastic for 50% delamination compared to 25% delamination.

15. Decrease in the FPF load is estimated using Tsai-Wu criterion with the rise of fiber inclination angle (θ) from 15^0 to 90^0 for $[\theta/\text{-}\theta]_2$ laminates. At $\theta=15^0$ the slope of the FPF curve is very steep and becomes asymptotic as θ approaches 90^0.

5.2 Impact Induced First Ply Failure of Delaminated Conical Shells

At first critical velocity of impact are predicted using existing FE formulation at different condition considering aspect ratio, size of delamination, location of delamination, number of delamination and location of impact. Critical velocity is the velocity at which FPF of the composite conical shell begins based on Tsai-Wu failure criterion. Critical velocity decreases on increase of aspect ratio and size of delamination. It is found that contact force, shell displacement, impactor displacement, impactor velocity decreases on increasing of aspect ratio, size & number of delamination. When the impact location moves from near fixed end to near free end contact force, shell displacement, impactor displacement, impactor velocity decreases.

CHAPTER 6

Research Contribution and Innovativeness:

The present research work contributes on first-ply failure load prediction and failed element location of pretwisted delaminated rotating composite conical shells under some well-established theories like maximum strain, maximum stress (Independent and polynomial based), Hoffmann, Tsai-Hill, and Tsai-Wu. Under static loading, vital parameters like size and location of delamination, pretwist angle, fibre orientation angle and rotation are considered to find out their impact on first-ply failure load. During impact loading, first the critical velocity of impact is calculated at which first-ply failure begins using Tsai-Wu failure criteria. The findings of critical velocity of impact is rare as most of the available literature explained transient response of low velocity impact. Then transient response of composite conical shells with single and multiple delamination with different size and location are studied. The variation of contact force, shell displacement, impactor velocity, impactor displacement with time of delaminated shell with different location of impact are also included in the present analysis.

CHAPTER 7

Future Scope of Work

Numerous research area are existing, which can be discovered or investigated in framework to the present work either in extension of the same or can be taken as a original research work. Some of which are cited below:

a. Structural damping can be added to the existing work to observe the effect of damping of delaminated composite conical shell under dynamic situations. Dynamic response of composites can be investigated by introducing visco-elastic material in intermediate layers.
b. The failure analysis of FGM, stiffened composites and sandwich composites structures can be done considering delamination, structural parameters and other operational conditions.
c. Progressive failure analysis of conical shell can be done considering different structural parameters and operational conditions.

REFERENCES:

[1] K.M. Liew, CM Lim and LS Ong, Vibration of pretwisted cantilever shallow conical shells. Int. J. Sol. Struct. 31 (1994) 2463–2474.

[2] S. Sreenivasamurthy, V. Ramamurti, A parametric study of vibration of rotating pre- twisted and tapered low aspect ratio cantilever plates, J. Sound Vib. 76(3) (1981) 311-328.

[3] Y.V.S. Kumar and A. Srivastava, First ply failure analysis of laminated stiffened plates, Compos. Struct. 60 (2003) 307–315.

[4] A.W. Leissa, J.K. Lee and A.J. Wang, Vibrations of twisted rotating blades. J. Vib. Acous. Stress. Reliab. 10 (1984) 251–257.

[5] X.J. Gu, Y.X. Hao , W. Zhang , L.T. Liu and J. Chen, Free vibration of rotating cantilever pre-twisted panel with initial exponential function type geometric imperfection, Appl. Math. Model.,11(037), 2018

[6] W. Carnegie, C. Stirlingt and J. Fleming, Vibration Characteristics of Turbine Blading Under Rotation-Results of an Initial Investigation and Details of a High Speed Test Installation, Proc. Inst. Mech. Engg. 180 (1965) 125-132

[7] M. A. Dokainish and S. Rawtani, Vibration Analysis of Rotating Cantilever Plates, Int. J Numer. Methods Eng., 3(1971), 233-248

[8] K Gupta and J.S Rao, Torsional Vibrations of Pretwisted Cantilever Plates, J Mech. Des., Transaction of ASME, 100(1978), 528-534

[9] R Henry and M Lalanne, Vibration Analysis of Rotating Compressor Blades, J Mech. Eng. Ind., Transaction of ASME, (1974), 1028-1035

[10] R. E Kielb, A.W Leissa and J.C Macbain, Vibration of Twisted Cantilever Plates- A Comparisson of Theoretical Results, Int. J Numer. Methods Eng., 21(1985), 1365-1380

[11] C. Li and H. Cheng, Free vibration analysis of a rotating varying-thickness-twisted blade with arbitrary boundary conditions. J Sound Vib. 492 (2021): 115791.

[12] D.X. Cao, B. Y. Liu, M. H. Yao, and W. Zhang., Free vibration analysis of a pre-twisted sandwich blade with thermal barrier coatings layers. Sci. China Technol. Sci. 60 (2017): 1747-1761.

[13] S. K. Sinha and K. E. Turner. Natural frequencies of a pre-twisted blade in a centrifugal force field. J Sound Vib. 330, no. 11 (2011): 2655-2681.

[14] S. Sreenivasamurthy and V. Ramamurti. A parametric study of vibration of rotating pre-twisted and tapered low aspect ratio cantilever plates. J Sound Vib. 76, no. 3 (1981): 311-328.

[15] D.N. Vadiraja and A. D. Sahasrabudhe. Vibration analysis and optimal control of rotating pre-twisted thin-walled beams using MFC actuators and sensors. Thin-Walled Struct. 47, no. 5 (2009): 555-567.

[16] M.S. Qatu and A.W. Wang, Vibration studies for laminated composite twisted cantilever plates, Int. J. Mech. Sci. 33(11) (1991) 927–40.

[17] O.G. Mcgee, H.R. Chu, Three-dimensional vibration analysis of rotating laminated composite blades, J. Eng. Gas Turb. Power, Trans ASME 116 (1994) 663–671

[18] J.N. Reddy, C.E. Liu, A higher-order shear deformation theory of laminated elastic shells, Int. J. Eng. Sci. 23(3) (1985) 319-330.

[19] M.O. Belarbi, A. Tati, H. Ounis, A. Benchabane, A. Development of a 2D isoparametric finite

element model based on the layerwise approach for the bending analysis of sandwich plates. Struct. Eng. Mech. 57(3) (2016) 473-506.

[20] M.O. Belarbi, A. Tati, H. Ounis, A. Khechai. On the free vibration analysis of laminated composite and sandwich plates: A layerwise finite element formulation. Lat. Am. J. Solids Struct. 14 (2017) 2265-2290.

[21] M. O. Belarbi, A. M. Zenkour, A. Tati, S. J. Salami, A. Khechai, M. S. Houari. An efficient eight-node quadrilateral element for free vibration analysis of multilayer sandwich plates. Int. J. Numer. Methods Eng. 122(9) (2021) 2360-2387.

[22] M. F. Caliri, A.J.M. Ferreira, V. Tita. A new finite element for thick laminates and sandwich structures using a generalized and unified plate theory. Int. J. Numer. Methods Eng. 109 (2) (2017) 290-304.

[23] Plannic I, Schnabl S, Saje M, Lopatic J and Cas B, Numerical and experimental analysis of timber composite beams with interlayer slip. Engg. Struct. 2008; 30; 2959-2969.

[24] J. Chen and Q.S. Li. Vibration characteristics of a rotating pre-twisted composite laminated blade. Compos. Struct. 208 (2019): 78-90.

[25] Z. Z Pan, X. Chen and Lu-Wen Zhang. Modeling large amplitude vibration of pretwisted hybrid composite blades containing CNTRC layers and matrix cracked FRC layers. App. Math. Model. 83 (2020): 640-659.

[26] R. Xiang, Z. Z. Pan, H. Ouyang and L. W. Zhang. A study of the vibration and lay-up optimization of rotating cross-ply laminated nanocomposite blades. Compos. Struct. 235 (2020): 111775.

[27] T. Y. Zhao, L P. Jiang, H. G. Pan, J. Yang and S. Kitipornchai. Coupled free vibration of a functionally graded pre-twisted blade-shaft system reinforced with graphene nanoplatelets. Compo. Struct. 262 (2021): 113362.

[28] W. Zhang, G. Liu and B. Siriguleng. "Saturation phenomena and nonlinear resonances of rotating pretwisted laminated composite blade under subsonic air flow excitation. J Sound Vib. 478 (2020): 115353.

[29] Y. Chen, T. Ye, G. Jin, S. Li and C. Yang. Vibration analysis of rotating pretwist FG sandwich blades operating in thermal environment. Int. J Mech. Sci.205 (2021): 106596.

[30] Y. Chen, G. Jin, T. Ye and M. Chen. A quasi-3D dynamic model for free vibration analysis of rotating pre-twisted functionally graded blades. J Sound Vib. 499 (2021): 115990.

[31] M. Hajianmaleki and M.S. Qatu. Vibrations of straight and curved composite beams: A review, Compos. Struct. 100 (2013): 218-232.

[32] E. Kumari, Free vibration analysis of rotating laminated composite plate type blades with variable thickness, Mater. Today: Proc. 43 (2021): 1762-1773.

[33] S. Mohamed Nabi and N. Ganesan. Comparison of beam and plate theories for free vibrations of metal matrix composite pre-twisted blades.J Sound Vib. 189, no. 2 (1996): 149-160.

[34] L. W. Zhang, Z. Z. Pan and X. Chen. Vibration characteristics of matrix cracked pretwisted hybrid composite blades containing CNTRC layers. J Sound Vib. 473 (2020): 115242.

[35] M. Teotia and R.K. Soni, Applications of finite element modelling in failure analysis of laminated glass composites: A review, Eng. Fail. Anal. 94 (2018) 412-437.

[36] K.J. Bathe. Finite element procedures in engineering analysis (1990), Prentice Hall of India,

New Delhi.

[37] C.K. Gim, Plate finite element modeling of laminated plates, J. Comp. Struct. 52(1) (1994) 157–168.

[38] J.N. Reddy and C.E. Liu, A higher-order shear deformation theory of laminated elastic shells, Int. J. Eng. Sci. 23(3) (1985) 319-330.

[39] K. Alnefaie, Finite element modeling of composite plates with internal delamination, Compos. Struct. 90, no. 1 (2009): 21-27.

[40] S.B. Beheshti-Aval and M. Lezgy-Nazargah. "A finite element model for composite beams with piezoelectric layers using a sinus model." Journal of Mech. 26, no. 3 (2010): 335-344.

[41] W. Chung and Elisa D. Sotelino. "Three-dimensional finite element modeling of composite girder bridges." Eng. Struct. 28, no. 1 (2006): 63-71.

[42] B. A. Gama and J. W. Gillespie Jr, Finite element modeling of impact, damage evolution and penetration of thick-section composites, Int. J Impact Eng. 38, 4(2011): 181-197.

[43] S. M. R Khalili, M. Soroush, A. Davar and O. Rahmani, Finite element modeling of low-velocity impact on laminated composite plates and cylindrical shells, Compos. Struct. 93, no. 5 (2011): 1363-1375.

[44] C. J. Mitchell, L. M. Dangora and J. A. Sherwood. "Investigation into a robust finite element model for composite materials, Finite Elem. Anal. Des. 115 (2016): 1-8.

[45] M. Peeters, G. Santo, J. Degroote, and W. V. Paepegem, High-fidelity finite element models of composite wind turbine blades with shell and solid elements, Compos. Struct. 200 (2018): 521-531.

[46] J. N Reddy and D. H. Robbins Jr., Theories and computational models for composite laminates, (1994): 147-169.

[47] G. Shi, K. Y. Lam and T. E. Tay, On efficient finite element modeling of composite beams and plates using higher-order theories and an accurate composite beam element, Compos. Struct. 41, no. 2 (1998): 159-165.

[48] A.D. Stemple and S W. Lee, A finite element model for composite beams undergoing large deflection with arbitrary cross-sectional warping, Int. J Numer.Methods. Eng. 28, no. 9 (1989): 2143-2160.

[49] M.H.H. Shen and J.E. Grady, Free vibrations of delaminated beams, AIAA 30(5) (1992) 1361-1370.

[50] M. Krawczuk, W. Ostachowicz and A. Zak, Dynamics of cracked composite material structures, J. Comput. Mech. 20 (1997) 79-83.

[51] J.J. Tracy and G.C. Pardoen, Effect of delamination on the natural frequencies of composite laminates, J Compos. Mater. 23(12) (1989) 1200–1215.

[52] C.K. Gim, Plate finite element modeling of laminated plates, J. Comp. Struct. 52(1) (1994) 157–168.

[53] A. Zak, M. Krawczuk and W. Ostachowicz, Vibration of a laminated composite plate with closing delamination, J Intell. Mater. Syst. Struct. 12(8) (2001) 545-551.

[54] T. Bandyopadhyay and A. Karmakar, Bending characteristics of delaminated cross-plycomposite shallow conical shells in hygrothermal environment, J. Reinf. Plast. Compos. 34(20) (2015) 1724-1735.

[55] T. Bandyopadhyay, A. Karmakar and K. Kishimoto. Hygrothermal effects on the free vibration characteristics of delaminated composite pretwisted rotating conical shells. JSME Mech. Eng. J. 1 (2014) 1-18.

[56] T. Bandyopadhyay, A. Karmakar and K. Kishimoto, Transient response of delaminated composite conical shells due to multiple low velocity impacts in hygrothermal environment, Compos. Struct. 143 (2016) 202–219.

[57] T.D. Singha, M. Rout, T. Bandyopadhyay and A. Karmakar, Free vibration analysis of rotating pretwisted composite sandwich conical shells with multiple debonding in hygrothermal environment, Eng. Struct. 204 (2020) 110058.

[58] A. Parhi, B. N. Singh and S. K. Panda, Nonlinear free vibration analysis of composite conical shell panel with cluster of delamination in hygrothermal environment, Eng. Comput. 37 (2021) 1565–1577.

[59] M. S. Rao and P. Shu D, Buckling analysis of two layer beams with an asymmetric delamination. Engg. Struct. 2004; 26; 651-658.

[60] Yin W. L, The effects of laminated structure on delamination buckling and growth, J. Comp. Mater, 1988; 22; 502-517.

[61] Yin W. L, Sallam S. N and Simitses G. J, Ultimate axial load capacity of a delaminated beam-plate, AIAA J; 1986; 24; 123-128.

[62] Xiaoping Shu. A generalised model of laminated composite plates with interfacial damage. Compos. Struct. 2006; 74(2), 237-246

[63] Shen MHH and Grady JE. Free vibrations of delaminated beams. J. AIAA 1992; 30(5):1361-1370.

[64] Paolozzi A and Peroni I, Detection of debonding damage in a composite plate through natural frequency variations. J. Reinf. Plast. Compos 1992; 9:369-389.

[65] Tracy JJ and Pardoen GC. Effect of delamination on the natural frequencies of composite laminates. J Compos. Mater, 1989; 23:1200-1215.

[66] Tenek LH, Hennekell EG and Gunzburger MD. Vibration of delaminated composite plates and some applications to non-destructive testing. Compos. Struct, 1993; 23:253-262.

[67] Fangliang Chen, Pizhong Qiao, Buckling of delaminated bi-layer beam-columns, Int. J. of Solids and Struct., 2011, 48(18), 2485-2495

[68] S. Wang, Y. Zhang, Buckling, post-buckling and delamination propagation in debonded composite laminates: Part 1: Theoretical development, Compos. Struct.2009, 88(1), 121-130

[69] M.S.R. Parlapalli, Dongwei Shu and Gin B.Chai, Buckling of composite beams with two enveloped delaminations: Lower and upper bounds, Comput. & Struct. 2008, 86(23–24), 2155-2165

[70] A. Parhi, B. N. Singh, and S. K. Panda, Nonlinear free vibration analysis of composite conical shell panel with cluster of delamination in hygrothermal environment, Eng. Comput. 37 (2021): 1565-1577.

[71] B. Qin, R. Zhong, T. Wang, Q. Wang, Y. Xu and Z. Hu, A unified Fourier series solution for vibration analysis of FG-CNTRC cylindrical, conical shells and annular plates with arbitrary boundary conditions,Compos. Struct. 232 (2020): 111549.

[72] M. Safarpour, A. R. Rahimi, and A. Alibeigloo, Static and free vibration analysis of graphene platelets reinforced composite truncated conical shell, cylindrical shell, and annular plate using theory of elasticity and DQM. Mech. Based Des. Struct. Mach.48,4 (2020): 496-524.

[73] P. Maji, M. Rout, and A. Karmakar, Free vibration response of carbon nanotube reinforced pretwisted conical shell under thermal environment. Proc. Inst. Mech. Eng., Part C: J Mech. Eng. Sci. 234, 3 (2020): 770-783.

[74] T. D. Singha, T. Bandyopadhyay, and A. Karmakar, Thermoelastic free vibration of rotating pretwisted sandwich conical shell panels with functionally graded carbon nanotube-reinforced composite face sheets using higher-order shear deformation theory. Proc. Inst. Mech. Eng., Part L: J Mater. Des. Appl. 235, 10 (2021): 2227-2253.

[75] B.P. Patel, M. Ganapathi and S. Kamat, Free vibration characteristics of laminated composite joined conical-cylindrical shells. J Sound Vib. 237,5 (2000): 920-930.

[76] D. He, D. Shi, Q. Wang and C. Ma, A unified power series method for vibration analysis of composite laminate conical, cylindrical shell and annular plate. In Struct. 29, 305-327. Elsevier, 2021.

[77] A. Kamaloo, M. Jabbari, M. Y. Tooski and M. Javadi, Nonlinear free vibrations analysis of delaminated composite conical shells. Int.l J Struc. Stab. Dyn. 20, 01 (2020): 2050010.

[78] A. Karmakar, H. Roy and K. Kishimoto. "Free vibration analysis of delaminated composite pretwisted shells." Aircr. Eng. Aerosp. Technol. 77, 6 (2005): 486-490.

[79] A. Karmakar and K. Kishimoto, Free vibration analysis of delaminated composite pretwisted rotating shells─ A Finite Element Approach. JSME Int. J Series A Solid Mech. Mater. Eng. 49, 4 (2006): 492-502.

[80] P. Maji and B.N. Singh, Free vibration responses of 3D braided rotating cylindrical shells based on third-order shear deformation. Compos. Struct. 260 (2021): 113255.

[81] S. Mohammadrezazadeh and A. A. Jafari, Nonlinear vibration analysis of laminated composite angle-ply cylindrical and conical shells." Compos. Struct. 255 (2021): 112867.

[82] M. Rout, T. Bandyopadhyay and A. Karmakar. "Free vibration analysis of pretwisted delaminated composite stiffened shallow shells: a finite element approach. J Reinf. Plast. Compos. 36, 8 (2017): 619-636.

[83] M. Rout, S.S. Hota and A. Karmakar, Free vibration characteristics of delaminated composite pretwisted stiffened cylindrical shell. Proc. Inst. Mech. Eng. Part C: J Mech. Eng. Sci. 232, 4 (2018): 595-611.

[84] E. Sobhani, A. R. Masoodi and A. R. Ahmadi-Pari, Vibration of FG-CNT and FG-GNP sandwich composite coupled Conical-Cylindrical-Conical shell, Compos. Struct. 273 (2021): 114281.

[85] H. N. R. Wagner, C. Hühne and S. Niemann, Robust knockdown factors for the design of axially loaded cylindrical and conical composite shells–development and validation, Compos. Struct. 173 (2017): 281-303.

[86] C.W. Lim, K.M. Liew and S. Kitipornchai, Free vibration of pretwisted, cantilevered composite shallow conical shells, AIAA J. 35 (1997) 327-333.

[87] M. Karimiasl, F. Ebrahimi, and B. Akgöz. Buckling and post-buckling responses of smart doubly curved composite shallow shells embedded in SMA fiber under hygro-thermal loading. Compo. Struct. 223 (2019): 110988.

[88] A. Beakou, and M. Touratier, A rectangular finite element for analysing composite multilayered shallow shells in statics, vibration and buckling. Int. J Numer. Methods Eng. 36, 4 (1993): 627-653.

[89] M. Biswal, S. K. Sahu, and A. V. Asha, Experimental and numerical studies on free vibration of laminated composite shallow shells in hygrothermal environment. Compos. Struct.127 (2015):

165-174.

[90] M. Di Sciuva, M. Gherlone, and L. Librescu, Implications of damaged interfaces and of other non-classical effects on the load carrying capacity of multilayered composite shallow shells, Int. J. Non-linear Mech. 37, 4-5 (2002): 851-867.

[91] N. D. Duc, K. Seung-Eock, P. H. Cong, N. T. Anh, and N. D. Khoa. Dynamic response and vibration of composite double curved shallow shells with negative Poisson's ratio in auxetic honeycombs core layer on elastic foundations subjected to blast and damping loads, Int. J. Mech. Sci. 133 (2017): 504-512.

[92] X Guo, Y. Y Lee and C. Mei, Non-linear random response of laminated composite shallow shells using finite element modal method. Int. J Numer. Methods Eng. 67(2006), 1467-1489

[93] C. K Hirwani, S. K Panda, T. R Mahapatra, and S.S Mahapatra, Nonlinear transient finite-element analysis of delaminated composite shallow shell panels. Aiaa J. 55(5), 2017.1734-1748.

[94] M.S.H. Fatt, and D. Sirivolu. Blast response of double curvature, composite sandwich shallow shells. Engg. Struct. 100,2015, 696-706.

[95] S. Huang and P. Qiao. A new semi-analytical method for nonlinear stability analysis of stiffened laminated composite doubly-curved shallow shells. Compos. Struct. 251, 2020.112526.

[96] H. Kurtaran. Geometrically nonlinear transient analysis of moderately thick laminated composite shallow shells with generalized differential quadrature method. Compos. Struct. 125, 2015. 605-614.

[97] H. Li, F. Pang, C. Gao and R. Huo. A Jacobi-Ritz method for dynamic analysis of laminated composite shallow shells with general elastic restraints. Compos. Struct. 242, 2020. 112091.

[98] H. Matsunaga. Vibration and stability of cross-ply laminated composite shallow shells subjected to in-plane stresses. Compos. Struct. 78(3), 2007. 377-391.

[99] D.D. Nguyen, Q.Q. Tran and D.K. Nguyen. New approach to investigate nonlinear dynamic response and vibration of imperfect functionally graded carbon nanotube reinforced composite double curved shallow shells subjected to blast load and temperature. Aerosp. Sci. Technol. 71, 2017.360-372.

[100] V.K Singh and S.K. Panda. Nonlinear free vibration analysis of single/doubly curved composite shallow shell panels. Thin-Walled Struct. 85, 2014.341-349.

[101] M.S. Qatu and A.W. Leissa. Free vibrations of completely free doubly curved laminated composite shallow shells. J. Sound Vib. 151(1), 1991.9-29.

[102] B.E. Said and S. R. Hallett, Parametric failure manifolds for laminated composites, Compos. Struct. 253 (2020) 112798.

[103] N. Zimmermann and P. H. Wang, A review of failure modes and fracture analysis of aircraft composite materials, Eng. Fail. Anal. 115 (2020) 104692.

[104] T.Y. Kam, H.F. Sher, T.N. Chao and R.R. Chang, Predictions of deflection and first-ply failure load of thin laminated composite plates via the finite element approach, Int. J. Solids Struct. 33(3) (1996) 375-398.

[105] J.N. Reddy and A.K. Pandey, A first-ply failure analysis of composite laminates, Comput. Struct. 25(3) (1987) 371-393.

[106] T.Y. Kam and F.M. Lai, Experimental and theoretical predictions of first-ply failure strength of laminated composite plates, Int. J. Solids Struct. 36 (1999) 2379-2395.

[107] B.G. Prusty, S.K. Satsangi and C. Ray, First ply failure analysis of laminated panels under transverse loading, J. Reinf. Plast. Compos. 20(8) (2001) 671-684.

[108] J. Błachut, Buckling and first ply failure of composite toroidal pressure hull, Comput. Struct. 82 (2004) 1981–1992.

[109] G.S. Ramtekkar, Y.M. Desai and A.H. Shah, First ply failure of laminated composite plates-a mixed finite element approach, J. Reinf. Plast. Compos. 23(3) (2004) 291-315.

[110] K. Bakshi and D. Chakravorty, First ply failure study of thin composite conoidal shells subjected to uniformly distributed load, Thin-Walled Struct. 76 (2014) 1–7.

[111] K. Bakshi and D. Chakravorty, Geometrically linear and nonlinear first-ply failure loads of composite cylindrical shells, ASCE (2014) 1-10.

[112] M. Romanowicz, Determination of the first ply failure load for a cross ply laminate subjected to uniaxial tension through computational micromechanics, Int. J. Solids Struct. 51 (2014) 2549–2556.

[113] T.Y. Kam, H.M. Su, C.Y. Huang, Quasi-static buckling and first-ply failure loads of shear web reinforced glass-fabric composite wind blades, Compos. Struct. 160 (2017) 1225-1235.

[114] A Karmakar, P.K. Sinha, Failure analysis of laminated composite pretwisted rotating plates, J. Reinf. Plast. Compos. 20(14-15) (2001) 1326-1357.

[115] D. Biswas, C. Ray, Effect of hybridisation in laminated composites on the first ply failure behaviour: Experimental and numerical studies, Int. J. Mech. Sci. 161–162 (2019) 105057.

[116] S. Gohari, S. Sharifi, Z. Vrcelj, Md. Y. Yahya, First-ply failure prediction of an

unsymmetrical laminated ellipsoidal woven GFRP composite shell with incorporated surface-bounded sensors and internally pressurized, Compos. B Eng. 77 (2015) 502-518.

[117] N. N. Rao and Pavuluri M. V. Rao, First ply failure analysis of rectangular fiber metal laminated composite plates subjected to uniformly distributed loads, J. Fail. Anal. Prev. 19 (2019) 1683–1690.

[118] S. Mondal, L.S. Ramachandra, Stability and failure analyses of delaminated composite plates subjected to localized heating, Compos. Struct. 209 (2019) 258-267.

[119] A. Kumar, A. Chakrabarti, P. Bhargava, V. Prakash, Efficient failure analysis of laminated composites and sandwich cylindrical shells based on higher-order zigzag theory, J. Aerosp. Eng. 28 (2015) 4014100.

[120] Anish, A. Kumar, A. Chakrabarti, Failure mode analysis of laminated composite sandwich plate, Eng. Fail. Anal. 104 (2019) 950–976.

[121] J.Y. Ang, M.S.A. Majid, A. Md. Nor, S. Yaacob, M.J.M. Ridzuan, First-ply failure prediction of glass/epoxy composite pipes using an artificial neural network model, Compos. Struct. 200 (2018) 579-588.

[122] G. Mustafa, A. Suleman, C. Crawford, Probabilistic first ply failure prediction of composite laminates using a multi-scale M-SaF and Bayesian inference approach, J Compos. Mater. 52(2) (2018) 169–195.

[123] J. R. Martinez, P. L. Bishay, On the stochastic first-ply failure analysis of laminated composite plates under in-plane tensile loading, Composites Part C: Open Access. 4 (2021) 100102

[124] A. Saha, A. Das, A. Karmakar, Parametric study on the first ply failure load of delaminated shallow pretwisted conical shells–a finite element approach. Materials Today:

Proceedings 11 (2019) 818-829.

[125] S. Timoshenko, D.H. Young, Vibration Problems in Engineering, 3rd ed. Dordrecht: Von Nostrand Reinhold, 1955:413-16

[126] V. Sairam, S. K Kanna & P. S. R. Kumar, Analysis of low-velocity impact response in Aa5083 plate. In IOP Conference Series: Mater. Sci.Engg. , April, 2021, Vol. 1123, No. 1, p. 012040.

[127] M. V Shitikova. Impact response of a viscoelastic plate made of a material with negative Poisson's ratio. Mech. of Adv. Mater. & Struct. 2022, 1-13.

[128] E. Mehrdad, S. Feli, S. & R. Das, Low-Velocity Impact Response Analysis of Functionally Graded Piezoelectric Plates Using Finite-Element Method and a Two-Degrees-of-Freedom Spring-Mass Model. Adv. Engg. Mater. 2023, 2201731.

[129] C.T. Sun, and S. Chattopadhyay, Dynamic response of anisotropic laminated plates under initial stress to impact of a mass. J. Appl. Mech. 1975; 42(3):693-698.

[130] C.T. Sun, and J. K Chen, On the Impact of initially stressed Composite Laminates, J. Compos Mater, 1985; 19; 490-504

[131] R. W. Mortimer, P. C. Chou and B. T. Rodini, In-Plane and Shear-Bending Impact of Laminated Composite Plates, J. Appl. Mech. Jun 1976, 43(2): 275-280

[132] E. H. Lee, The Impact of a Mass Striking a Beam, J. Appl. Mech. 1940, 7(4): A129-A138

[133] Li C. Shen, H. S. Yang, & H. Wang. Low-velocity impact response of sandwich plates with GRC face sheets and FG auxetic 3D lattice cores. Engg. Anal. Bound. Elem. 2021, 132, 335-344.

[134] M. Song, X. Li, S. Kitipornchai, Q. Bi & J. Yang, Low-velocity impact response of geometrically nonlinear functionally graded graphene platelet-reinforced nanocomposite plates. Nonlinear Dyn. 2019, 95, 2333-2352.

[135] J. He, L. He and B. Yang, Analysis on the impact response of fiber-reinforced composite laminates: An emphasis on the FEM simulation. Sci. Engg. Compos. Mater. 2019, 26(1), 1-11.

[136] F. Ebrahimi and S. Habibi. Low-velocity impact response of laminated FG-CNT reinforced composite plates in thermal environment. Adv. Nano Res. 2017, 5(2), 69.

[137] A. K. I. N Ceyla and M. Şenel. An experimental study of low velocity impact response for composite laminated plates. J. Sci. & Tech. Dumlupınar University, 2010, (021), 77-90.

[138] M. M Ansari and A. Chakrabarti. Behaviour of GFRP composite plate under ballistic impact: experimental and FE analyses. Struct. Engg. Mech. 2016, 60(5), 829-849.

[139] L.U. Chun and K.Y. Lam. Dynamic response of fully-clamped laminated composite plates subjected to low-velocity impact of a mass. Int. J Solids and Struct. 1988, 35(11):963-979

[140] N. Hu, H Sekine, H. Fukunaga and Z.H. Yao. Impact analysis of composite laminates with multiple delaminations. Int. J. Impact Engg. 1999; 22:633–648.

[141] H. Sekine, T. Hu, T. Natsume and H. Fukunaga, Impact response analysis of partially delaminated composite laminates. Trans. JSME, Series A 1997; 63:131–137. 22.

[142] A. Karmakar and K. Kishimoto. Transient dynamic response of delaminated composite rotating shallow shells subjected to impact. Shock. Vib. 2006; 13:619–628

[143] T. Bandyopadhyay, A. Karmakar, K Kisimoto. Transient Response of Delaminated Composite Conical Shells Due to Multiple Low Velocity Impacts in Hygrothermal Environment, Compos. Struct, 2016, 143:202-219

[144] P. N. B Reis, P. Sousa, L.M. Ferreira & C.A. Coelho, Multi-impact response of semicylindrical composite laminated shells with different thicknesses. Compos. Struct. 2023, 310, 116771.

[145] S. Sharifi, T. A. D. M. S Almula, S. Gohari, G. Sharifishourabi, Y. Saed & M.Y.B. Yahya. Impact response of laminated composite cylindrical shell: finite element simulation approach. Appl. Mech. Mater.2013, Vol. 393, pp. 387-392, Trans Tech Publ. Ltd.

[146] M. Rout, S.S. Hota, and A. Karmakar. Prediction of impact response of delaminated pretwisted stiffened shell. Aust. J. of Mech. Engg. 2021, 19(2), 173-185.

[147] C. A. C. P. Coelho, F. V Navalho and P. N. B. Reis. Impact response of laminated cylindrical shells. Frat. ed Integrità Strutt. 2019, 13(48), 411-418.

[148] S. Paramasivam, & A.J.T. Johnson. Experimental and numerical studies on the low-velocity impact response of carbon fibre- reinforced polymer anisogrid cylindrical shells. Poly. Compos. 2022, 43(6), 3831-3845.

[149] P.K. Parhi, P.K. Sinha, S.K. Bhattacharya, Dynamic Behaviour and Impact Induced First Ply Failure of Multiple Delaminated Composite Shells, J. Reinf. Plast. Compos, 2001, 20, 15: 1276-1300

[150] C. K. Hirwani, R K. Patil, S. K. Panda, S. S. Mahapatra, S. K. Mandal, L Srivastava and M K. Buragohain, Experimental and numerical analysis of free vibration of delaminated curved panel, Aerosp. Sci. Technol., Vol. 54, July 2016, 353-370

[151] C. K Hirwani, S K Panda and T R Mahapatra, Nonlinear Finite Element Analysis of Transient Behavior of Delaminated Composite Plate, J. Vib. Acoust. Apr 2018, 140(2): 021001

[152] C. K Hirwani, S K Panda, S. S Mahapatra, S K Mandal, L. Srivastava and M. K Buragohain, Flexural strength of delaminated composite plate – An experimental validation, Int. J. Damage Mech. Vol. 27, Issue 2

[153] C. K Hirwani, S K Panda, T R Mahapatra and S. S Mahapatra, Numerical Study and Experimental Validation of Dynamic Characteristics of Delaminated Composite Flat and Curved Shallow Shell Structure, J. Aerosp. Eng. August 2017, 30(5)

[154] C. K Hirwani and S K Panda, Nonlinear thermal free vibration frequency analysis of delaminated shell panel using FEM, Compos. Struct. Vol. 224, 15 September 2019, 111011

[155] C. K Hirwani, S K Panda and T R Mahapatra, Thermomechanical deflection and stress responses of delaminated shallow shell structure using higher-order theories, Compos. Struct. Vol. 184, 15 January 2018, 135-145

[156] H. C. Dewangan, N. Sharma, C. K Hirwani and S K Panda, Numerical eigen frequency and experimental verification of variable cutout (square/rectangular) borne layered glass/epoxy flat/curved panel structure, Mech. Based Des. Struct. Mach , 2020, 50 (5), 1640-1657

[157] C. K Hirwani and S K Panda, Numerical nonlinear frequency analysis of pre-damaged curved layered composite structure using higher-order finite element method, Int. J. Non-Linear Mech. 2018, 102, 14-24.

[158] C. K Hirwani, S K Panda, T R Mahapatra and S. S Mahapatra, Nonlinear Transient Finite-Element Analysis of Delaminated Composite Shallow Shell Panels, 2017, AIAA J. 55(5):1-15

[159] C.K. Hirwani, T.R. Mahapatra, S. K. Panda, S.S. Sahoo, V.K. Singh and B.K. Patle, Nonlinear Free Vibration Analysis of Laminated Carbon/Epoxy Curved Panels, Def. Sci. J. 2017, Vol 67 No 2

[160] C. K Hirwani and S K Panda, Nonlinear finite element solutions of thermoelastic deflection and stress responses of internally damaged curved panel structure, Appl. Math. Model, 2019, Vol. 65, 303-317,

[161] C. K Hirwani and S K Panda, Numerical and experimental validation of nonlinear deflection and stress responses of pre-damaged glass-fibre reinforced composite structure, Ocean Eng, 2018, 159, 237- 252

[162] C. K Hirwani, S K Panda and B. K. Patle, Theoretical and experimental validation of nonlinear deflection and stress responses of an internally debonded layer structure using different higher-order theories, Acta Mech. 2018, 229, 3453-3473.

[163] C. K Hirwani and S K Panda, Nonlinear transient analysis of delaminated curved composite structure under blast/pulse load, *Eng. Comput.*2020, 36, 1201 -1214

[164] L Srivastava, L Krishnanand, N. K Nath, C K Hirwani and S K Panda, Effect of blast load on dynamic deflection responses of internally damaged carbon–epoxy laminated composite shallow shell panel using experimental properties, *Trans. Indian Inst. Met.* 2023, 76 (1), 157-164

[165] K K Erukala, P K Mishra, H C Dewangan, S K Panda and M Dwivedi, Damaged composite structural strength enhancement under elevated thermal environment using shape memory alloy fiber, Acta Mech., 2022, 233 (8), 3133-3155,

[166] K K Erukala, P Pattanayak and S K Panda, Large Deformation Dynamic Characteristics of Cracked Laminated Panel and Improvement of Stiffness Using Shape Memory Alloy Fiber, J. Press. Vessel Technol. 2024, 146 (2)

[167] V Kumar, H C Dewangan, N Sharma, S K Panda, Numerical prediction of static and vibration responses of damaged (crack and delamination) laminated shell structure: an experimental verification, Mech. Syst. Signal Process. 2022, 293, 115709.

[168] V Kumar, S K Panda, S.R. Mahmoud and M Balubaid, Numerical investigation of transient thermo-mechanical loading effect on combined damaged (crack and delamination) curved shell structure: an experimental verification, Ocean Eng. 2022, 266 (4), 113009

[169] R. M Jones, Mechanics of Composite Materials, 1998, Taylor and Francis

[170] R D Cook, Finite Element Modelling for Stress Analysis, 1995, John Willey & Sons

APPENDIX

Flow chart for the FPF analysis of rotating composite conical shells

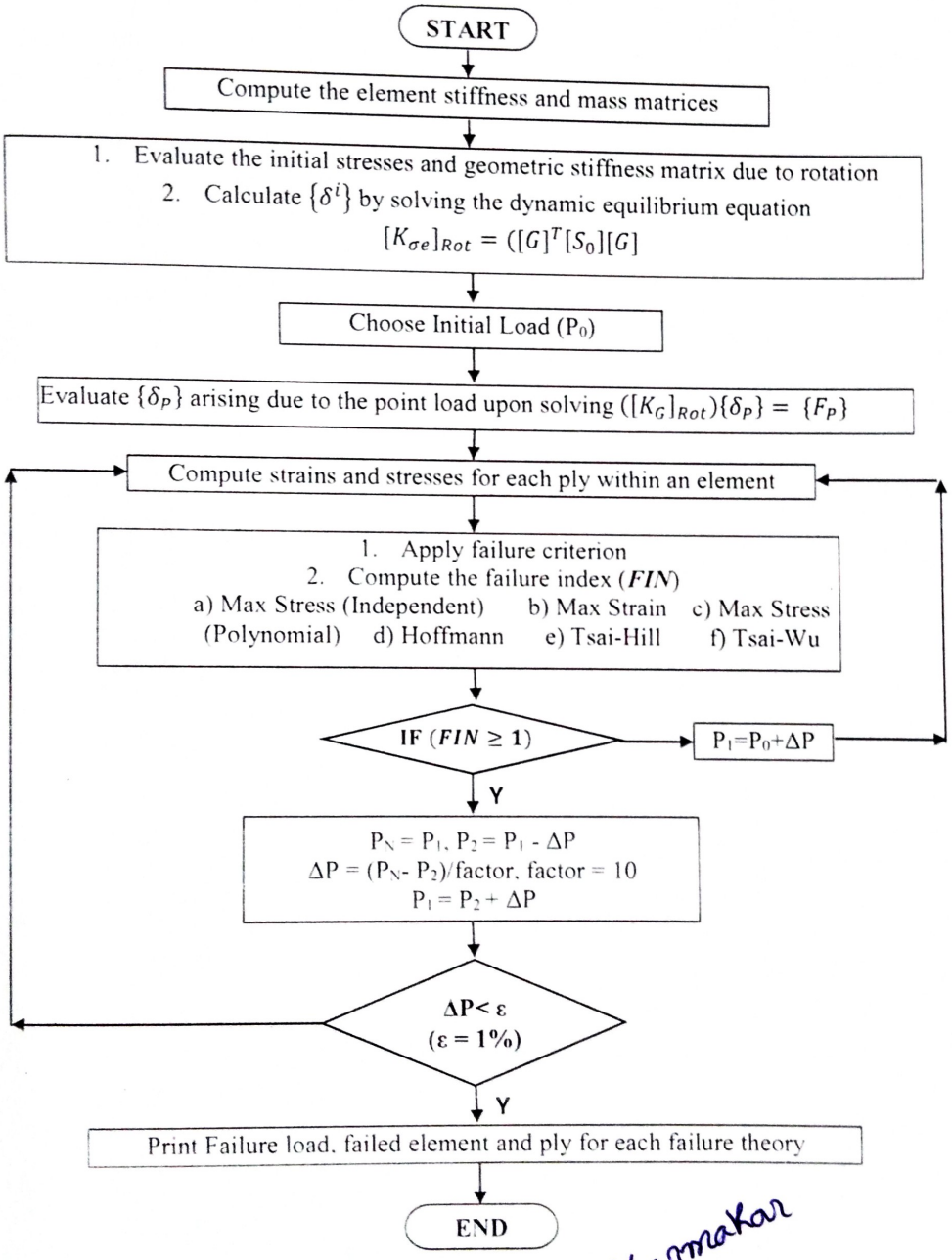

Suman Karmakar